The Impact of Harmonics on the Power Cable Stress Grading System

by

Utkarsh Patel

A thesis
presented to the University of Waterloo
in fulfillment of the
thesis requirement for the degree of
Master of Applied Science
in
Electrical and Computer Engineering

Waterloo, Ontario, Canada, 2012

AUTHOR'S DECLARATION

I hereby declare that I am the sole author of this thesis. This is a true copy of the thesis, including any required final revisions, as accepted by my examiners.

I understand that my thesis may be made electronically available to the public.

Abstract

With the continuous growth of non-linear power electronic components and the increasing penetration of the distributed generation (DG), the potential for degradation in the power quality of the existing grid exists. There are concerns that the total harmonic distortion (THD) could reach unacceptable levels of 5% or higher. Moreover, there is additional potential of the presence of amplified harmonic components in the power network grid when the harmonic frequencies align with the resonant frequencies that are being injected by power electronic components of the DG. The above conditions could increase the electrical stresses on the insulation system of the power system components, and in particular, cable terminations are a concern.

Standard cable terminations are designed to operate under power frequency in the power system network and their service life is considered accordingly. The research work aims to provide an understanding of the performance of the stress grading (SG) system of a commercial cable termination when the voltage waveform is distorted due to the presence of harmonics and when the high frequency and high $\frac{dV}{dt}$ voltage waveforms are present from a typical power electronic drive. An aging experiment was performed for over a 600 hour time period using the pulse width modulated (PWM) high-voltage generator to quantify the impact of high frequency stress on SG system of cable termination. Furthermore, the cable termination was tested under power frequency, distorted voltage waveforms composed of fundamental and low order harmonics using an experiment setup that generate distorted voltage waveforms. Diagnostic techniques such as surface potential distribution measurements and surface temperature monitoring are used to analyze the termination performance. The surface tangential field is calculated based on the gradient of the termination surface potential as measured with an electrostatic voltmeter.

The study shows that distorted voltage waveforms with high frequency and high $\frac{dV}{dt}$ components, increase the electric field, resistive heating, and surface temperature rise in the terminations that use the field-dependent SG materials. The rise of electric field by as high as 27.1% and surface temperature rise of as high as 17°C demonstrates the severity on the cable terminations. Such electric field enhancements for a period of time have a potential to initiate partial discharge that could lead to degradation of the termination. Moreover, surface temperature rise of 17°C could reduce the allowable ampacity of the cable conductor, reduce the short circuit levels, and reduce the feeder loading limits. The field-dependent electrical conductivity ($\sigma(E, T)$), permittivity (ε), and the temperature dependencies of ($\sigma(E, T)$ and ε) have strong impact to degrade the electrical and thermal properties of the termination due to stress from

the non-sinusoidal distorted voltage waveform. In order to minimize the surface temperature rise from the hotspot and electrical stress enhancement that eventually lead to insulation degradation and failure, the following recommendations are made for a suitable SG design for a termination to handle the severe voltage stress:

1. Apply the capacitively graded termination in the grid where the distortion levels are low. Under the increased total harmonic distortion levels and HF components, resistively grading with higher degree of nonlinearity (achieved through the use of ZnO filler) is beneficial.

2. The utilities could take preventive maintenance on medium voltage power cable accessories to prevent the termination failure before it actually occurs.

3. Researchers could focus to resolve and minimize the rising power quality issues when the distribution generations are operated, improve the power electronic converters, and provide cost-effective harmonic filter solutions for harmonic mitigation.

Acknowledgements

Dedication

To my Guru Pramukh Swami Maharaj.

Table of Contents

List of Figures

List of Tables

Chapter 1

Introduction

This chapter provides an overview of the power quality issues on the changing power system network. Important power quality issues of harmonics and system resonance are described along with the issues created from the power electronic drives on power system insulation systems. The effects of the contaminated power on the insulation systems are highlighted. The research objective and thesis outline are provided at the end.

1.1 Overview

In an effort to make the power system network more reliable and sustainable, there have been ongoing changes in the existing grid. New design practices and operating techniques are being developed to continually improve the reliability of the grid. Emerging smart grid technologies are accelerating the transformation of the current distribution system into the smart distribution system of the future. The notion of the smart grid is to develop tools and applications to be integrated with today's technologies for resilience of the distribution system and to achieve a self-healing grid. The smart grid vision implies a huge increase in the number of entities that will communicate and interact in distribution systems and bulk power operation. With the increasing energy demand, grid modernization is ongoing and expected to rise with the integration of cost-effective sources of renewable energy or distribution generation (DG). The renewable plant owners are being provided with financial incentives to allow great investment in renewable development and offer their products to a larger market. Since generation of wind and solar power, for instance, is intermittent and variable nature, integrating large amounts of wind and solar power can lead to a degradation of network power quality and stability issues.

Since power electronic devices are a key component of the DG, increased switching power electronic devices can create many issues pertaining to voltage waveform quality, such as substantial amount of amplified harmonics injection resulting from the resonance condition. Such power quality issues can induce severe stresses on the electrical insulation system of various power system components. The increased power quality issues on the grid means significantly higher stresses on the electrical insulation system of power system components including cable terminations. The reliability of the insulation system is one of the essential concerns which are linked to the changing operating environment.

1

The sole purpose of the cable termination through the surface stress relief system is to ease the electric field intensity around the end of the insulation shield at the cable end. An ideal stress grading (SG) system would produce a uniform distribution of electric field. The SG system plays a crucial role in the reliability of the insulation system. Even a small malfunction in the SG system could lead to the breakdown of the main insulation. Developing electrical stresses is generally manifested by surface discharges in the vicinity or hot spots in the SG system and/or in the cable insulation shield layer. The presence of enhanced stresses could significantly increase the threat to the SG system of the cable termination. In this work, cable terminations were experimentally shown to degrade and fail under the poor power quality.

The following sections provide background of some common power quality issues and their causes. An overview is provided on the insulation integrity of various power system components under the influence of poor power quality.

1.2 Power Quality Issues

Power quality is a term used in a different context within the power system industry. From the utility perspective, power quality refers to the distribution system reliability, while power quality for the load equipment manufacturers means certain characteristics of the power supply that enable the equipment to function in their intended manner. From the perspective of insulation system manufacturers, power quality refers to the certain electrical properties that enable the insulation system to last long without significant loss of life. The power quality issue is ultimately the one that is consumer-focused because the issue is linked with the huge economic value.

The IEEE Standard Dictionary of Electrical and Electronics Terms defines power quality as "the concept of powering and grounding sensitive electronic equipment in a manner that is suitable to the operation of that equipment [1]." There are numerous standards and guidelines for power quality. IEEE Std. 141-1995, IEEE Std. 519-1992, IEEE Std. 1159-2009, IEEE Std. 1100-1999, IEEE Std. 1346-1998, IEEE Std. 446-1995, IEEE Std. P1564, and IEEE 1250-1995 are some of the significant ones that are often referenced. Many such standards provide definitions and indices of power quality, which are often application specific and pertain to various electrical engineering disciplines.

IEEE Std. 1159-2009 has classified the power quality issues for the single-phase and polyphase AC power systems, which are charted in Figure 1.1. IEEE Std. 1159-2009 explains that the main reason for developing different categories is that there are different ways to solve power quality issues depending on the particular variation that is of concern [2].

2
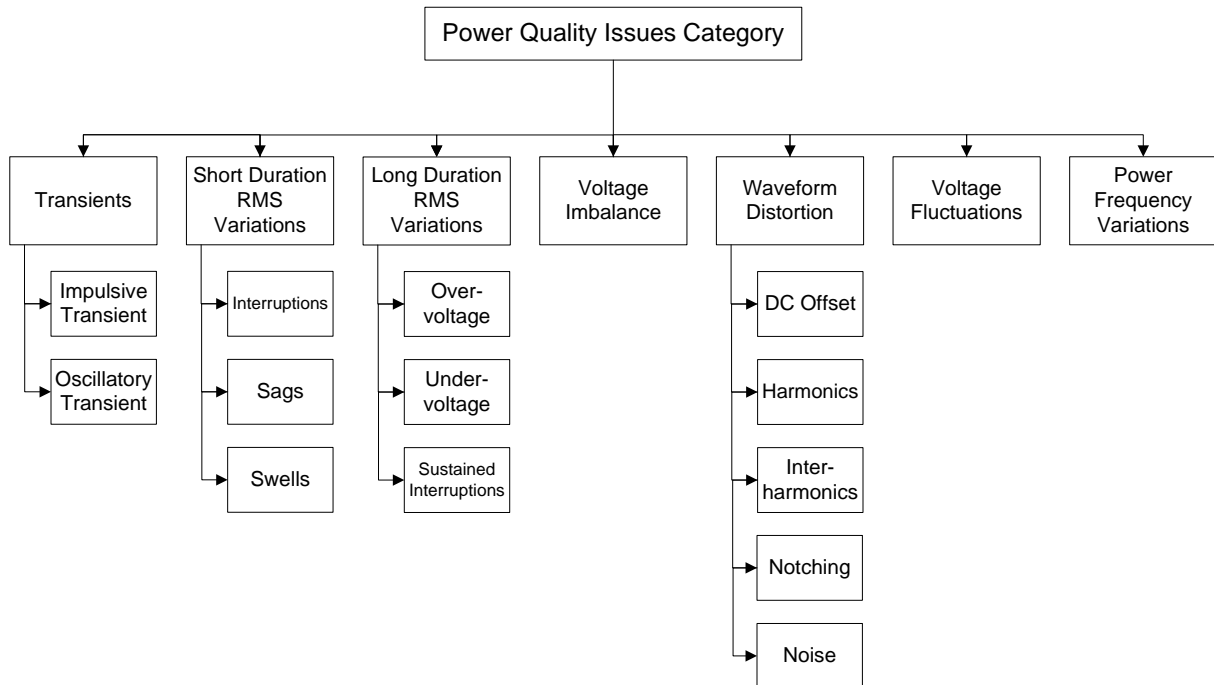
Figure 1.1: Framework of power quality issues classified in IEEE Std. 1159-2009

The source of the power quality related issue in the utility distribution system is the distribution system, customer load, or a combination of both. Traditionally, the North American electric power systems have had very good power quality. However, the power quality is deteriorating due to proliferation of different non-linear loads such as rectifiers, cycloconverters, and large variable-frequency drive (VFD) type loads [3-5]. Moreover, the implementation of DG in the distribution system has grown significantly in recent years. The integration of DG on the distribution system network is expected to increase in North America because of cost-effective sources of sustainable energy with incentives driven by reduced emissions, government policy and promotional programs such as Ontario's Feed-in Tariff Program and United States' Federal Renewable Energy Grant Program [6-7].

The increased use of non-linear power electronic devices linking the modern non-linear loads and distributed generation to the existing grid can also create many issues pertaining to power quality such as harmonic contamination, network resonance based harmonic amplification, complex repetitive transients, voltage sags, overvoltages, power frequency variations, etc. [4-5, 8-12]. To this day, most of the existing load is still linear and the non-linear devices are small; however, the larger linear loads are increasingly being replaced by multiple smaller non-linear loads in addition to integration of the power-electronics-based distributed generation [4, 9, 12-17]. The resulting increment of non-linear devices on these systems

threatens to deteriorate the quality of this power. Besides, there is always a possibility for the local power quality issues to travel through the distribution network and affect other customers.

There is research and development taking place in several areas such as (1) improving the active power filters (APF) with their respective control strategies [18-19], (2) improving the control operation of the Distribution STATic Synchronous COMpensator (DSTATCOM) [20-21], (3) improving the existing distributed generation interface [13, 22], (4) increasing the distributed generation penetration [23-24], (5) improving the network architecture [25], and potentially many others to improve the grid power quality and to minimize the growing power quality issues. The research work in the above mentioned area directly or indirectly intends to limit the grid power quality issues to the permissible limits as stated in the Std. IEEE-519. The decades-old power quality issue is expected to see even more contamination in power quality [5, 9, 12, 26]. With the explosive growth of the non-linear power electronic components and increasing penetration of the DGs having unconventional characteristics, the power system industry is currently in a somewhat challenging and unique period. Several crucial power quality issues are examined broadly in the following sub-sections.

1.2.1 Harmonic Component Related Issues

Originally, a power system network was designed to flow power in one direction, i.e. power would flow from the generator terminal to the load terminal. In this conventional design, power comes from the reliable generators, which are far away from the load and are able to produce large amounts of electricity. These include nuclear power plants, hydro stations, and fossil-fuel power stations. However, there are losses involved in this procedure due to generators being long distance away from the load.

The conventional power system network is experiencing changes with the integration of the DGs including wind turbines, photovoltaic solar panels, fuel cells, small hydro, and biomass plants. Since these types of generators depend a lot on geographical locations, they are spread all around the power system grid. The DGs are typically connected near the load on the distribution network to minimize the line losses. They challenge conventional design by creating power flow that goes both way, downstream as well as upstream. Moreover, DGs would be connected on the feeder with the power electronic converter and seldom by using the rotating mechanisms such as synchronous and induction generator. Harmonic is one of the serious power quality issues because the distortions in the waveforms are continuous. The voltage and current harmonics can produce various problems in the power system such as conductor overheating, equipment heating, equipment malfunction, dielectric failure, communication interference,

false operation and trips of fuses and circuit breakers, utility meter measurement errors, and operation instability [27].

Power electronic converters connected with the DG function to convert DC power or unregulated AC power into regulated AC power. An AC/DC converter and an inverter are used in various combinations depending on the type of DG to carry power back to the power grid. A typical DG would at least include a three-phase converter that interfaces the DG to the distribution network. An example of a grid connected Photovoltaic (PV) Solar System with the three-phase power electronic converter is shown in Figure 1.2.
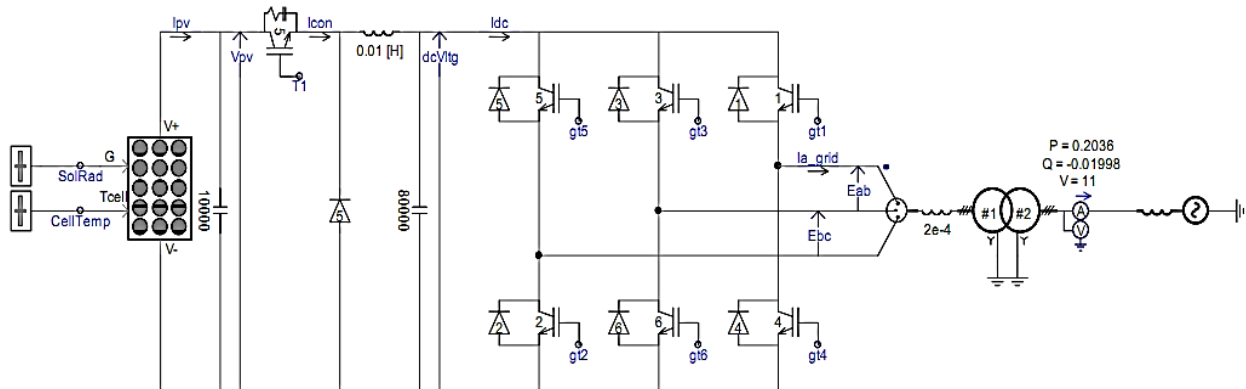
Figure 1.2: Schematic of the three-phase converter interfacing 250kW PV solar system to the distribution network [28]

Power electronic converters with different topologies and operating at different switching frequencies up to 10 kHz would inject a wide range of voltage and current harmonics into the network. Harmonics exist in the power system due to non-linear loads. Typical examples of non-linear loads include switch-mode power supplies, UPS units, electric arc furnaces, static VAR compensators, inverters, DC converters, AC or DC motor drives, and ferromagnetic devices [29]. The term 'non-linear' is used for such types of loads that draw current from the power source having a dissimilar shape to that of the applied voltage. The distorted current drawn by the non-linear load passes through the line impedance between the system source and the non-linear load as shown in Figure 1.3.
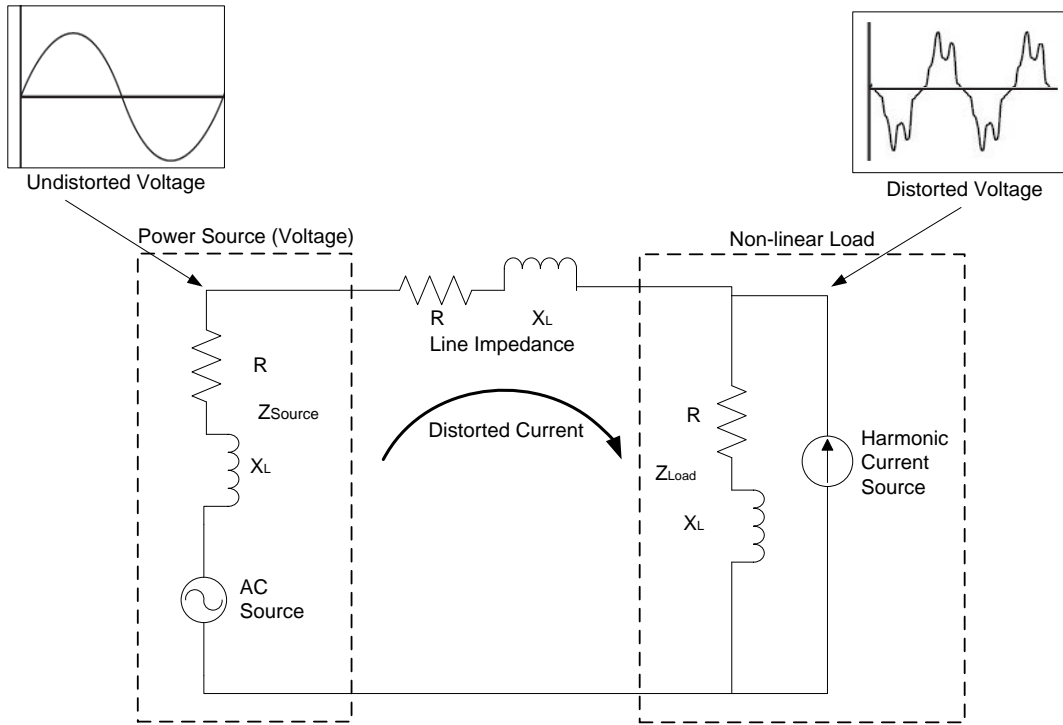
Figure 1.3: Distorted-current inducing distorted voltage through the non-linear load

When this distorted current runs around in the system and reflects through the system impedance, voltage drop occurs or harmonic voltage distortion is produced. To illustrate this point, a simple line diagram is shown in Figure 1.4 that comprises of source voltage (u) and source impedance (L_N). The harmonic current (i_N) passing through the source impedance (L_N) produces a voltage drop (U_L) according to the formula:

$$U_L = L_N \frac{\mathrm{d}i_N}{\mathrm{dt}} \tag{1.1}$$
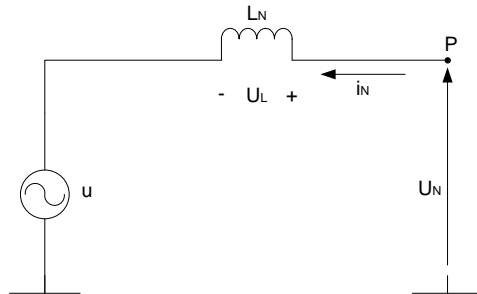
Figure 1.4: Simple line diagram illustrating production of voltage distortion

6

The distortion of the supply voltage waveform is simply a voltage drop across the source impedance (U_L) minus the induced voltage (u). The voltage drop occurs for each harmonic frequency based on Ohm's Law ($V_h = I_h \times Z_h$). The vector sum of the entire voltage drop is the total voltage distortion. Equation 1.1 indicates that the magnitude of the voltage drop depends on the system impedance and current at each harmonic frequency. In other words, the voltage can increase significantly if a large portion of the load becomes non-linear (i.e. if harmonic current increases).

In a power system network, the power frequency (PF) waveform has several additional waveforms superimposed upon it, creating multiple frequencies within the PF waveform. The contribution of all the harmonic frequencies to the fundamental is defined as total harmonic distortion (THD) [27]. The resulting waveforms of the current and voltage of non-linear loads are non-sinusoidal in nature and have high degree of distortions. The production of the characteristic current harmonics is determined by the pulse number, which is given by the following equation.

$$h = (k \times q) \pm 1 \tag{1.2}$$

In equation 1.2, h is the harmonic number or the integer multiple of the fundamental, k is any positive integer, and q is the pulse number of the converter. A 6-pulse bridge or a three-phase full wave diode rectifier bridge will exhibit harmonics at 5th, 7th, 11th, 13th, 17th, 19th, and other such multiples of the fundamental. A three-wire distribution system with mixed linear and non-linear loads generally includes harmonic currents in the order of 5th, 7th, 11th, 13th, etc. A four-wire distribution with mixed linear and non-linear loads mainly includes 3rd harmonic and other triplets in the neutral wire [30]. Pulse width modulation (PWM) technique based voltage source converters (VSC) also exhibit triplet harmonics along with other power quality issues, which are described in Section 1.2.3. Some additional sources of harmonics, though negligible, are rotating machines and transformers when in saturation mode.

The problem with harmonics in the industry has existed for such a long time and has already been addressed to prevent the system from destabilizing itself. There are some solutions available in the industry, which have been in operation to mitigate the harmonic issues. The harmonic mitigation may be performed using the integral part of non-linear equipment, such as an AC line reactor for PWM drive, or using a discrete item of mitigation equipment, such as an active power filter connected to the switchboard [30]. Common harmonic mitigation solutions are also available for a group of non-linear equipment. Current industry practice uses neutral current eliminators and phase shift systems, standard AC line and DC bus reactors, duplex reactors, passive LC filters, multi-pulse (phase shifting), quasi-multi-phase (phase staggering), active filters, and active front ends [30].

In reality, power systems are able to absorb a considerable amount of current distortion [31]. The THD levels on a power system network have been low over the years and meeting the levels recommended in Std. IEEE-519 1992. Std. IEEE-519 1992 is a standard developed by IEEE for acceptable voltage distortion to distribution system in order to address harmonic related concerns and to control them. The standard is called, "Recommended Practices and Requirements for Harmonics Control in Electric Power Systems," which was developed in 1981 and revised again in 1992. This document is well known in the industry by the name of IEEE-519 and has been widely applied in establishing needed harmonic correction throughout the industry.

The IEEE-519 suggests that since harmonics voltages are generated by the passage of harmonics currents through distribution system impedances, they can be controlled by the currents or system impedances within the industrial facility [32]. To achieve this, IEEE 519 document defines the level of harmonic currents that a customer can inject into the distribution system. The means to measure the current distortion level is the Total Demand Distortion (TDD). The definition of TDD according to IEEE 519-1992 is "the total root-sum-square harmonic current distortion, in percent of the maximum demand load current." TDD, not THD, serves as the basis for the practices and procedures in IEEE 519-1992. TDD is only provided for odd harmonics because even harmonics do not contribute much to the total distortion. These values are explicitly shown below in Table 1.1, where limit is described from the ratio of short circuit current (I_{SC}) and load current (I_L).

Table 1.1: Current distortion limits for 120 V to 69 kV Utility Distribution System as defined in IEEE 519-1992 [27]

I_{SC}/I_L	Maximum Harmonic Current Distortion in % of I_L Individual Harmonic Order (Odd Harmonics)[1,2]					TDD
	<11	$11 \leq h \leq 17$	$17 \leq h \leq 23$	$23 \leq h \leq 35$	$35 \leq h$	
<20[3]	4.0	2.0	1.5	.6	.3	5.0
20 < 50	7.0	3.5	2.5	1.0	.5	8.0
50 < 100	10.0	4.5	4.0	1.5	.7	12.0
100 < 1000	12.0	5.5	5.0	2.0	1.0	15.0
>1000	15.0	7.0	6.0	2.5	1.4	20.0

[1] Even harmonics are limited to 25% of the odd harmonic limits above.

[2] Current distortions that result in a DC offset, e.g., half-wave converters, are not allowed.

[3] All power generation equipment is limited to these values of current distortion, regardless of actual I_{SC}/I_L, where I_{SC} = maximum short circuit current at PCC and I_L = maximum demand load current (fundamental frequency component) at PCC.

For example, if at a Point of Common Coupling (PCC) the I_{SC}/I_L is less than 20, then the maximum TDD allowed is 5% which includes most of the contribution from harmonics under the 11th order. As the I_{SC}/I_L ratio increases, the allowable TDD increases. Even a small current and the resulting low TDD can have a high THD which could be of a significant threat to the distribution system. IEEE 519-1992 also defines the voltage distortion limits as listed in Table 1.2, which is another requirement check for the customers and utilities in addition to the TDD. The IEEE 519-1992 standard has been very helpful in realizing the required levels of harmonics and loading conditions.

Table 1.2: Individual Voltage distortion limits and THD limits as defined in IEEE 519-1992 [27,

Bus Voltage at PCC	Individual Voltage Distortion (%)	Total Harmonic Voltage Distortion THD (%)[1]
69 kV and below	3.0	5.0
69.0001 kV through 161 kV	1.5	2.5
161.001 kV and above	1.0	1.5

[4] High voltage systems can have up to 2.0% THD where the cause is an HVDC terminal that will attenuate by the time it is tapped for a user.

The severity of the harmonic issue is such that the issue has only been minimized over the years but not completely eliminated from the system. The best engineered hybrid harmonic mitigation techniques can significantly attenuate the harmonic components but cannot completely cancel out every harmonic component. A steady-state distortion of waveforms would still result and high harmonic impedance would be present at the DG three-phase converter, for instance. The collective effect of the increasing non-linear loads with the integration of DGs and FACTS devices have the potential to increase the THD levels specified in IEEE-519 and impact the distribution system. The problems associated with the increasing harmonics can get more complex since the harmonic components can add or subtract.

Under the influence of non-linear loads, New Zealand's low voltage distribution network is already seeing a THD level close to the limit of 5% and is expecting it to increase beyond 5% [5]. The PSCAD/EMTDC simulation results by Kadir, et al. showed that the THD exceeds its limit of 5% when four DFIG-based DG units are installed in the distribution system [33]. A 5 MW photovoltaic (PV) system connected to the 20 kV line of the rural distribution grid in the southwest of Spain exceeded the TDD limits set by IEEE-519 [34]. There are potentially many other distribution networks around the globe which are continuously exceeding the THD and TDD limits resulting from the increasing non-linear loads. Hence, there lies ahead a serious challenge for the North American power system industry to

comply with the IEEE-519-1992 recommended practices and to control the industrial system designs with the threat of increasing current and voltage distortion levels.

1.2.2 System Resonance Related Issues

The harmonics related issue is generally thought to be a harmonic injection in the network. Another severe issue is that of the harmonic resonance where certain harmonic currents may amplify under the resonance phenomenon. Harmonic resonance is not present when the system is operating under the fundamental frequency during which the inductance of the system is much lower compared to the system capacitance [35]. When harmonics are present, the impedances in the system change, which in turn produce resonance conditions at some buses. There is always a potential of the presence of amplified harmonic components in the power network grid when the resonant frequencies align with the harmonic frequencies that are being injected, for instance, by the power electronic converter of the DG. At the resonance condition by any bus, the harmonic current injection into the system would see the overvoltage condition and the amplification of current.

Resonance can be classified into two categories: parallel resonance and series resonance. Parallel resonance is related to high impedance levels at resonance frequency, which results in high harmonic currents injection and heavy voltage distortion [36]. A simplified parallel resonance model is shown in Figure 1.5, where the capacitive and inductive components are in a parallel combination.
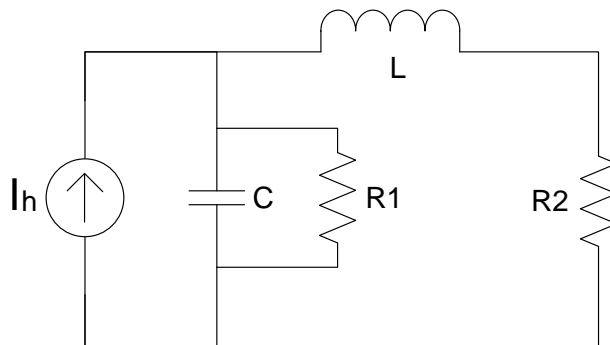
Figure 1.5: Equivalent circuit for parallel resonance including resistances [36]

Upon neglecting the resistance, the impedance seen by the harmonic source is given by [36]:

$$Z(\omega) = \frac{j\omega L}{1 - \omega^2 LC} \tag{1.3}$$

10

$$\text{where, } \omega = h \times 2\pi f_o \tag{1.4}$$

At the resonance frequency, f_{rp}, the impedance becomes infinite (i.e. $Z(\omega) \rightarrow \infty$)

$$f_{rp} = \frac{1}{2\pi \sqrt{LC}} \tag{1.5}$$

Since the harmonic source is mainly a current source, high harmonic voltage would be seen, and the harmonic current would be amplified to an infinite value in the capacitive branch.

$$\frac{I_{Cap}}{I_h} = \left| 1 - \frac{1}{1 - h^2 \omega^2 LC} \right| \tag{1.6}$$

But the impedance cannot be infinite in a real system because some resistance will always be present. Even though the resistances do not influence the resonance frequency, resistance will still be the main determining factor for the impedance and amplification close to the resonance frequency.

Series resonance, on the other hand, is opposite to parallel resonance in that it leads to low impedance at the resonance frequency causing high current and a high voltage distortion even in a location where there is little or no harmonic emission [36]. An equivalent circuit of series resonance is shown in Figure 1.6
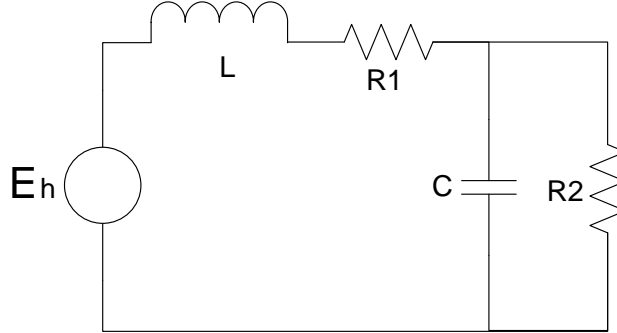
Figure 1.6: Equivalent circuit for series resonance including resistances [36]

Similar to parallel resonance, the resonance frequency, f_{rs}, is:

$$f_{rs} = \frac{1}{2\pi \sqrt{LC}} \tag{1.7}$$

When the resistances are taken into account, the resonance order will not change significantly, but the amplification of the voltage distortion will become finite [36]. Zheng, et al. [36] studied the impact of a grid-connected wind farm on the parallel harmonic resonance. The authors accurately modeled various

power components using the power-system analysis simulation software DIgSILENT PowerFactory 14.0 and MATLAB in order to calculate the resonance frequency and amplitude of the impedance. The large system under test used 100 wind turbines with a rated power of 2 MW and terminal voltage of 690 V each, and 100 turbine transformer and underground cables of 34.5 kV, which are used to connect wind turbines to the MV substation. By processing the frequency sweep, the resonance order was obtained as shown in Figure 1.7.
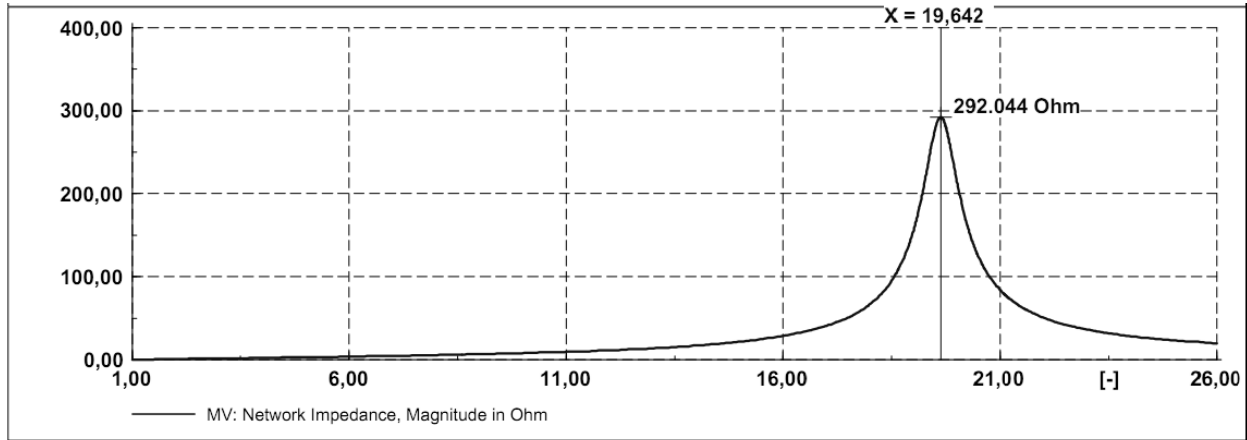
(a) $Q_{cap} = 0M$ var
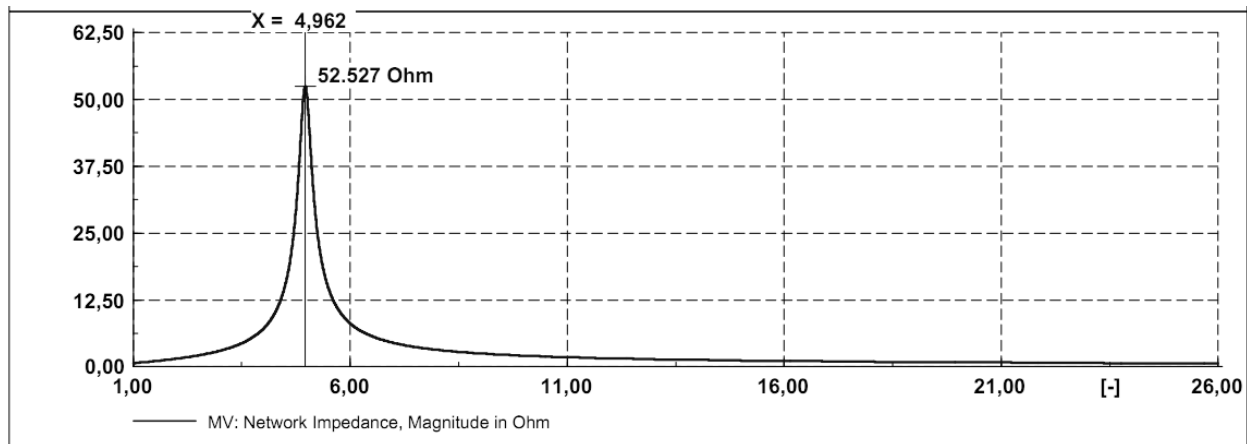
(b) $Q_{cap} = 72M$ var

Figure 1.7: Results of frequency sweep at the MV bus (a) without and (b) with capacitance [36]

The simulation results in Figure 1.7 indicate that the added capacitive component from the wind farm connected to capacitor banks (Q_{cap} = 72 MVar) changes the resonance frequencies of the existing harmonic resonance. Resonance occurring around harmonic order 33 (1.98 kHz) without a capacitor bank

is shifted down to harmonic order 7 (420 Hz) when all 72 MVar of capacitor bank is connected. The 5th harmonic is amplified 1.8 times. Many such low-order harmonic components would amplify and could cause THD to exceed beyond 5% and breach Std. IEEE 519-1992.

The distribution feeder is generally equipped with the capacitor bank for power factor correction purposes, adding to the system capacitance and contributing to the resonance of the system. The capacitor banks are also connected at the terminal of the DGs to meet the reactive power requirements laid by the utilities. The reactive power compensation would depend on the operating condition of the DGs. This means that system capacitance would vary and so would the feeder resonant points. The introduction of DGs on the distribution feeder can have multiple and shifting resonance peaks. This is observed in the simulation performed by Patel, et al. in [37]. The authors have carried out a simulation on the actual Hydro One distribution feeder system to investigate the impact of Wind Turbine Generators (WTGs) connections on resonant modes of system impedance and THD in the network. The simulation results in Figure 1.8 show that resonant frequencies change after subsequent switching of the WTGs. The first resonance frequency shifts towards the 7th harmonic frequency and the second resonance frequency shifts towards the 17th harmonic because the WTGs are added to the distribution feeder system. The THD results indicate that THD of 7% in voltage and THD of 38.93% in current would occur as the worst case scenario when two WTGs are connected to the system.
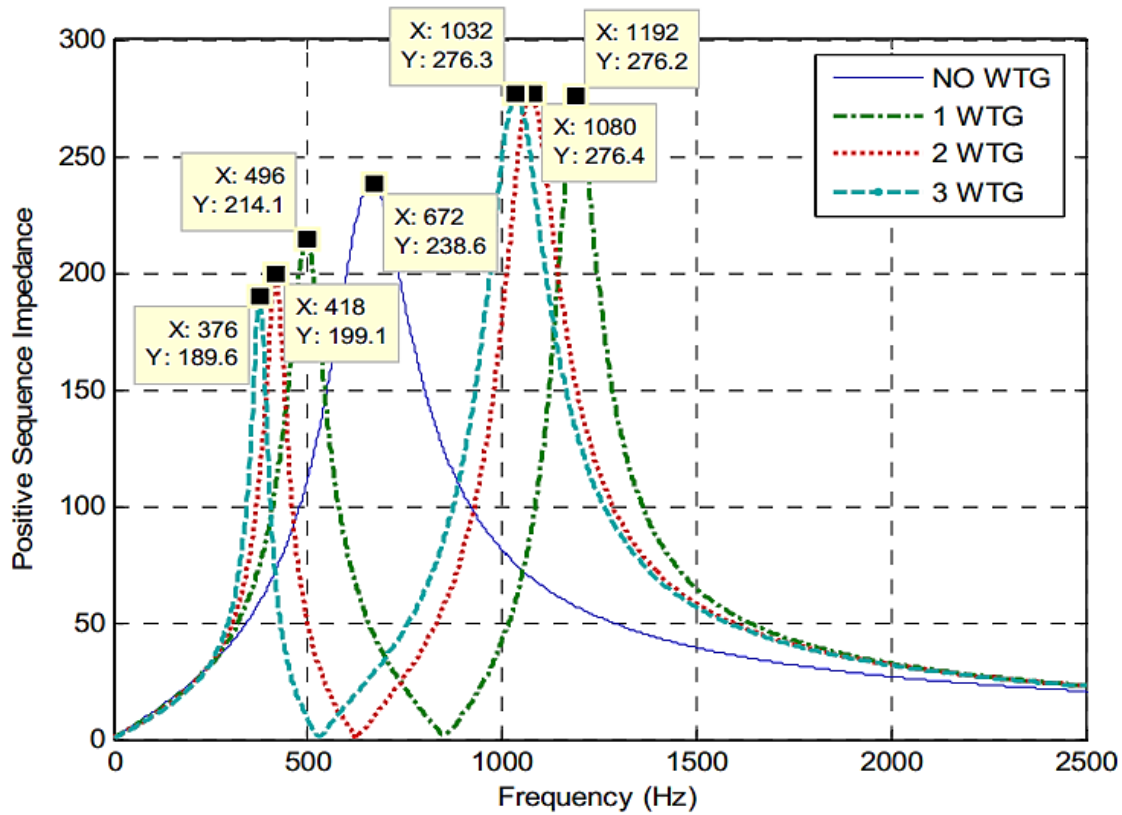
Figure 1.8: Frequency sweep indicating resonance dependence on the operating conditions of WTGs [37]

A severe general concern is at the 5th and 7th harmonics because these frequencies are normally present in the power system network. Harmonic resonance occurring at around 5th and 7th harmonic components would cause severe amplification of the harmonic voltage distortion. A certain combination of capacitive and inductive components would shift the floating resonance plot. In the past when DGs were not connected to the distribution feeder, the feeder resonant frequencies were known for which appropriate precautions could be taken. However, the distribution system is becoming an increasingly active system with the smart-grid initiatives and unpredictable operation of various DGs on the distribution feeders in several different combinations. As a result, the distribution system capacitance and inductance are very difficult to predict. The resonant points on feeders are thus virtually impossible to identify and could cause the system to resonant at several anonymous frequencies depending on a feeder's operating condition. Appropriate filters or converter switching could be designed to mitigate the resonant frequency components but continuously changing resonant frequencies makes it impractical. The unacceptable THD could significantly enhance the electrical stresses on the insulation materials of the distribution system.

14

1.2.3 PWM-VSCs Related Issues

The role of a power electronic converter is becoming more significant in the power system grid. They can be found almost everywhere functioning at the renewable energy plants primarily influenced by the availability of high power semiconductor devices. In the late 1970s and early 1980s, AC VFDs were developed in various forms. In the mid 1980s, AC drive technologies started to appear, most notably in the form of the PWM type inverters, which revolutionized the operation and control of the machines. The newer solid state drives provided several advantages over the older methods of speed control including better reliability, reduced downtime, improved overall system efficiency, improved power factor, reduced harmonic current levels, soft starting and over-speed capabilities, and improved product quality [38-39].

In high power range, the power electronic converters can be classified into two categories: voltage source converters (VSC) and current source converters (CSC). The differences in these two types of converters are their mode of operation and type of DC-link energy storage. DC-link capacitor is used for VSC, and DC-link inductor is used for CSC. The VSC has more advantages over the current source converter such as better efficiency, faster transient response, lighter weight, lower price, and greater flexibility of operation with either closed-loop or open-loop control [40-43]; therefore, use of VSC has become dominant in the industry. In particular, PWM-based VSC is a dominant method in the industry and is used to supply electrical power to motors.

The availability of high power semiconductor switches and growing power demand of the semiconductor switches have facilitated the trend of increasing the voltage ratings of the PWM-VSC. Now it is possible to for VSC to operate at 13.8 kV for motor drives, while VSC for power system applications can be at higher voltages [44]. Two main semiconductor switches that can withstand high power are the insulated gate bipolar transistor (IGBT) and the integrated gate commutated thyristor (IGCT). Both of these power electronic devices are in use in high power-high voltage PWM-VSC; IGBT is more common primarily due to its advantage of higher frequency capabilities, low cost, and more mature technology [45-46]. Today, IGBTs up to current rating of 3.5 kA and switching frequency of as high as 10 kHz are available in the industry for 13.8 kV voltage ratings.

The converter scheme or topology is one important design factor for a VSC. There are various topologies for PWM-VSC depending on how the semiconductor switches are connected. A simple, cost-effective, and reliable PWM-VSC topology is the 2-Level VSC which is very common for low voltage power applications [47-48]. A 2-Level VSC is a three-phase twelve-pulse converter bridge having two semiconductor switches on each phase leg. The reason for calling such a converter "2-Level" is because

each of the three terminals on the AC side can assume two voltage levels, i.e. +VDC and –VDC with respect to n point. Two-way power flow can occur with this topology. Though 2-Level VSC is also common for medium and high voltage power applications [49], there is one drawback each switch of 2-Level VSC has to withstand full DC voltage in the off-state, which demands switches at higher voltage ratings implying very high costs. An alternative approach to overcome this issue is to use multiple switches in series. This approach adds complexity to the design as all the switches in one switching cell need to operate at the same instant with the inclusion of a snubber circuit to divide the voltage equally. The snubber circuits could be very lossy in nature especially for high power applications and could increase the overall operational cost. As a result, for medium and high voltage applications, 3-Level or other multi-level topologies are preferred though there is no dominant topology. A 3-Level VSC is a three-phase twelve-pulse converter bridge having four semiconductor switches on each phase leg [50]. The multi-level VSC could be complex to implement and expensive compared to the 2-Level SVC, but it provides improved power quality, reduced operational losses, and eliminates the need for switches of high voltage ratings.

PWM-VSCs are facing a challenging situation in balancing between the power size and power quality requirements at the PCC. Even though there have been huge improvements in the semiconductor devices in the past decade, respecting the power quality requirements imposed by the international standards are challenging. The harmonics and harmonic resonance related issues result from the solid state drives which are already discussed in section 1.2.1 and 1.2.2. In addition, there are output voltage waveform related issues from the operation of PWM-VSC. There are certainly improvements in the controllability of the output voltage waveform in terms of amplitude and frequency, and reduced lower-order harmonics; however, the converter losses have increased due to higher frequencies, high order harmonics were produced, and increased levels of electro-magnetic interference (EMI) could be seen [30]. The major problems associated with the PWM-VSC output voltage waveform are the pulse rise-time that causes high $\frac{dv}{dt}$ stresses, the pulse repetition frequency, and the overvoltage that causes large overshoots [51-53]. Several harmonic components at well-defined frequencies and magnitudes are generated from various PWM-VSC schemes.

These days, there are numerous solutions available to supress the transient overvoltage and harmonic components. Common practices are to include a passive filter at the inverter side or use motor terminal filters to mitigate the harmonic components and reduce the rise time of the voltage pulses. These filters are imperfect and they normally slow down the rise time and the overshoot; however, they do not have

any particular effect on the repetition frequency of the fast pulses; they also add to the cost, weight, and size [54].

1.3 Effects of Distorted Voltage Waveform on the Insulation Material

The insulation system is vulnerable to the steady state power quality issues. Poor power quality can have adverse effects on the generators, induction motors, transformers, cables, and cable accessories. The effect of harmonic components and harmonic resonance condition is significant to generators because their source impedance is typically three to four times that of a utility transformer. Voltage and current harmonics cause increased machine heating that is caused by copper and iron losses, both frequency dependent. Transformer losses are heavily dependent on the harmonic current levels and load losses, which significantly rise at harmonic frequencies when transformers supply non-linear current. The harmonic current components in transformers cause an increase in core losses. The losses in AC induction motors caused by harmonic distortion are very similar to that of the losses in generators and transformers. Copper losses and iron losses in stator windings, rotor circuit and rotor laminations dissipate heat in the induction motor. Cable losses, dissipated as heat, are harmonic current dependent due to their "skin effect".

Copper losses are $I_{rms}^2 R$ losses caused by the current passing through the winding resistance and are influenced by a phenomenon termed "skin effect". The skin effect theory refers to the tendency of current to flow near the outer region of the conductor. At fundamental power frequency, the skin effect is negligible and has uniform current distribution across the conductor. At higher frequencies, such as at harmonic frequencies, skin effect is significant and substantially reduces the effective cross sectional area of the cable's conductor and increases the resistance. As a result, $I_{rms}^2 R$ copper losses increases at harmonic frequencies. Iron losses can be divided in two different types: (1) hysteresis losses and (2) eddy current losses. Hysteresis losses occur by power consumed from the non-linearity of the generator or transformer flux density/magnetization force curve. Generator or transformer's flux density causes reversal in the core magnetic every time the current changes polarity, which occurs, for instance, every 120 times in a second for 60 Hz supplies. At harmonic frequencies, more rapid reversal would occur. Hence, hysteresis losses would increase at harmonic frequencies. Eddy current losses result from the current circulation in the iron core, winding, and other parts, which are induced by the stray magnetic fields around the turns in the windings. Eddy currents are proportional to the square of the frequencies. Hence, at harmonic frequencies, eddy current would rise significantly [30].

The industry is well aware of these losses in the machines, transformers, cables, and cable accessories. Even the newer equipment designs that are developed with great precautions have seen early failures due to dielectric heating, i.e., temperature rise brought on by the power developed in a dielectric material due to its dielectric losses. In 2009, Sonerud, et al. [55] associated dielectric heating with the highly distorted voltage waveforms. The study is distinct because the authors analytically proposed a modified power loss equation that incorporates the effects of voltage harmonics and have identified voltage distortion to potentially add to the power loss of the solid dielectric material.

On the other hand, the fast pulse drives such as PWM-VSC are known to have adverse effects on the machine insulation system. There are a number of cases where fast switching has produced complex transients and severely stressed the motor insulation, which is designed to operate at 50 or 60 Hz. Some of the issues include premature insulation and mechanical (bearing) failure, electromagnetic interference, acoustic noise, and torsion vibration. The use of PWM-VSCs has reported a variety of motor failures as well as motor side challenges during the early stages of using these drives. The nature of the PWM waveform is such that high peak voltages of short durations are produced, which create stresses that cause motor insulation to deteriorate and fail [52, 56-59]. High $\frac{dv}{dt}$ or short rise time is of concern because it causes the voltage peaks to be unevenly distributed across the motor windings. Each voltage peak has a potential to cause a small breakdown called a partial discharge (PD) in any air-filled voids in the insulation material. Repeated PD breakdowns have the potential to gradually destroy the insulation. So the rate of deterioration is greater at higher frequencies and can reduce the insulation life significantly. The added stresses on the insulation systems from the PWM-SVCs could result in Joule and dielectric heating, space charge accumulation, and surface discharge activities, along with the PD, all of which lead to accelerated insulation degradation [60].

Experimental work and industry experience have shown the adverse effects of the contaminated power quality on various insulation systems. The life of polymeric electrical insulation is highly influenced by temperature [56]. The high repletion frequency and the high $\frac{dv}{dt}$ create additional joule and dielectric power losses in the insulation system, which manifest as hot spots in the conductive armour tape and the semiconductive stress grading tape and also influence their performance [52, 56-57]. The performance of conductive armour tape and the semiconductive stress grading tape is poor in the presence of highly repetitive steep-front PWM pulses as opposed to the power frequency which can lead to early failure of the coatings. The high repetition rate also has other negative effects on the groundwall, strand, and turn insulation [56].

18

Koltunowicz, et al. [61] experimentally showed that the fast repeating transients reduce the dielectric quality and lifetime of the paper impregnated transformer by a factor of 3.5 when the frequency is varied from 1 kHz to 10 kHz. Degradation of the insulation in terms of tan delta values is higher with repetition frequency of the transient. Koltunowicz, et al. [62] have experimentally showed the aging effect of high frequency voltages on the transformer paper insulation. In their experiment, the authors have shown times to breakdown the impregnated paper insulation under a clean sinusoidal waveform and a 5 kHz 1 kV repetitive impulse superimposed on a 50 Hz sinusoidal waveform. The results have indicated that samples aged under high frequency failed twice as fast as those aged under power frequency.

The negative effects of the amplified high frequency harmonics occurring from the harmonic resonance condition at the Eagle Pass Back-to-Back (B2B) VSC installation led to the failure of cable termination [8]. The experience at the Eagle Pass saw that harmonic frequency around 12 kHz got amplified up to 40% of the fundamental voltage leading to the thermal runaway of the cable termination. Ming, et al. [63] have experimentally analyzed the thermal behaviour of the cable terminations, using frequencies between 5 to 20 kHz in addition to thermal field studies using finite element methods (FEM). The results of the experiment and simulation showed that the severity of the terminations' surface temperature rise under high frequencies voltages, as opposed to power frequency.

1.4 Research Objectives

The study of the deteriorative effects of distorted voltage waveforms on insulation degradation is an emerging research area. A significant amount of the work has already been done on machine insulation under the influence of steep front pulses. However, research in the area of distorted voltage waveform effects on cable accessories is still very limited. This is concerning because the rate of the failures of cable termination and joints are becoming more significant in the cable systems [64-66]. The industry is becoming aware of the growing failures of the cable terminations and joints. This research work extends Banerjee's work [67], who has presented the work on impact of the network resonance based harmonic amplification on the cable termination, to study the stress grading system of the cable termination under the influence of high harmonic and high frequency components. Due to similarity in the stress grading system of the machine and cable termination, the proposition is that the cable termination degradation would occur in a similar fashion to that of the machine insulation degradation.

Standard cable terminations are designed to operate under power frequency in the power system network. Manufacturers estimate the life of cable termination considering their operation under power frequency

19

voltage. So it becomes important to investigate and understand the performance of the cable termination when the voltage waveform is distorted due to the presence of harmonics.

The research objectives set for this work are as follows:

- Design an experimental setup to generate power frequency and distorted voltage waveforms, and utilize a PWM high-voltage generator for testing of the cable terminations with protection provisions.
- Prepare commercial cable terminations with extreme care as to avoid any workmanship errors. Test cable terminations under power frequency, distorted voltage waveforms composed of fundamental and low order harmonics, and PWM voltage waveforms. Investigate the stress grading areas of the cable termination with surface potential distribution and thermal behaviour under pseudo-field conditions.
- Compare and analyze experimental and simulation results.

1.5 Thesis Outline

The thesis is organized accordingly:

- Chapter 1 introduces the power quality issues of the power system network. Harmonic and harmonic resonance issues are explained briefly. In addition, issues of high frequency stresses due to PWM-VSCs are also explained. A brief review is provided on how the power quality issues have affected the electrical insulation system of various power system components.
- Chapter 2 reviews knowledge on power cable system. Semiconductive shield properties are reviewed to show their dependence on the cable insulation integrity. The stress grading systems of cable termination to date are reviewed. Various failure modes of terminations are described.
- Chapter 3 provides the details of the preparation of the cable termination test samples used in this research. This includes commercial MV cable terminations and Haefley^{TM} oil-test terminations.
- Chapter 4 describes the experimental designs along with the experiment procedure sequence. In addition, diagnostic methods are described.
- Chapter 5 provides results obtained from experimental measurements. The experimental and simulation results are also discussed along with their implications to cable termination design for the smart grid environment.

- Chapter 6 provides a brief summary, conclusions, and future work suggestions related to the cable termination study under the non-sinusoidal distorted waveform.

Chapter 2
Cable System

This chapter describes the cable structure and properties of some of the important components of the cable. A relation is explained between the properties of the semiconductive shields and the cable integrity. Cable termination, an important cable accessory, is introduced and its importance in the cable system is explained. An overview of the stress grading system of the cable termination is provided along with the cable termination failure modes.

2.1 Cable Structure

In order to appreciate the cable termination technology and its purpose, an understanding of a power cable structure is important. The power cable has a coaxial structure and consists of several layers whose cross-sectional diagram is shown in Figure 2.1. A typical power cable comprises a current-carrying conductor at line voltage in the interior, an insulation surrounding the conductor, and an outer conductor at earth potential. The conductor material is copper or aluminum that is stranded. The next major layer is the polymeric dielectric insulation. Today, a prevalent global dielectric choice is XLPE (Crosslinked Polyethylene) for cable insulation in high voltage extruded cables rated up to 500 kV. The copper or aluminium neutral wires are wound in many possible ways around the insulation and carry loss or fault currents. The uppermost layer covers the neutral wires with a thermoplastic polyethylene jacket, which provides mechanical support to bind internal layers. The jacket prevents stray currents in the ground from causing corrosion of the neutral conductors.
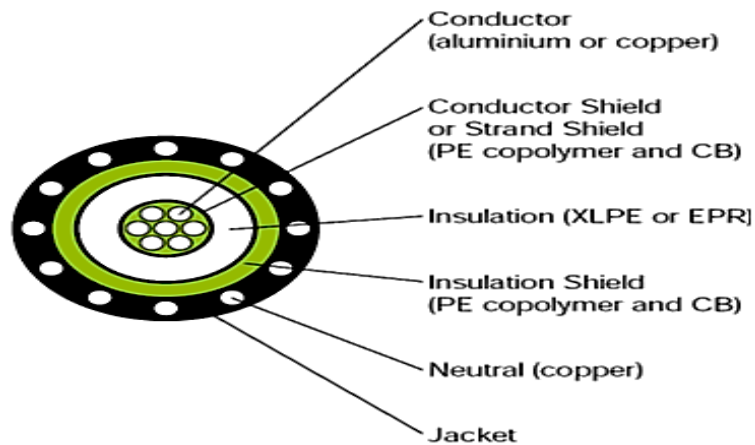
Figure 2.1: Cross-sectional view of the cable consisting of several layers [69]

22

The interfaces between the metal conductors and the polymeric insulation would tend to include protrusions and voids that would cause electrical stress enhancement and premature failure [70]. To overcome this issue, a 'polymer semicon' or 'semiconductive shield' is attached on both sides of the polymer insulation at the interfaces of conductor. As observed from the cross-sectional view of the cable in Figure 2.1, there are two semiconductive shields. The first semicon layer is between the conductor and the inner side of polymer insulation. The second semicon layer is between the outer side of polymer insulation and the concentric neutral conductor. In order to differentiate the two semiconductive shields, the semicon layer on the outer part of the cable is referred to as 'outer semicon', 'core screen', and more commonly as 'insulation shield', while the semicon layer on the inner part of cable is referred to as 'inner semicon', 'conductor screen', 'strand shield', and more commonly as 'conductor shield' [70]. The conductor shield, the insulation, and the insulation shield are co-extruded (triple extrusion process) to ensure the interfaces are smooth and free of contamination. The semiconductive shields would help equalize the electrical stresses over a large area. The next section explains the importance, properties, and performance measure of the semiconductive shield for cable insulation integrity.

2.2 Semiconductive Shield

At the interfaces of the conductors and polymer insulation, protrusions and voids could be present. The outer surface of the conductors may not be perfectly smooth and could have several ridges where the individual conductor strands meet one another. These critical spots will stress the polymeric insulation leading to a premature failure of the cable. Hence, the primary purpose of the semiconductive shields between the metal conductors and polymeric insulation is to reduce electrical stress enhancement with reduced potential gradient and avoid the premature failure of cable. The conductor shield provides a uniform electrical gradient to polymeric insulation so that the long term viability of cables can be ensured, while the insulation shield protects the insulation from the damaging effects of ionization at the outside of insulation surface and provides a permanent group contact around the insulation [71]. In short, semiconductive shields are a key component of power cable insulation system, essentially because they are preventing partial discharge (PD) at the interfaces.

The quality of the semiconductive shields would have an impact on the dielectric loss, space charge dynamics, and cable life. This quality could vary depending on the physical and electrical properties, which also serves to measure its performance.

2.2.1 Semiconductive Shield Properties and Performance Measure

The physical and electrical properties of (1) smoothness, (2) cleanliness, (3) extrusion processability, (4) strippability, (5) conductivity, and (6) ease of dispersion are used to measure the performance of the semiconductive shield.

The **smoothness** is measured in terms of the physical imperfections at the surface of the semicon on the polymeric insulation. Mechanical imperfections protruding from the semicon surface into the polymeric insulation (i.e. protrusions) could amplify electrical stresses to the magnitude that would lead to PD [69]. This would promote localized electrical stress and induce undesired tree growth at the tip of the sharp edge towards the polymeric insulation and may cause premature failure of the cable.

The localized electrical stress enhancement factor, δ, due to protrusions at the semicon surface can be estimated by Mason's equation [72]:

$$\delta \approx \frac{2L}{r \ln\left(1 + \frac{4L}{r}\right)}$$ (2.1)

Here, L is a distance between the protrusion point and plane distance (i.e. the insulation thickness), and r is a radius of the protrusion (assumed to be half hyperboloid). Based on the estimation from Mason's equation, Figure 2.2 illustrates the stress enhancement factors for various cable constructions. The ratio L/r is a governing parameter in stress enhancement. The localized stress enhancement increases as the protrusion tip radius gets smaller or sharper in the same dielectric insulation thickness. The electrical stress enhancement increases approximately ten fold when the protrusion tip radius becomes ten times smaller. Heavy damage to the dielectric insulation could result in the case of a sharp protrusion. With the same protrusion tip radius, stress enhancement at a protrusion tip increases with the insulation thickness. This implies that higher insulation thickness in power cables may not necessarily be useful because thicker insulation can actually cause higher stress enhancement at a protrusion tip, under a specific applied voltage.
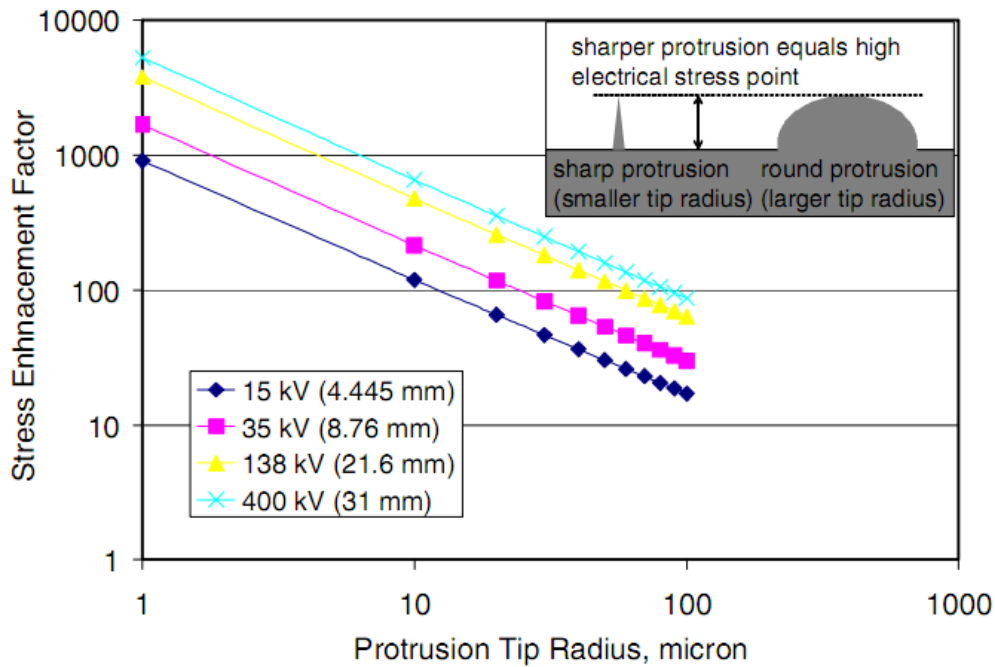
Figure 2.2: Stress enhancement factor for power cables with varied ratings [71]

The **cleanliness** can be measured in terms of level of the ionic impurities present in the semicon compounds. Generally, water-soluble ionic impurities in the semicon compound affect the number and size of water trees developed in the XLPE insulation [73]. These ions have been found to initiate and also accelerate the growth of water trees, as shown in Figure 2.3. The water trees would eventually "convert" to electrical trees through the PD activity [74-75]. The electrical tree conversion is considered as the final breakdown leading to power cable failure in a very short time. The presence of ions in the semicon is highly detrimental to the cable dielectric insulation life. For this reason, water trees are considered a major issue leading to premature cable degradation [76].

One of the processes to measure and evaluate the cleanliness of the semicon is Induction Coupling Plasma (ICP) spectroscopy. Han, et al. [71] has performed elemental analysis using ICP spectroscopy for different types of semiconductive shields, the results of which are provided in Figure 2.4.

Figure 2.3: Accelerated growth of water trees from the conductor shield (left) and insulation shield (right) due to water-soluble ionic impurities [77]
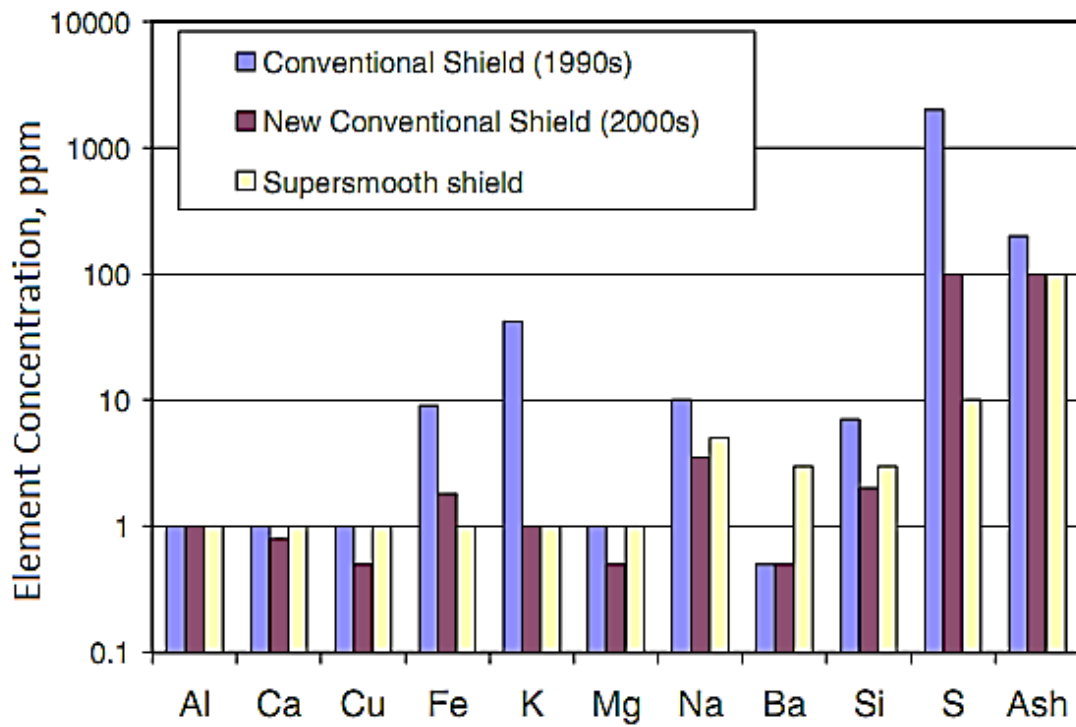
Figure 2.4: Contamination levels of different semiconductive shields [71]

Figure 2.4 compares the ionic impurities level for conventional shield of the 1990s, the new conventional shield of the 2000s, and supersmooth shield. One important observation is that the supersmooth shields and new conventional shields of the 2000s exhibit low level of ionic impurities, resulting in improved cleanliness over the years.

One important requirement for semiconductive shields is **extrusion processability**, which indicates the manufacturing rate of the semiconductive shield. As the rate of cable production increases, the semiconductive shields could pose a limitation in cable processability due to its ever increasing viscosity, which can induce scorch in an extruder [71]. The scorch build-up of a semiconductive shield is an important factor because it can be embedded at the interface with insulation and cause protrusions. There are new conventional shields in process that would tend to address the issue of extrusion processability [78]. The viscosity of the new conventional shield in process would be much lower compared to the former conventional shield to allow higher extrusion processability and reduced scorch build-up.

Strippability can be thought of as the ease of peeling off an insulation shield from the cable. A better strippability is a representation of the least amount of strip force that is required to separate the layers. The criterion is that the insulation shield can strip easily at various installation temperature conditions and for different insulations while minimizing any pick-off residues after peeling off insulation shields on the insulation surface, which may act as electrical stress points [71].

In practicality, the semiconductive shield properties would tend to degrade over time. For example, there may be protrusion appearing due to unexpected physical event which could cause premature failure of the cable. The extruded semicon compound should have suitable physical and electrical properties that offer excellent surface smoothness, low level of ionic impurities, reasonable extrusion processability, ease of strippability, ease of dispersion, and good conductivity.

A semiconductive shield is a layer of extruded polymeric stress-control material which is made up of semi-conductive compounds containing carbon black as conductive agent. The improvement in the semiconductive shields since their introduction in 1960s can be explained by improvements in the carbon blacks in semicon compounds. The improvements in the carbon blacks over the decades has helped achieve longer power cable life and reduced premature failure.

Conductivity and **ease of dispersion** are other important semiconductive shield properties that are dependent on the carbon black of the semicon compounds. Volume resistivity of the semiconductive compounds at equal carbon black loading is used to measure the conductivity. Ease of dispersion

indicates the ease at which the pigment can be wetted with resin and subsequently de-agglomerated [69]. It represents the attractive forces one needs to overcome in order to separate the agglomerates into discrete carbon black aggregates [69].

2.2.2 Impact of Carbon Black on the Physical Properties of Semicon

The material chosen to develop semicon compound is carbon black, which influences semicon properties. Carbon black material is manufactured by the thermal decomposition of various types of hydrocarbons. Carbon black used in semiconductive shields is pure and conductive. In semicon, furnace black and acetylene black have been widely used. Furnace black is produced by partial oxidation of hydrocarbon oil or gas, while acetylene black is produced by continuous thermal decomposition of acetylene gas. Shields based on furnace black are commonly referred as 'conventional shields' and are widely used, while the shields based on acetylene black are commonly referred as 'supersmooth shields' and rarely used. The major breakthrough in semiconductive shield technology in the 1990's was the development of supersmooth semiconductive shields based on acetylene black. By nature of feedstock and reaction conditions, acetylene black has lower grit and ionic impurities levels than furnace black, resulting in smoother surfaces and is cleaner than the conventional semiconductive shields when extruded on cable. However, the quality of electrical grade furnace black has improved over the years in terms of cleanliness and is more cost-effective [71].

Carbon black is filtered in order to obtain conductivity. When carbon black is added into a polymer matrix, carbon black aggregates form a continuous path and becomes a conductive polymer composite. In the tunneling theory, electron flow occurs when the carbon black aggregates are either in contact or separated by less than a percolation distance (critical distance) [79]. In other words, electrons tunnel through the polymer from aggregate to aggregate. In the process when aggregates are getting increasingly closer, the tunneling would occur. This increases the electrical conductivity of the polymer composite. The term 'percolation' is used in this context to describe a point where the polymer composite makes a transition from an insulating to a conducting system [79]. Hence, the percolation behavior of carbon black determines the conduction level in semiconductive shield.

Surface smoothness of a semiconductive shield is affected by carbon black dispersibility and grit from carbon black. [69, 71] Nevertheless, physical cleanliness, polymer gels, contamination from the environment, and mixing technology at the compound manufacturer do affect surface smoothness in addition to carbon black. A special strippable carbon black shows excellent strippability as compared to the conventional conductive black. A carbon black that can enhance the strippability factor is also shown

28

to have helped reduce the formulation cost [69]. There are few macroscopic properties of carbon black such as particle size, aggregate structure, porosity, and surface chemistry that impact the semiconductive shield characteristics [71]. The semicon properties are primarily affected by two properties of the carbon black: particle size and aggregate structure. Table 1 demonstrates how physical and electrical properties of semiconductive shields are affected by two properties of the carbon black.

Table 2.1: Effect of carbon black colloidal properties on physical and electrical properties of semiconductive shields [71]

For a smaller carbon black particle, the viscosity and conductivity of the semicon would be higher and dispersibility would be lower. For a larger carbon black particle, the viscosity and conductivity would be lower but dispersibility would improve, which applied for aggregates as well. Therefore, the selection of properties of carbon black is critical in order to balance the physical and electrical properties of semiconductive shields and to obtain high quality semicon compound. Hence, carbon blacks are given such an importance. Today, carbon blacks with low levels of ions and sulfur with reasonable particle size and reasonable aggregate structure are used in the semicon compounds to help achieve the long life of power cables desired by the power industry [69].

2.2.2 Dependence of Semiconductive Shield on the Cable Insulation Integrity

The quality of the carbon blank and associated semiconductive shield affects the overall cable insulation integrity. The properties of semicon layers affect dielectric loss and cable aging.

Liu, et al. [80] investigated the influence of semicon layers on the dielectric loss of the cables. Transformer ratio bridge technique is utilized for low-loss dielectric measurement. Two types of semicon material are utilized in the study: conventional shield and supersmooth shield. The measurement results on a conventional shield are shown in Figure 2.5 and that on a supersmooth shield are show in Figure 2.6.

(a)   (b)
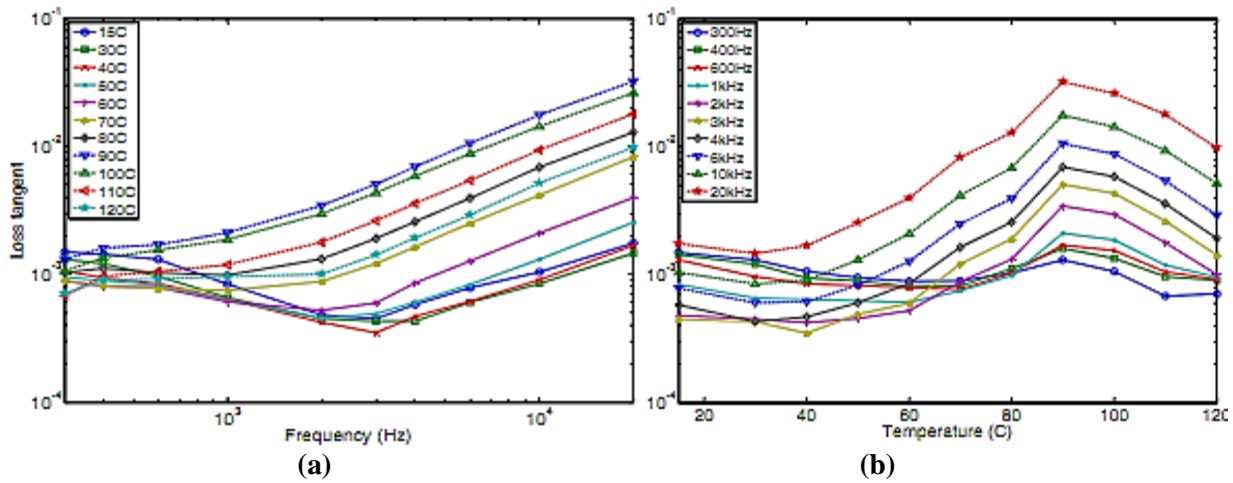
Figure 2.5: Results for XLPE cable with conventional shield showing (a) Frequency Spectra, and (b) Temperature Spectra [80]

(a)   (b)
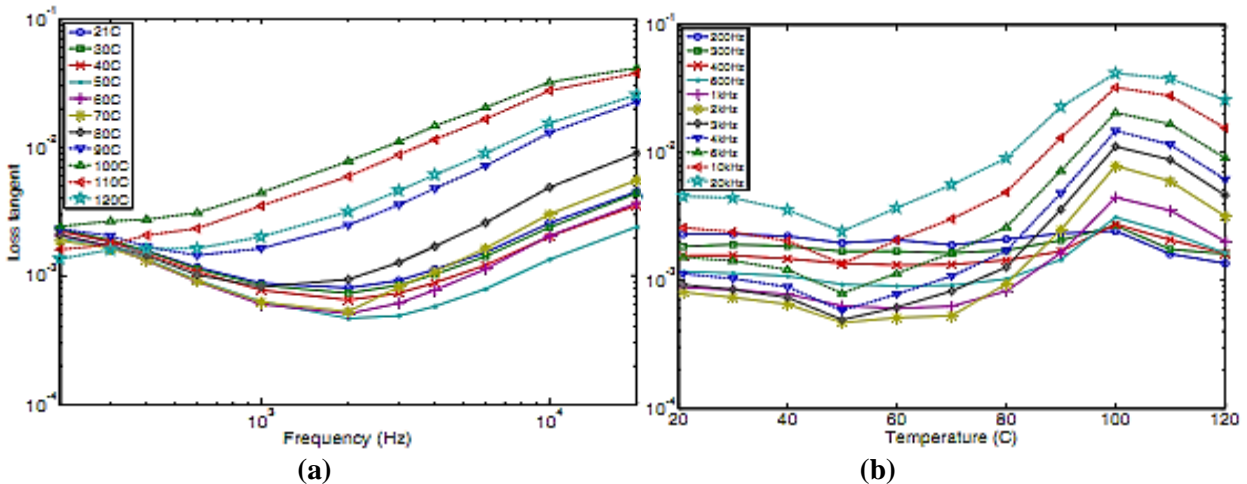
Figure 2.6: Results for XLPE cable with supersmooth shield showing (a) Frequency Spectra, and (b) Temperature Spectra [80]

30

The frequency spectra for both shields are similar. The dielectric loss tangent increases as the frequencies increase for all temperatures. The temperature spectra are also similar except the temperature of maximum loss tangent is at 90 °C for conventional shield and 100 °C for supersmooth shield. An interesting observation is in the case of temperatures below 60 °C where the dielectric loss tangent decreases up to 3 kHz. To explain these results, the authors claim that there are two dielectric loss behaviour are present. One dielectric loss behaviour is dominant for the lower temperatures while the other dielectric loss behaviour is dominant for the higher temperatures. To determine the cause of the increasing dielectric loss and difference of loss peak temperatures, the authors carried out DC resistivity measurement on two semicon materials under various temperatures. The findings show that the axial resistance of both semicon materials is the main contributor for the dielectric loss tangent. The authors also carried out an equivalent circuit modeling to study the effects of semicon layers on the dielectric loss of power cables. The semicon layers of the XLPE cables have been found to be dominant in the dielectric loss in the frequency range of 200Hz to 20 kHz. The radial resistance of semicon layers was found to have given rise to dielectric loss tangent at higher frequencies under higher temperatures. Semicon was seen to dominate the dielectric loss in the insulation system of the XLPE cables, when the outer semicon was treated like an electrode.

There will be electrical stress, thermal stress, and mechanical stress to the cables throughout the cable's life. These stresses influence the aging of the cable. Aging is an important factor since replacement costs, maintenance costs, and installation costs are involved and decisions about cables need to be made. The quality of semicon compound plays an important role in influencing a cable's life. Experiments by Gross, et al. [81] have showed that the accelerated cable life performance of XLPE cables with supersmooth conductor shields is significantly better than for conventional conductor shields. Han, et al. in [78] proved that the new conventional shields with improved furnace black provided better cable life performance. The semiconductive shield properties of smoothness and cleanliness are at the root of obtaining better cable service life. The smoothness at interfaces between the polymeric insulation and semiconductive shields is very critical for the long term electrical performance and life of the cables

With high degree of attention to details on the semicon compound, though it appears to bring little immediate benefit, the long reliable cable service life can be achieved. Semiconductive shields are capable of being produced with a high degree of cleanliness and with an excellent combination of electrical properties. Their quality adds ultimate value to the power cable.

2.3 Medium Voltage Cable Terminations

Good semiconductive shield properties ensure gradual transition and even distribution of electric field lines between the insulating property of the polymeric insulation and conducting property of the neutral wires. When the cable is required to be terminated by stripping the semiconductive shield and cutting the neutral wires up to a certain length, the lines of electric field will concentrate over the small area at the interface of the semiconductive shield and the insulation. The reason for removing these layers in the first place is to avoid the flashover between the neutral wires and inner conductor at the cable end when high test voltage is applied. The cable ending abruptly creates discontinuity that can result in high electric field concentration in that small area, which is commonly referred to as the triple point. Triple point occurs because the neutral wire and insulation shield are moved up to a certain length from the cable's end. Triple point normally occurs at any interface where a solid, gaseous or liquid insulation and grounded concentric screen meet. This modification introduces a tangential field component, and the field in the cable's end is no longer radial. Figure 2.7 illustrates the normalized electric field concentration at the triple point (near point A) of a cable which is beyond the discharge threshold (3 kV/mm) as observed from the finite element method analysis. The end of the cable can be modeled in a simple form as a circuit having impedances Z_1 and Z_2 with HV source from the cable conductor and ground at the insulation shield, which is also indicated in Figure 2.7. The voltage division between the impedances Z_1 and Z_2 helps in determining the potential at point B. Z_2 can be considered purely capacitive because polymeric insulation can be assumed to have zero conductivity. So,

$$Z_2 = {}^1\!/_{j\omega C_2} \tag{2.2}$$

$$Z_1 = {}^1\!/_{j\omega C_1} \tag{2.3}$$

Usually, the case is that $C_1 \ll C_2$. Hence, the voltage drop occurring between point A and B is almost the total voltage drop. So this would create a very high electric field in this region. The increase in the localized stress at the triple point can possibly exceed the breakdown strength of the gaseous insulating media and give rise to partial/surface discharges. The PD activity can erode the semiconductive shield and polymeric insulation, and can potentially cause premature failure of the cable. To avoid PD in the triple point and control the divergent field, stress control layer which is an important component of the cable termination must be applied as a corrective measure [69, 82-85].
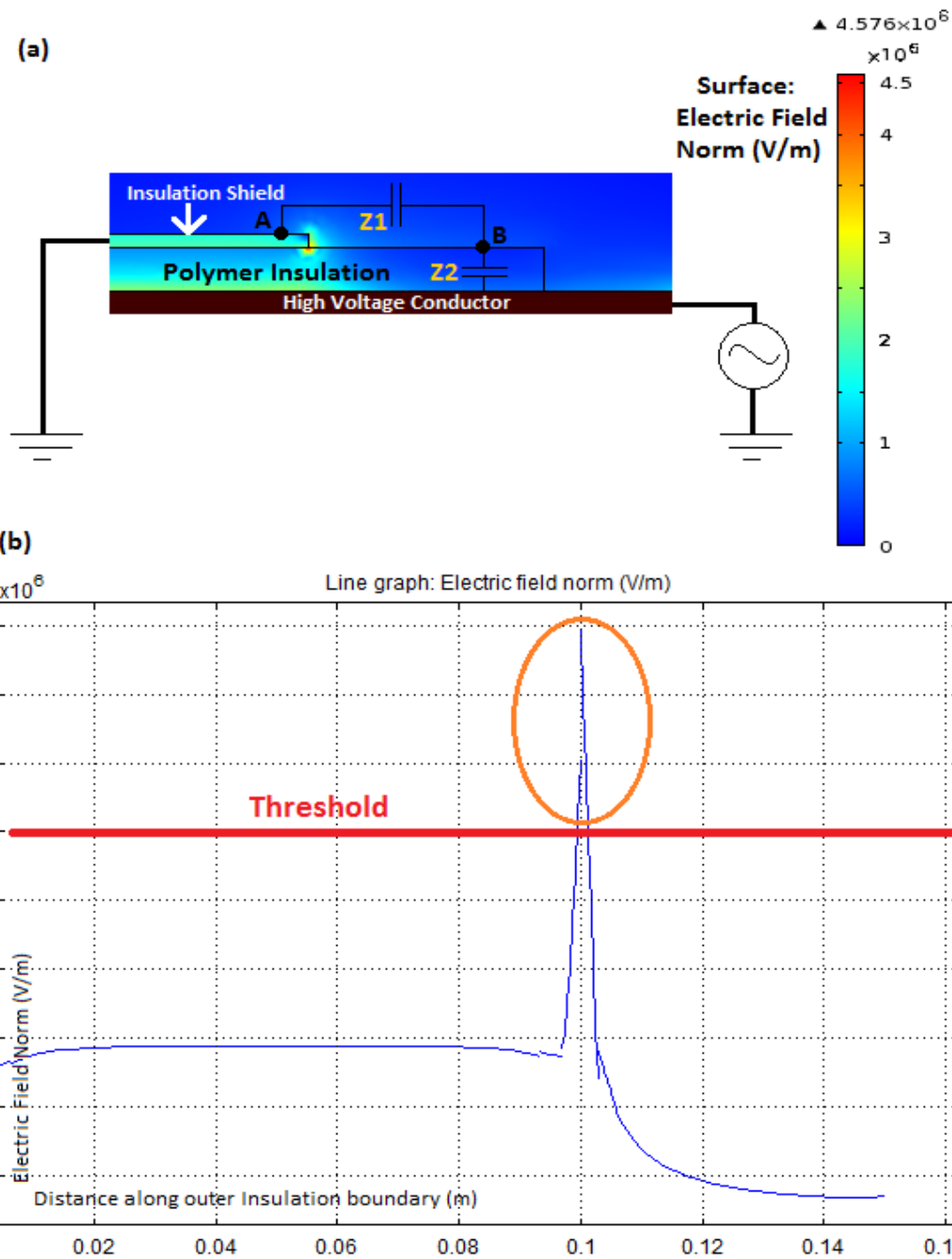
Figure 2.7: (a) Normalized electric field distribution on an energized HV cable where the field is enhanced at the triple point (near point A) as observed from the finite element method analysis, and (b) Normalized electric field (V/m) profile along the outer insultion boundary where the electric field exceeds the discharge threshold of 3 kV/mm at the triple point

IEEE Std-48-1996 defines high-voltage cable termination as a device for terminating alternative-current power cables having laminated or extruded insulation rated for 2.5 kV and above [87]. IEEE Std-48 classifies the termination into three different classes based on their competency to (1) provide electric stress control for the cable insulation shield terminus, (2) provide complete external leakage insulation between the cable conductor(s) and ground, and (3) seal against moisture entry. For example, Class 1A are the terminations that hold all three conditions for use on extruded dielectric insulation system, such as XLPE. The predominant engineering considerations are thus **electric field control**, **creepage distance**, and **physical and environmental protection**.

Electric field control is essential for all classes of cable termination to avoid tracking and insulation failure, which is achieved by stress grading systems. Stress grading (SG) systems are further explained in section 2.4. **Creepage distance** is the surface path between the insulation shield and bare cable conductor terminal pad measured along the length of the cable. This creepage distance must be sufficient to protect against tracking, avoid leakage current flow, and avoid flashover when weathersheds are not used at the Basic Impulse Level (BIL). In order to reduce the probability of tracking, leakage current flow, and flashover under polluted and wet conditions, sheds are incorporated for outdoor termination designs [87]. To protect the termination **physically and environmentally**, it is enclosed in a material such as moulded ethylene propylene diene monomer (EPDM), ethylene vinyl acetate (EVA), or Silicone Rubber [88]. The level of contamination and moisture can be prevalent even in the indoor environment such industrial mills, and oil and gas industries. Therefore, there is a general recommendation to use Class 1 termination because IEEE classes do not make provision for "indoor" or "outdoor" environments.

Commercially available cable terminations have been in market since late 1960s. There are a number of terminations which were developed over the last few decades. Practice in the industry prior to 1960s was to wrap a tape on the exposed cable end. A self-amalgamating tape was used to form a cone which is then layered with a semiconductive tape forming a "stress cone". The challenge with this method was significant installation time especially during severe weather conditions, and skill level requirements. So the installation practices have improved over the years with the technology advances. Today, the installation considerations are predominantly based on termination type and field workmanship. Current medium voltage (MV) termination types are either pre-moulded, heat-shrink, or cold-shrink.

Pre-moulded termination types built with pre-fabricated capacitive stress cones were the next evolution after the hand-taped termination. They have remained in usage predominantly for high voltage (HV) applications (i.e. 69-500 kV) and specialized MV application [89]. The drawbacks of pre-moulded

34

termination type design are their large size, high production cost, difficulty to install, and less flexibility in applying to different conductor sizes and insulation thickness [90]. When heat-shrink and cold-shrink terminations appeared in 1970s, they addressed the drawbacks of pre-moulded termination types. Heat-shrink termination design is developed by applying SG material at the end of the insulation shield, and positing and shrinking the insulating tube by heat over the mastic [87]. Cold-shrink termination design includes moulded skirts, SG material, and sealing mastics, loaded onto a removable core tube [87]. Unlike the heat-shrink type, after positioning the cold-shrink termination over the prepared cable, the core tube is removed. Heat-shrink and cold-shrink termination designs are compact, have low manufacturing costs, and are simple to install. As a result, heat-shrink and cold-shrink designs have become the predominant type for modern MV terminations.

2.4 Stress Grading Systems

Stress grading layer is an essential part of termination for electric field control near the end of the cable, reducing the electric field tangential component, and improving the voltage distribution to avoid partial discharge that leads to tracking and insulation failure [82]. Stress grading is another term for electric field grading. There is great importance of the SG in many types of high voltage power system equipment because a lifetime of the insulation depends heavily on the reliability of its electric stress grading layers. The electric potential and electric field distribution along the length of the cable termination is an indication of the quality of the SG system [83-84]. SG systems are traditionally a vital part of the insulation systems in MV and HV devices.

There are basically two primary stress grading techniques: (1) resistive field grading (realized by means of a resistive layer with appropriate current-field characteristics), and (2) capacitive field grading (e.g., stress cone, geometric electrode grading, refractive grading with high-permittivity materials, condenser grading, etc) [82, 91-93]. The difference in these two field grading mechanisms is the dominance of the type of current. For a capacitive field grading method, the displacement, i.e. capacitive current dominates, while resistive current dominates for the resistive field grading method. As a general rule of thumb, conductivity $\sigma(E,T)$ which is proportional to resistive current density, should be compared with the product of the dielectric constant, ε, times the frequency, ω, i.e., $\epsilon\omega$, which is proportional to capacitive current density. If $\sigma(E,T)$ is larger than $\epsilon\omega$, then the system is resistively graded, and if $\epsilon\omega$ is larger than $\sigma(E,T)$, then the system is capacitively graded. In some cases, both capacitive and resistive field grading methods are active when a combination of both methods is used, for example, when nonlinear resistive field grading tubes are used together with capacitive stress cones [93-94].

35

During the product development stage, the main task is to identify the best field grading technology for a given application. The termination designs used for power system industry are designed for power frequency applications. In last few years, the maturity of the nonlinear resistive field grading technology has considerably progressed for both AC and DC applications. This has resulted in its usage for the higher system voltages. Nonlinear resistive field grading layer has the electric conductivity that changes with electric field. The electric conductivity is a function of the electric field generally with the following empirical equation, where σ_0 and κ are positive constants:

$$\sigma(E) = \sigma_0 e^{-kE} \tag{2.4}$$

These nonlinear resistive field grading materials are usually composites that are filled with fillers such as silicon carbide (SiC) and doped zinc oxide (ZnO) [69, 84]. These are high dielectric constant materials and their concentration determines the degree of nonlinearity that helps relieve the electric stress. Virsberg and Ware [91] found that the concentration and content of the fillers affect the resistive layer's field grading properties in a very critical way. The fundamental property of a nonlinear resistive field grading layer with high dielectric constant and high permittivity can be represented as a controlled resistor connected electrically to the insulation shield as shown in Figure 2.8. For simplicity, the semiconductive shield is grounded in the equivalent circuit representation.
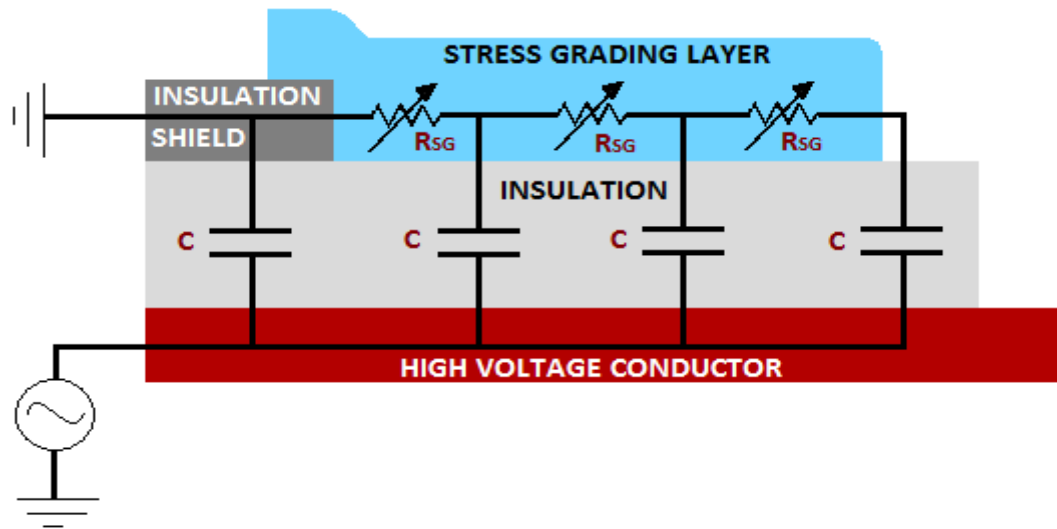
Figure 2.8: Equivalent circuit representation of a resistive stress grading system as a controlled resistor connected electrically to the insulation shield

36

The controlled resistor in cylindrical form extending past the insulation shield onto the polymeric insulation allows the electric stress to distribute along the length of the stress grading layer. Nonlinearity of the material is represented by the variability of the resistor that has a diode-like current-voltage characteristic. The stress relief is achieved by utilizing such a nonlinear resistive material. Figure 2.9 illustrates the difference in the electric field lines for a cable end with and without the nonlinear resistive stress grading layer. The electric field and potential distribution across the cable length is better for the case of nonlinear resistive layer.
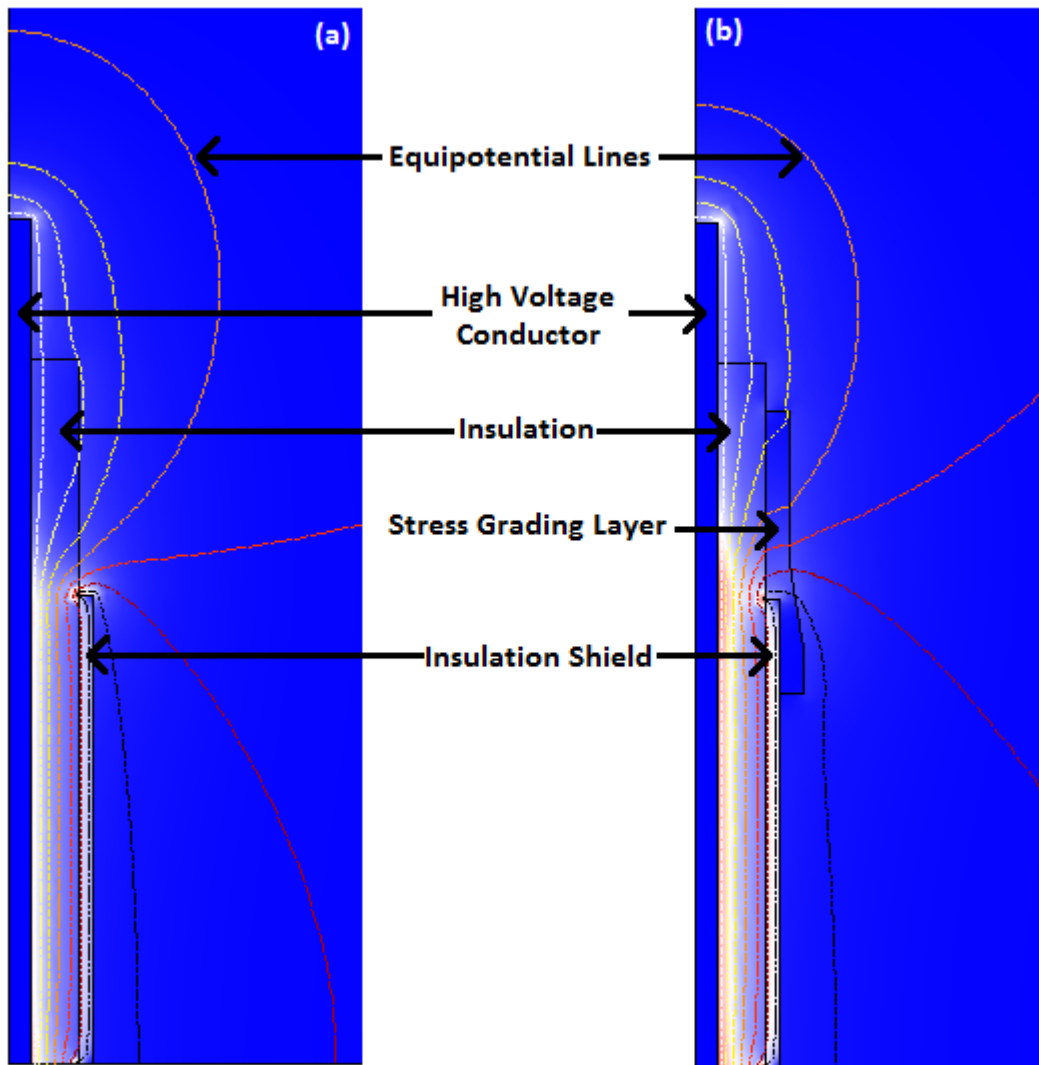
Figure 2.9: Comparison of electric field lines at the terminus of insulation shield (a) without, and (b) with the stress grading layer, indicating the importance of stress grading layer in distributing the unrelieved electric stress

The nonlinear resistive SG layer can control the magnitude of the electric stress with the field dependence nature, but consequently produces ohmic heat (Q) due to conduction currents. The level of dissipation energy may be beyond acceptable level under normal operating conditions but are not problematic under few tens of microseconds of an impulse [64, 84, 95]. The produced ohmic heat (Q) under low frequency, such as power frequency, does not represent a problem for the nonlinear resistive field grading system and performs great. For rare events such as short time impulse-type stresses, the resistive field grading material remains insulating with low losses. However, ohmic heat (Q) increases with frequency $\left(\frac{dV}{dt}\right)$ [93, 95]. The joule heating, which develops the hot-spot, is a concern if the impulse or overshoot condition occurs frequently. Qi, et al. [84] showed that the maximum field does not necessarily occur at the peak applied voltage but is sensitive to the rate of change of the voltage. The influence of the joule heating is subject to the dependency of resistive field grading system's electric field to its conductivity. An excellent stress grading material is the one with very strong nonlinearity, which is an important designing criterion.

Capacitive field graded termination, on the other hand, were dominating during 1960s, mainly because it was difficult to obtain the flexibility required for a termination with a resistive layer. Capacitive graded materials possess an ability to produce a voltage gradient along their length when the potential difference exists across their length due to high permittivity material. This allows electric stress lines to spread and reduces the voltage stress per unit length. Stress cone, which is one of the prevalent applications of the capacitive field grading, is time consuming to construct and much insulation material is required. Stress cones and similar arrangements create tedious work and add high material costs [91, 95]. Moreover, the capacitive SG method requires thick layers in order to produce sufficient relief of the electric field even at lower frequencies. Under the impulse conditions, the capacitive grading may not be adequate. As a result, the nonlinear resistive method is an attractive solution with respect to its superior functioning and to its lower demands on labour and material. Therefore, the research work focuses on the cable termination with nonlinear resistive stress grading system.

2.5 Cable Termination Failure Modes

Cable terminations are installed at abundant locations, especially in the power system industry. MV cable terminations are part of the complex MV power cable infrastructure. Within the power system network, MV cable termination can be found in the collector system, collector substations, interconnection substations, transformers, breakers, switchgears, poles, underground network of wind farm and solar farm, HVDC static inverter plant, STATCOM, SVC, etc. [66, 96-97], as shown in Figure 2.10. Cable

terminations connecting at the transformer are connected to the motor through softstarter that operates under high switching frequencies. In addition, cable terminations are located at the cable termination station, which is a point at which the submarine cable connects into the land-based infrastructure or network.

Figure 2.10: MV cable terminations installed at the (a) pole [99], (b) incoming compartment of a harmonic filter bank [99], (c) switchgear [100], (d) substation [101], and (e) electric meter panel [102]

The failure of the terminations is becoming a reality at these locations. Terminations are failing at the collector system, interconnection substations, transformers connecting to motors, SVC, etc [8, 66, 103]. For example, many collector systems in service today in Colorado, Kansas, Texas, New Mexico, Iowa, Oklahoma, and Minnesota are failing soon after their 2-5 years warranty periods instead of operating successfully for its useful life of around 20-25 years [66]. The reliability of the complex MV power cable

infrastructure continually shows that it is the backbone of several power system components such as substation and collector system. The failure rate of the cable in the wide insulation system is low because cable accessories such as cable termination and cable joints generally fail earlier compared to cables. The failure rates of the cable termination are substantial within the cable system that causes great economic loss [66, 92, 104-105]. Even though cable terminations have been used for more than 50 years, premature insulation failures do occur. The problem of cable terminations still remains incompletely solved. There are various factors contributing to the failure.

Poor workmanship is one of the major causes of termination failure. A good termination is assembled with a lot of care and precaution. Very essential in all types of terminations is that the layers of the stress control make good contact with the insulation and insulation shield. Terminations should have no air gaps or air pockets remaining at the interface of the insulation shield and stress grading layer. Without care and precaution by qualified cable jointers, there could easily be pockets of air trapped inside the stress grading layer when it is applied over the interface of the insulation and insulation shield. Such air pockets or air gaps dangerously enhance the electric stress at the air gap that may lead to PD when the cable is energized. The failures resulting from the workmanship are reported from the experience and are also experimentally verified. Naderian and Haddock from Kinectrics performed root cause analysis on a termination and cable for a hydro company located in Ontario [103]. The failure of the 28 kV rated termination occurred one year after installation in 2006 that had caused an outage and pole fire. The examination of the failed termination revealed that the fault was found right in the boundary of the stress grading layer and semicon layer of the cable, where a 2 mm gap was found. This error in the construction has certainly resulted in increased stress on the insulation surface, left a potential spot for cable failure, overheated the stress grading material near the gap, and punctured the cable termination as shown in Figure 2.11. Zarim, et al. [106] experimentally reported that cable termination in a MV circuit breaker compartment with a loose connection resulted in excessive heating phenomenon.

Figure 2.11: Puncture of the 28 kV cable termination located in Ontario due to workmanship error of leaving 2 mm gap at the boundary of stress grading layer and semicon of the cable [103].

Another workmanship error occurred when an incorrect length of stress control tube was used that resulted in premature failure of cable termination. Meng in [97] reported three cases of cable termination failures. A 22 kV cable termination located at the 22 kV switchgear of petrochemical plant in Jurong Island, Singapore broke down with 10 mm puncture at the interface of the insulation and semicon layer. The puncture went down through the entire thickness of the insulation and exposed the copper conductor beneath. The cause of this failure was the insufficient length of the stress control tube. Furthermore, cable jointers should also be careful as not to damage the insulation in anyway when assembling the termination. Workmanship error causing even a small scratch at the polymeric insulation could lead to PD and cause premature cable failure. Meng reported another failure case of 22 kV cable termination at the petrochemical plant in Jurong Island that was punctured with 15 mm diameter and burnt the surrounding metal cover of the cable box completely. The failure was a result of deep knife cuts at the interface of the XLPE insulation and insulation shield when the insulation shield was required to be removed. Moreover, the insufficient length of the stress control tube was used. The third case by Meng reported audible discharge noise at the area of the stress grading layers of both red phase and yellow phase at the back section of the 22 kV switchgear. The cause of the discharge was because of insufficient air clearance between two stress control tubes. Moore in [66] reported all major failure of the 35 kV cable accessories at the wind farm's collector system in Texas is attributed to workmanship, though root cause analysis was not performed. The qualified cable jointers should thus be very cautious when assembling a termination as to avoid any air pockets at the interface of stress grading layer and semicon, avoid scratches and cuts

on the insulation, use stress control tube with suitable length, and keep reasonable clearance distance between two phases.

The adverse effects of the high frequency stress on the MV motor insulation and transformer has already been determined [56-60, 63, 69, 107-112]. So a newer rising cause of failure in the cable termination is presumed and to a degree demonstrated to be the high frequency voltages. The recent field and research results extended into the stress grading of the cable terminations show the negative impact of the high frequency voltage waveforms. Cable breakdown often happens due to a strong electric field in the cable insulation, close to the boundary of the stress grading layer and semicon layer of the cable. The cause of the cable termination failure at the Eagle Pass Back-to-Back (B2B) VSC installation, a joint venture between ABB, EPRI, and AEP, was HF harmonic resonance around 12 kHz [8]. Paulsson, et al. [8] who investigated the root cause of the failure conducted accelerated aging tests with nonlinear resistive SG layer used in the installation. Authors noted that when high frequency voltage stress was superimposed on power frequency, as the terminations were subject to the field, the nonlinear resistive terminations all failed within 470 hours. Ming, et al. [64] at ABB Corporate Research showed through experiments and simulations that high frequency voltages over the range of 5-20 kHz and amplitude 0-20 kV$_{RMS}$ negatively affect the thermal behaviour of the cable termination, which plays a significant role in the failure mechanism. The high frequency voltages showed hot-spots on the surface of the cable termination with nonlinear resistive SG layer, which are caused by high ohmic loss in the resistive SG layer. IMCOP - Power Cable Reliability Consulting & Diagnostics reported the failure of a cable termination linking a substation with 100 MW wind generation plant [65]. Even though the termination was installed correctly and had passed the very low frequency (VLF) test, the termination failed within one month of installation. The cause of the failure was unknown though it could be due to the presence of HF voltage components. A few electrical engineers on a technical forum in October 2011 discussed the cause of the failure of 34.5 kV cable termination in a 34.5 kV/13.8 kV transformer during switching of a 24.5 MW motor through softstarter [113]. The failure was thought to have resulted from a switching that produced transient voltages and heat from the conducting current once the motor started to run, though no root cause analysis was performed. Figure 2.12 shows a picture of failed cable termination that was connected to a 13.8 kV/6.6 kV transformer powering a pump at one of Ontario's nuclear generation station in 2010. The wear on the termination is noticeable at the dark regions, which most likely occurred by excessive heat caused by HF voltage components that operate pump. The cable termination failures resulting from the presumed high switching frequency voltages and harmonic components are noticeably rising in the industry. Even ABB Switzerland is in agreement that the rates of failure of cable accessories are significantly increasing

at the wind farm, as learned from the interaction with personnel from ABB Switzerland at The Conference on Electrical Insulation and Dielectric Phenomena (CEIDP) 2011.

Figure 2.12: Failed cable termination that was connected to 13.8 kV/6.6 kV transformer powering a pump at one of Ontario's nuclear generation station

Such failures of cable terminations create huge economic loss. According to INCORP, over 150 collector-cable system failures have been documented since 2004, ranging from $30,000 to $500,000 each [65]. Mike Moore reports $35,000 as an average repair cost of cable accessories at the wind farm collector system [66]. This high cost is a result of freight charges on materials, rental earth removal equipment, test technician and repair crew stand time, and outage caused by the failure. The challenges ahead lie for the aged cable terminations currently installed in the grid since the past few decades. The cables and cable accessories are reaching the end of their service life. In some cases, the service life has now been exceeded. The question lies in whether the aged cable terminations in the grid and new improved terminations can bear the increased stresses caused by harmonic contamination and high frequency components. The threat of increasing power contamination is questionable.

Chapter 3
Materials and Sample Preparation

This chapter discusses the cable termination setup and the sample preparation. The descriptions of the commercial QT-II (or Type-I) and QT-III (or Type-II) test terminations, modified KEV-50 oil terminations, and 2 AWG tape-shielded XLPE cable are provided in the next section. The last section describes the process of preparing the cable and installing the termination.

3.1 Cable Termination Setup

Class 1A cable terminations in the MV range are considered in this research work. Since MV range, which is the phase-to-phase operating voltage range of $V_{L-L} = 2.5\text{-}44$ kV_{L-L}, represents the largest application of compact terminations, the research work focused on MV range cable terminations. Class 1A was chosen for being the best class and for its competency to provide electric field control, creepage distance, and physical and environmental protection. Figure 3.1 shows pictures of the Type-I and Type-II cable terminations rated for 5-8.7 kV_{L-N} that are considered in this study.

Figure 3.1: Cable termination samples that are considered in this study: (a) Type-II and (b) Type-I

The specific cable termination testing product for the research work was selected by considering several cable properties such as voltage ratings of the cable, cable insulation level, conductor AWG size, shielding type, and conductor material. The termination mounting location was also considered. Based on the requirements, 3M™ Cold Shrink Silicone Rubber Termination QT-III, 7621-T-95 (Type-II) kit with ratings of 5-8.7 kV was selected, which had met or exceeded the test requirements as specified in IEEE Std-48. The study focused on several samples of this termination design. The properties of this cable termination test sample are provided in the next section.

3.1.1 Cold Shrink 5-8.7 kV Cable Termination Properties

Type-II is a one-piece, dry-type, non-skirted termination based on cold shrink technology. The dimension and maximum wet creepage distance of this termination is 8.5 inches. The short installed length has the advantage of installations in limited space, such as those with transformers, motors, starters, switchgear, and variable speed drives. Another advantage of short termination is that sometimes the use of auxiliary boxes can only be eliminated when limited space is available. Since the 7621-T-95 termination kit is non-skirted, it can only be used in indoor (weather-protected) locations or moisture-free conditions such as in a plant or pad-mount transformer and installed upright or mounted with brackets [114].

The SG system of the cable termination test sample includes:

(1) High dielectric constant (Hi-K) stress control tube
(2) Built-in high dielectric constant (Hi-K) semicon void filling stress control compound
(3) Built-in silicone sealing compound or top seal
(4) Silicone rubber insulator

The Hi-K materials are specially formulated high dielectric constant materials that are an integral part of this termination. The Hi-K material with a dielectric constant greater than 15 minimizes surface stress by uniformly distributing the electrical field over the entire surface of the termination insulator [114]. All the SG system components are compatible with common solid dielectric insulations including XLPE insulation. 7621-T-95 is a shielded termination kit but can be used either on tape or concentric cables. The cable conductor should not exceed a maximum continuous operating temperature of 105°C and an emergency overload rating of 140°C.

The Hi-K stress control tube used modified Ethylene Propylene Diene Monomer (EPDM) to increase and equalize the positive and negative polarity impulse voltage withstand level performance [115]. The required Basic Impulse Level (BIL) of 95 kV was achieved by incorporating the improved tubing into the termination design and optimizing its thickness and length relative to the other design components [115]. The built-in Hi-K void filling stress control compound eliminates the step of applying silicone grease or any other void filling material. Being an integral part of the termination assembly, the material is developed primarily based on silicone rubber for thermal stability and has optimized dielectric constant and loss over a wide electrical stress range [115]. The compound remains with the termination assembly upon removal of the removable support core. The process of removing the support core allows the stress control compound to conform itself into and around the insulation shield step, which displaces air and fills any irregularities on the insulation and insulation shield surface. The built-in silicone sealing

compound replaces the use of sealing tape at the lug, which eliminates the taping and possible flagging. The silicone-based compound goes between the support core and top of the insulation and helps seal the termination and cable, which allows some tracking resistance and creates a waterproof seal [115]. The silicone rubber insulator with non-skirted tubular design is dark gray in colour with good tracking resistance, high hydrophobicity, high resistance to ultraviolet radiation, high resistance to weathering, and fine mechanical properties [115].

The complete termination assembly is pre-stretched and loaded onto a removable core or the support tube. Cold-shrink termination implies positioning the support tube precisely over the XLPE and insulation shield and then pulling out the core to shrink down the termination onto the cable. Thus, cold shrink allows quick and easy installation accommodating a wide range of cable sizes without requiring a force fit. Figure 3.2 shows the dissection of the prepared Type-II cable termination and the components of the SG system underneath the termination insulator along with their thickness.

The SG system components of the termination sample are specified to have high-permittivity; however, the conductivity was expected to be low and field dependent. The electrical properties of these components are given in Table 3.1 measured based on ASTM D150 and ASTM D149.
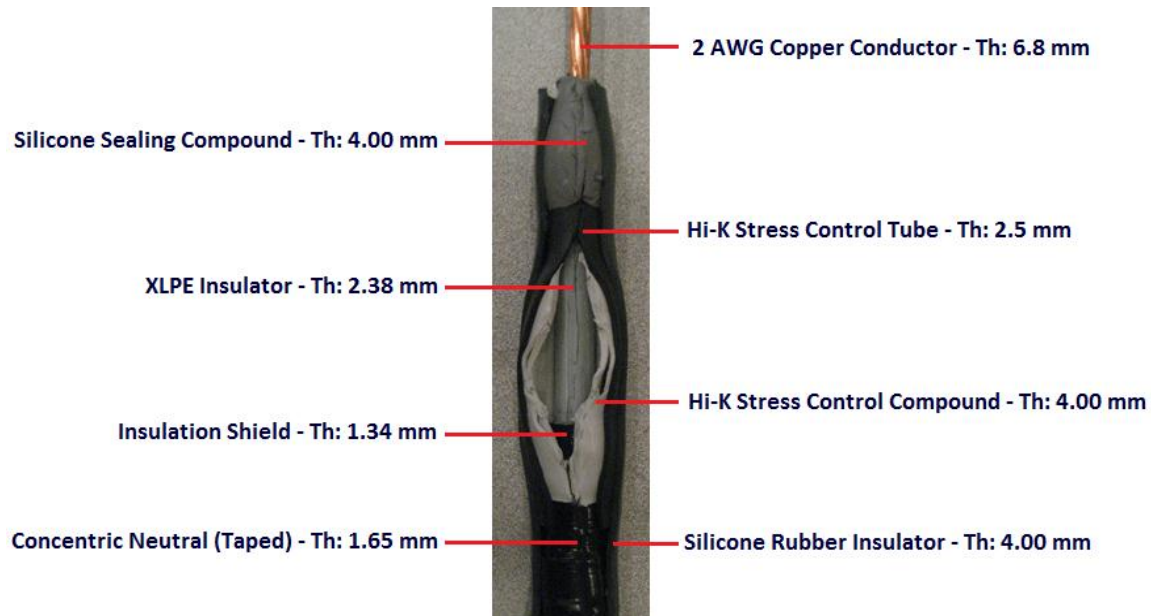
Figure 3.2: Dissection of the 5-8.7 kV Type-II showing the SG system components

Table 3.1: Electrical properties of the SG system components of the Type-II based on ASTM D150 and ASTM D149 [115]

	Hi-K Stress Control Tube	Hi-K Stress Controlling Compound	Silicone Sealing Compound	Silicone Rubber Insulator
Dielectric Constant 60 Hz; @ 1 kV, 23°C (ASTM D150)	**22**	**25**	**Not Available**	**3.6**
Dissipation Factor 60 Hz, 1 kV, 23°C (ASTM D150)	**0.10**	**0.90**	**Not Available**	**0.003**
Dielectric Strength 1.9 mm thickness (ASTM D149)	**Not Available**	**Not Available**	**300 V/mil**	**500 V/mil**

The selected termination test sample has a resistive-capacitive SG system. As mentioned in Section 2.4, the nonlinear resistive SG system has matured over the years and is also very common for the operating voltages under 44 kV as opposed to the capacitive SG system, which is more suitable for operating voltages above 44 kV. However, the dissipation factor of less than 1(i.e. $\tan \delta < 1$ or $I_R < I_C$) under the PF operating condition for both the stress control tube and the stress controlling compound suggests the termination is capacitively graded for the PF operating condition. The dissipation factor of both the SG layers increases (Figure 3.3) that suggests the termination is resistively graded for the HF operating condition.

The two different types of $3M^{TM}$ samples, Type-I and Type-II, are used in this study. Type-II termination technology is $3M^{TM}$'s latest introduction of 1996. Type-I uses a tape to fill in the air gap at the edge of the triple point and requires the installer to wrap tapes or mastic at the top of the termination and use the silicone grease, which differentiates it from the Type-II. Type-II does not require the installer to fill in the edge of the cable semicon because of the built-in Hi-K stress controlling compound that provides an excellent seal. The air pockets are convincingly eliminated to prevent premature failure of the Type-II termination sample. One major difference between Type-I and Type-II technologies is the improved

electrical properties of the Type-II's stress controlling compound as opposed to Type-I's wrapped tape and silicone grease. The dissipation factor of both the technologies is compared in Figure 3.3 where the operating conditions of the Type-II are indicated. The tubing (QT-II) is common in both Type-I and Type-II termination technology, while the new putty (QT-III) is an inclusion to the Type-II technology. Both layers when overlapped for Type-II technology would aid in minimizing the dissipation factor under the operation of wide range of electric stresses. The overall dissipation factor is the average of the dissipation factor of both the layers.
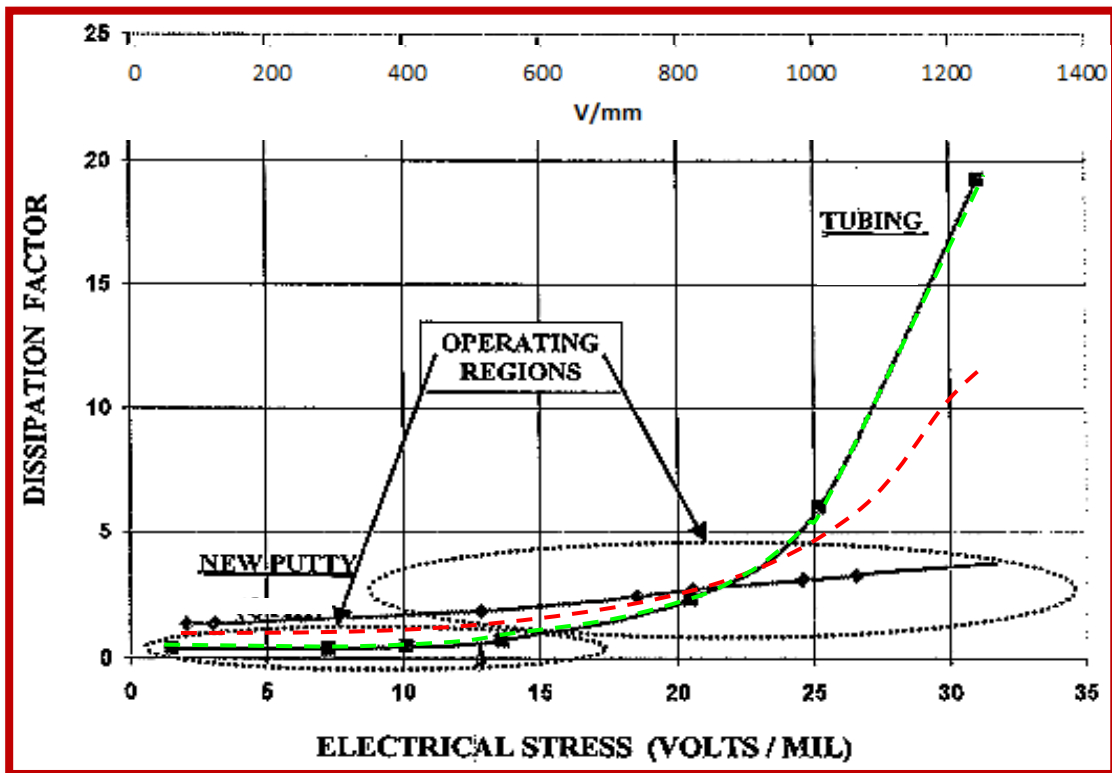
Figure 3.3: Plot of dissipation factor of the Type-II Hi-K stress controlling compound or putty and Type-I Hi-K stress control tube with respect to electrical stress is used to minimize the dielectric heating in Type-II technology where the green plot represents the Type-I dissipation factor and the red plot represents the Type-II dissipation factor

The newer Type-II termination technology has several advantages over the Type-I termination. Type-II allows simple installation, reduces termination preparation time, and minimizes the risk of error. However, the costs of Type-II termination kits are higher by 20-30% compared to Type-I termination kits. One of the reasons for considering Type-I for the study was that many distribution systems across North

America still have 3M™ Type-I terminations and similar types of terminations from other cable accessories companies installed in the grid prior to 1996 and are currently aged. In fact, there is still a market for Type-I terminations in the United States due to 20-30% lower costs. Type-II terminations are of interest because of being dominating termination types since 2000s.

3.1.2 Test Cable

The cable termination test sample in this study used a suitable sized cable. To prepare a cable termination for testing purposes, a 25 inch length of XLPE cable rated for 5 kV_{L-N} was used. The selected cable is tape-shielded, which is generally applied in underground distribution networks. It conforms to ICEA S-93-639/NEMA Shielded Power Cable 5-46 kV. This 5 kV_{L-N} cable is compatible with the 5-8.7 kV_{L-N} rated Type-I and Type-II cable termination kits. The reason for choosing a 25 inch length was to limit the capacitance of the test sample under HF and high $\frac{dv}{dt}$ stresses, thus reducing the generator loading and the overall power rating of the experimental setup. The characteristics of the XLPE cable structure components are provided in Table 3.2 below.

Table 3.2: Characteristics of a 5 kV_{L-N} XLPE Cable used in the preparation of test terminations

Cable Component	Material	Thickness	Outer Diameter
Conductor	Copper Strands (Tot: 7), 2 AWG, 90°C max. conductor temperature	3.43mm	6.86 mm
Conductor Shield	Semiconductive polymeric layer	0.7 mm	9.60 mm
Insulation	XLPE (133% insulation level)	2.38 mm	14.36 mm
Insulation Shield	Semiconductive polymeric layer	1.34 mm	17.04 mm
Concentric Neutral	Copper wire (tape shield)	0.13 mm	17.30 mm
Outer Jacket	Polyethylene	1.65 mm	20.60 mm

The cable was terminated on both ends to prepare a final test sample. The dry test termination was on one end of the cable while a modified Haefely KEV-50 oil-filled termination was on the other end.

3.1.3 Oil Termination

The bottom end of the cable was terminated in an oil-filled termination. From the existing three types of oil-insulated termination for different voltage levels, oil-filled cable test termination unit KEV-50^{TM} was chosen from HAEFELY^{TM}. KEV-50 was used to 'control' termination in the test sample since they have PD levels ≤ 1 ρC up to 50 kV$_{RMS}$, and are insensitive to distorted or HF voltages in the tested frequency range. The condition of PD ≤ 1 ρC levels up to 50 kV$_{RMS}$ ensured that any PD detected during the initial quality test would be localized to the test termination.

KEV-50 helps control the steep electric field gradients that occur during the cable test at the end of a cable from which the sheath has been removed by immersing the bared cable in an insulating fluid of high dielectric strength. The insulation degradation occurring under the distorted or HF components stress would be localized to the test termination when the KEV-50 is used on one end of the test samples. KEV-50 can thus be used for AC testing, and testing under HF and distorted voltage waveform, as well as for partial discharge and electrostatic measurements. The HF insensitivity of the KEV-50 can also be useful for long-term accelerated aging tests on the test terminations. The characteristics of the KEV-50 oil termination are listed in Table 3.3.

Table 3.3: Characteristics of KEV-50^{TM} oil termination [116]

Rated voltage at 50/60 Hz (kV)	**50**
PD level at rated voltage (ρC)	**≤ 1**
Test voltage (kV) at 50 Hz and 1 minute	**60**
Insulation Oil volume per termination (L)	**2**
Maximum cable diameter over insulation shield layer (mm)	**35**
Maximum conductor diameter (mm)	**30**
Length (mm)	**660**
Height (mm)	**595**
Width (mm)	**220**

The KEV-50 test termination consists of a trolley with a pillar which carries the plastic tube. The sealed end of the plastic tube is configured as a high-voltage electrode. This includes the high-voltage

connection and the cable plug-in. Figure 3.4 shows a cross-sectional diagram of the oil-filled cable test termination unit KEV-50^{TM} with steel supporting structure. The advantages offered by this termination structure are easy handling, short cable preparation time and short set up time. For testing conditions, at least 0.15 m clearance was required.
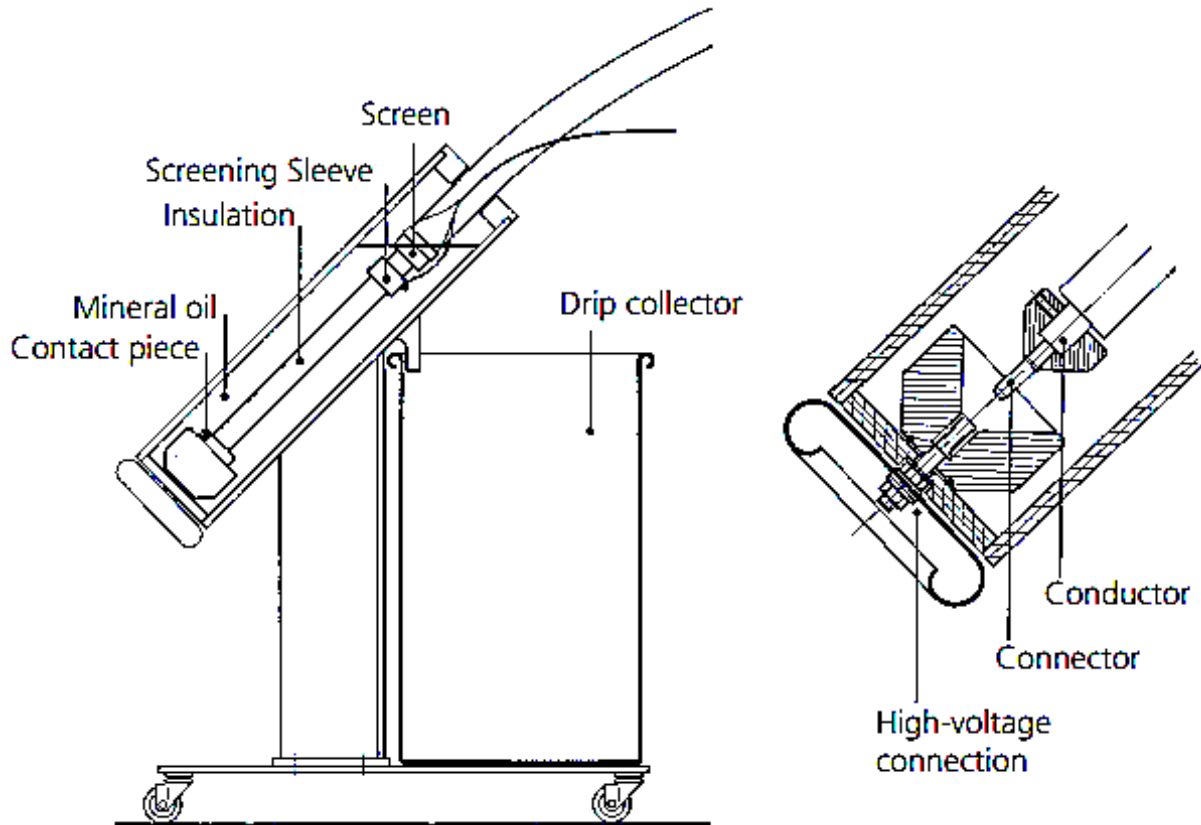
Figure 3.4: Cross-sectional diagram of the KEV-50^{TM} oil termination showing important components [116]

The commercial oil used with the KEV-50 termination was Shell Diala AX; however, Esso's Voltesso 35 oil was also used as an alternative. Both possess similar chemical and physical properties. The important electrical characteristics of both oils are shown in Table 3.4. The insulating oil used in the cable terminations can be used for several months before it needs to be replaced or filtered.

Table 3.4: Electrical characteristics of Voltesso 35 and Diala AX insulating oils [117,118]

Electrical Characteristics	Test Standard	ESSO Voltesso 35	Shell Diala AX
Dielectric Strength (kV) at 60 Hz	D3300 (2mm)	50	56
Impulse Strength (kV)	D3300	225	226
Power Factor at 60Hz, % @ 100°C	D924	0.07	0.04
Gassing Tendency, µL/min	D2300B	+17	+12

3.2 Sample Preparation

The following steps describe the process of preparing the cable termination samples. The preparation was done very carefully in a clean environment to attain precision and avoid workmanship error by a 20+ years experienced linesman at the Waterloo North Hydro.

Step 1- Preparation of the Cable: Before installing the termination kit on the XLPE cable sample, the cable ends were suitably prepared. Cable preparation is the foremost important step so it was necessary to begin with a good cable end. Cable dimensions were chosen and prepared considering the recommendations by KEV-50^{TM} oil termination and Type-II, which is shown in Figure 3.5. The first step of the cable preparation was to strip off the cable outer jacket and pull back the concentric neutral wires to form a ground connection. The entire process of cable preparation used sharp, high quality tools. The next step used a 'semi-con scoring' tool to helically cut and remove the insulation shield, without causing damage to the XLPE insulation. The XLPE insulation conductor shield was helically cut from the copper conductor using an insulation stripping tool.

The process of removing various layers cuts was extended only partially through the layers. When the cable insulation was being removed, care was taken not to cut completely through and damage the conductor strands. For the same reason, the resulting residue from the insulation shield was completely removed. The non-flammable cable cleaning solvent saturated pad from the 3M^{TM} Cable Preparation Kit CC-2 was used in a reasonable proportion. This ensured that no insulation shield particles remained on the XLPE insulation surface.
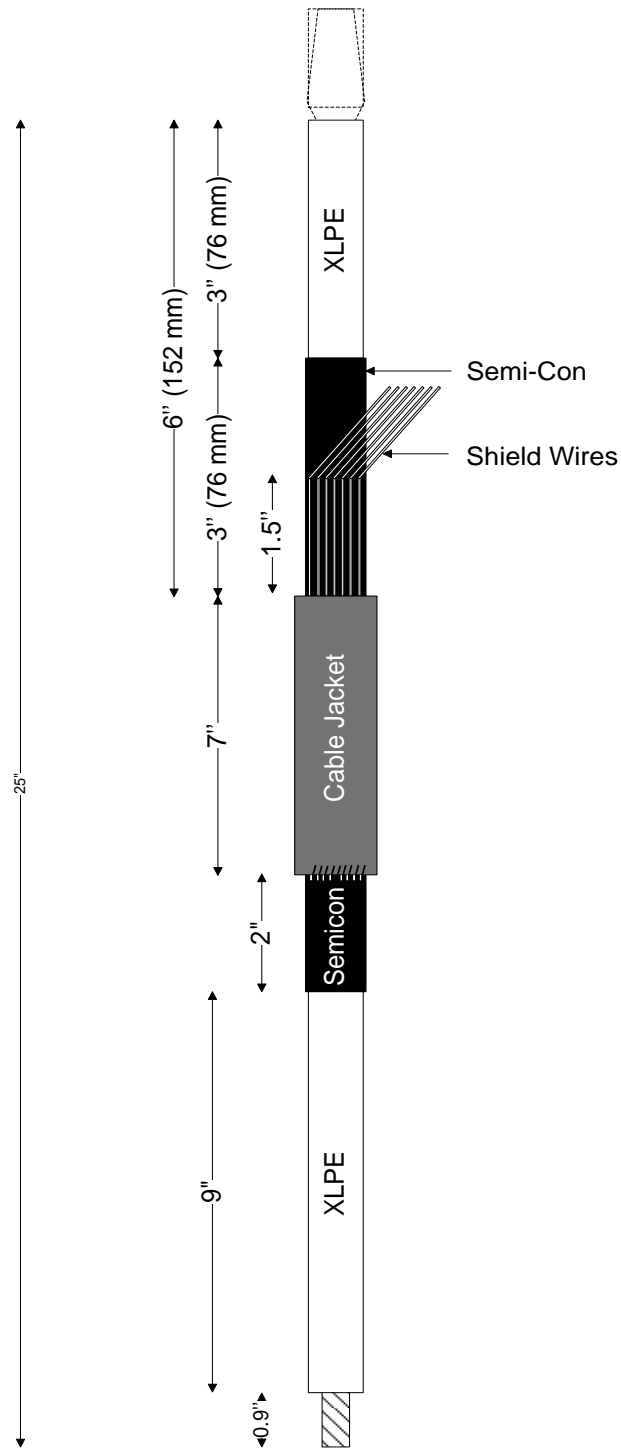
Figure 3.5: Dimensions incorporated from the recommended dimensions by KEV-50^{TM} oil termination and Type-II Termination to prepare a cable for terminating on both ends

Step 2 – Installation of the ground braid and lug: The pre-formed ground braid was positioned with the short tail over tape shield directly adjacent to the cable jacket cut edge. The long tail of ground braid was positioned extending over the cable jacket with a solder block over the mastic strip. Later the ground braid was secured to the cable jacket 114 mm from cable insulation shield edge using vinyl tape. The illustration in Figure 3.6 shows the initial step of the installed ground braid. Next, the ground braid around the cable tape shield was wrapped around once completely. The constant force spring was wrapped and tightened in the same direction as ground braid. A second mastic strip was used over the solder block on the ground braid and previously applied mastic. Finally, vinyl tape was wrapped in two half-lapped layers around mastic strip, constant force spring, and exposed tape shield. Care was taken not to cover the exposed insulation shield. A suitable lug was installed on the copper conductor by positioning and crimping.
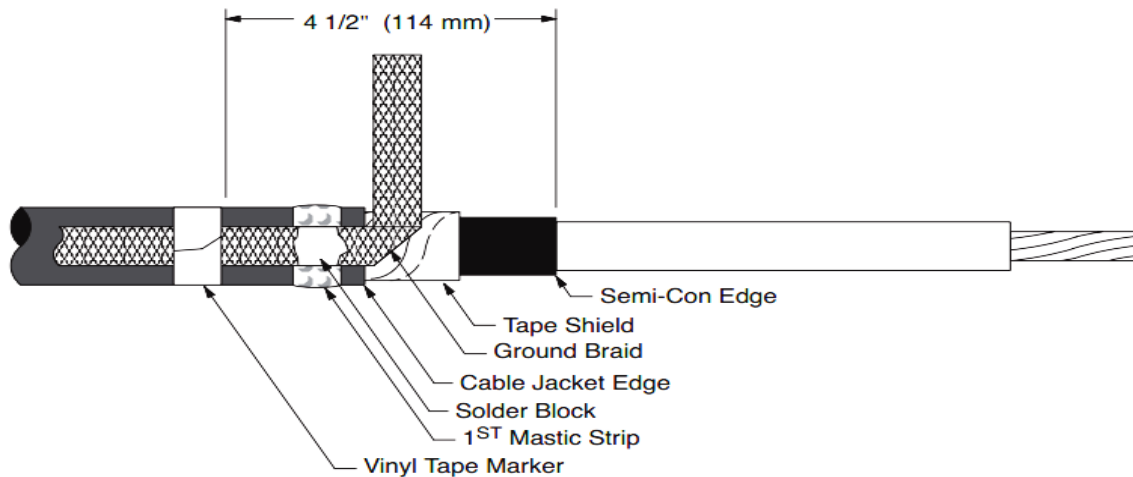
Figure 3.6: Intermediate step of positing and installing the ground braid [114]

Step 3 - Installation of the termination: The termination body was sided onto the cable and the removable core. The winding of the removable core was unwound and pulled in a counter-clockwise direction. The process created firm contact of termination with the mastic seal area, cable, and the supporting assembly.

Step 4 - Insertion of termination in the oil-filled insulating tube: The last step required inserting the prepared dry termination into the oil-filled insulating tube. Shell Diala AX oil was filled in the KEV-50™ plastic tube to a suitable level of 14 inches that completely separated the dry termination. The prepared 3M™ Cold Shrink Type-II termination cable was slowly inserted into the oil-filled insulating tube, as shown in Figure 3.7.
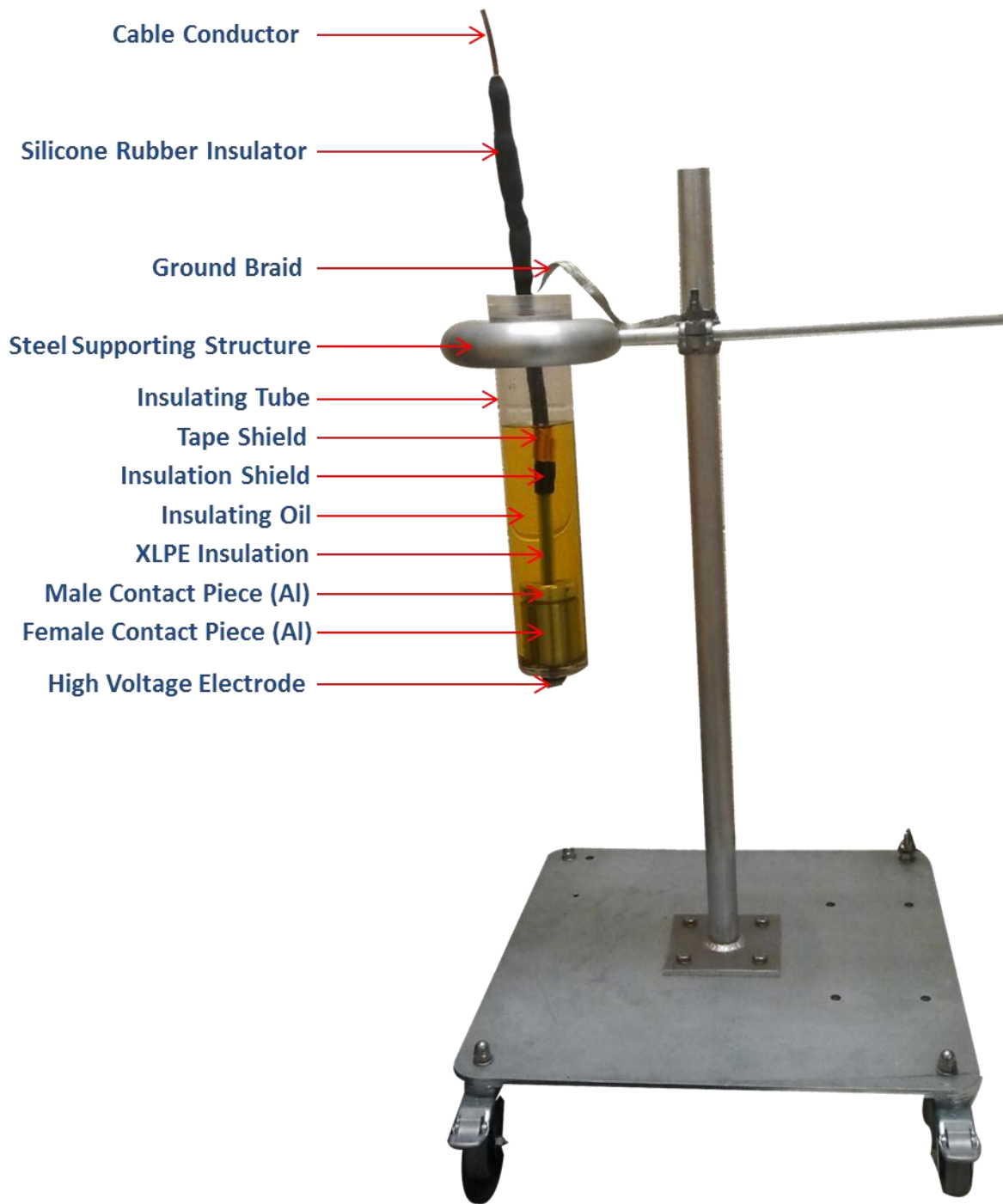
Figure 3.7: The prepared cable termination test sample with the KEV-50^{TM} oil termination and Type-II Termination

To verify the cable termination test sample preparation quality, initial PD measurements were conducted according to IEC 61442, for accessories with VL-N = 8.7kV [119]. The indication of PD < 10 ρC for the 25% higher testing voltage level of 15 kV_{RMS} ensured that the cable termination samples were prepared correctly without any human errors.

Chapter 4
Experiment Setup

This Chapter describes the experimental setup and diagnostic techniques used for in this work. A technique to generate the harmonic components is described along with the high frequency aging setup. The experimental procedure sequence is explained with the aid of tables for aging and electrostatic voltmeter measurements.

4.1 Experiment Setup

This section presents a description of the setups for the experimental work. The arrangements for the generation of the distorted voltage waveforms and PWM voltage waveforms are described. These experimental setups helped achieve primary design goals, which are mentioned in the sub-section below.

4.1.1 Harmonic Components Generation

The information that Hydro One Inc. had provided was steady state and transient state three-phase data at the Point of Common Coupling (PCC) when (a) DG was not connected and (b) DG was connected to the power system grid. Appendix A provides the waveforms of (1) RMS voltage and RMS current for the steady state when the DG was not connected on July 15, 2010 and Nov 12, 2010 (2) RMS voltage and RMS current for the steady state when the DG was connected on July 18, 2010 and Dec 25, 2010, (3) Instantaneous voltage and instantaneous current for the transient state when the DG is not connected on Mar 14, 2010, and (4) Instantaneous voltage and instantaneous current for the transient state when the DG is connected on Mar 09, 2011. The waveforms in Appendix A clearly show the enhancement in the voltage and current magnitudes and distortion levels when the DG is connected to the grid.

The Fast Fourier Transformer (FFT) was used to obtain the spectral analysis plots as shown in Figure 4.2 for the case of (a) DG not connected and (b) DG connected to the power system grid. FFT, a faster version of Discrete Fourier Transformer (DFT), was used to transform the voltage waveforms in the time domain into its discrete frequency domain representation. The built-in MATLAB's FFT function was utilized in the MATLAB^{TM} program that computed the discrete Fourier transform of a signal. Such harmonic distortion and over-voltage could occur at every almost every DG, capacitor, or power electronic drive connected to the grid.

The Hydro One Inc. data at the PCC emphasized the facts mentioned in Section 1.2.1 which specify the enhancement of the low order harmonics from the DG-connected power electronic drives and the three-wire distribution system with mixed linear and non-linear loads.
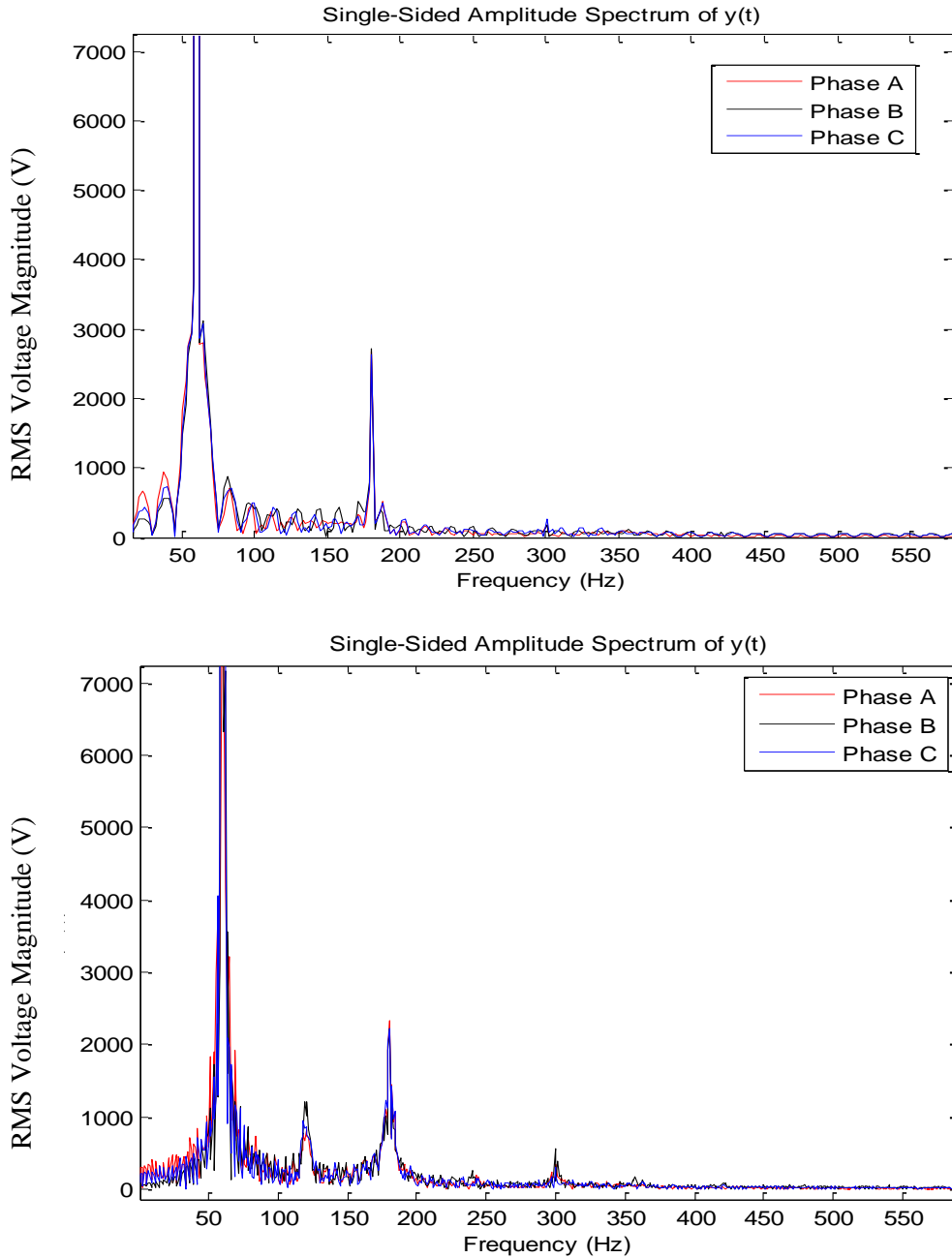

Figure 4.1: FFT Spectrum computed in a MATLAB$^{\text{TM}}$ program of three-phase voltage waveform for a typical transient state when (a) DG is not connected and (b) DG is connected to the grid

In order to generate a precise level of distortion in the output waveform, a unique technique adopted by Ghunem, et al. was utilized [120]. A schematic diagram of this is shown in Figure 4.2.
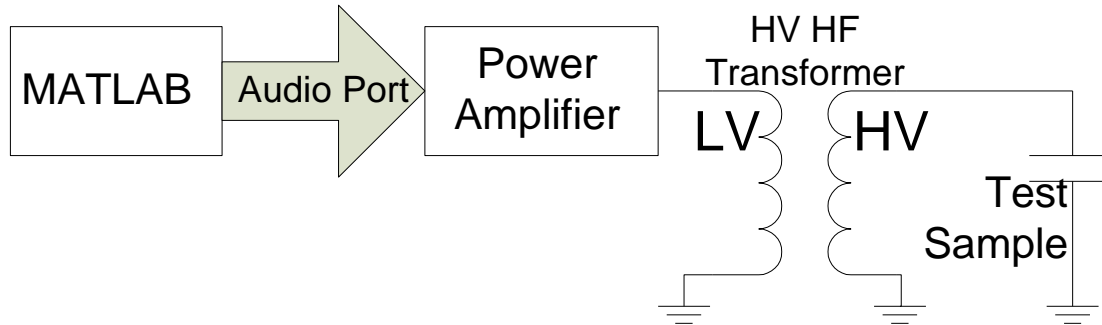

Figure 4.2: Schematic representation of distorted voltage waveform generator

The desired voltage waveform was generated in the computer through the MATLAB™ based software and the signal was passed onto the audio port. The audio signal was then fed to the power amplifier to get the required amplification, which was fed to a custom-built high voltage test transformer from Bey Electronics Corporation. The advantage is that this approach allows accurate adjustments of the amplitude, frequency, DC off set, and the phase shift. Hence, the desired level and shape of the distortion in the output waveform was achieved. The distortion voltage generation technique allowed production of PF, low order harmonic components, and PF and low order harmonic components superimposed voltage output waveforms.

This approach was limited by the frequency response of the custom transformer. The low order harmonic components were limited to 15th harmonic because of the limitation of the custom-built high voltage transformer, which can operate at a maximum of 100 V$_{RMS}$/10 kV$_{RMS}$, 1A, 60 -1000 Hz. The unique approach thus eliminates the need of superposition circuit setup. The setup presented here was used for the cable termination surface potential measurements using electrostatic voltmeter tested under the distorted voltage waveforms.

4.1.2 High Frequency Aging Setup

High frequency aging setup was achieved with an IGBT-based pulse voltage generator designed and patented by Yatong Yu in 2009 [121], which can produce high voltage square wave and PWM waveforms. The PWM pulse waveforms were chosen for aging purpose because of their high $\frac{dv}{dt}$ or short

rise time and high switching frequency features that help increase dielectric and thermal stresses. Moreover, the high frequency reduces the overall aging time period.

The generator has a potential to produce PWM waveforms with a peak voltage up to 17 kV and with a switching frequency from 600 Hz to 3 kHz. The fundamental frequency of the PWM waveform can vary from 20 Hz to 1200 Hz. The rise time is less than 200 ns and the pulse width can vary up to several milliseconds. The generator consists of wave shaping components including IGBT switches. The unique cascade connection circuit design with 10 stages enables the generator to produce the stable high voltage square wave and PWM waveforms. The generator fully charges the capacitors on each stage in parallel. When the IGBT switches on the discharging side are triggered, the charged capacitors in each stage discharges simultaneously in series and adds the series voltage, thus providing a high peak voltage. A microcontroller-based trigger signal generator with optical fiber cables is used to trigger the IGBT switches in the generator. The input to the generator was fed by a transformer. The voltage was varied by a dial on the variable transformer.

The setup presented here was used for thermal analysis of the cable termination for the aging test under the high frequency, high $\frac{dv}{dt}$ PWM voltage waveforms. The cable terminations were exposed to these PWM non-sinusoidal steep-front voltage waveforms.

Maximum ratings of 16 kV$_{P-P}$ and the additional 30% from the overshoot, and 3 kHz for the pulse repetition rates were adopted. Figure 4.3 illustrates a PWM-VSC output voltage waveform applied for the aging of the cable termination for 600 hours. The load characteristics highly influenced the rise and fall time of the pulses, as well as the output voltage. Since the loads, i.e. cable terminations, used in this study are inherently capacitive, the decay time for discharging ($\approx$RC) was too long relative to the pulse period. The pulse fall time depends strongly on the load characteristics, i.e., the impedance of cable termination. In the setup used in this study, the fall time is about 38 µs. The polarity is positive and fixed (unipolar). These values of pulse voltages and pulse repetition rates generate substantially dielectric and thermal stresses.
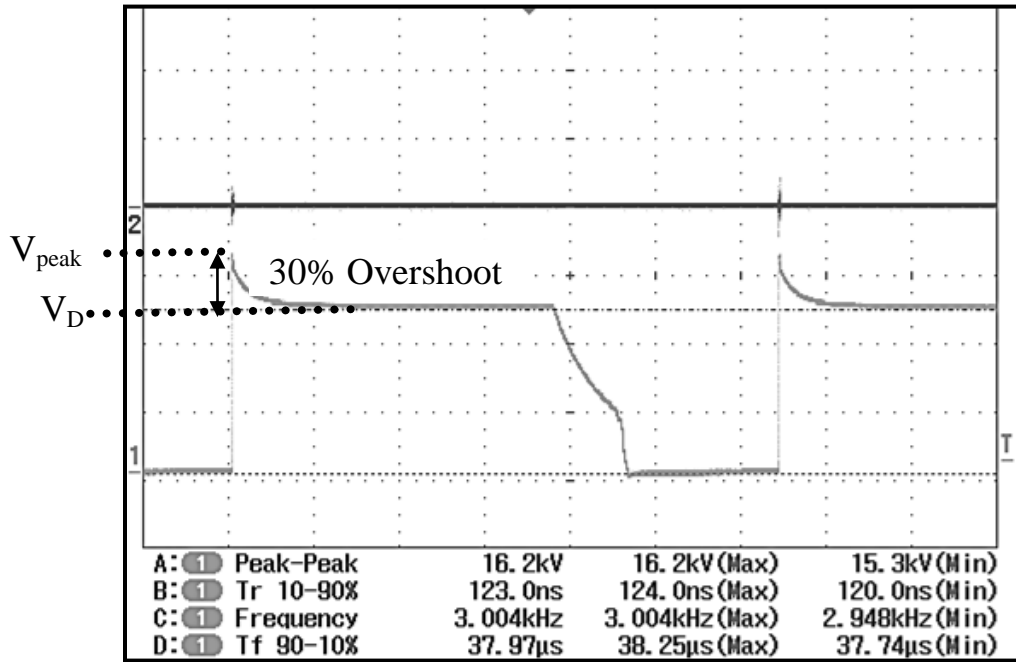
A:	①	Peak-Peak	16. 2kV	16. 2kV(Max)	15. 3kV(Min)
B:	①	Tr 10-90%	123. 0ns	124. 0ns(Max)	120. 0ns(Min)
C:	①	Frequency	3. 004kHz	3. 004kHz(Max)	2. 948kHz(Min)
D:	①	Tf 90-10%	37. 97μs	38. 25μs(Max)	37. 74μs(Min)

Figure 4.3: A single PWM pulse voltage waveform at 16 kV_{P-P} and additional 30% from the overshoot, 3 kHz switching frequency, 60 Hz fundamental frequency, and rise time of 123 ns

4.2 Diagnostic Techniques

This section presents a description of the diagnostic techniques used to evaluate the stress grading system of the cable termination. The setups of the surface potential measurement and the temperature profiles for the dielectric and thermal characterization of the cable termination are described. The potential distribution on a surface of the termination is used to understand the electric field at distorted waveforms.

4.2.1 Temperature Measurements using Infrared Camera

The temperature measurement is an important diagnostic technique because dielectric response of the insulation is highly temperature dependent. The temperature has a high dependency with the dielectric loss factor. So any significant temperature change observed on the cable termination surface is a sign of a high dielectric loss and discharges.

The temperature measuring system consists of a Flir-SC500 infrared camera having an emissivity spectrum between 7.5 μm and 13 μm displaying the temperature image in a 320 × 240 pixel array on the thermo-vision acquisition software, ThermaCAM™ Researcher 2.8 Pro SR-3. The accuracy of the thermal camera is 2 K over the range of 273 K to 773 K with the detector sensitivity of 0.07 K at a

61

temperature of 303 K [122]. Figure 4.4 depicts the setups used for measuring the surface temperature along the cable termination sample when it was energized by PWM pulses.
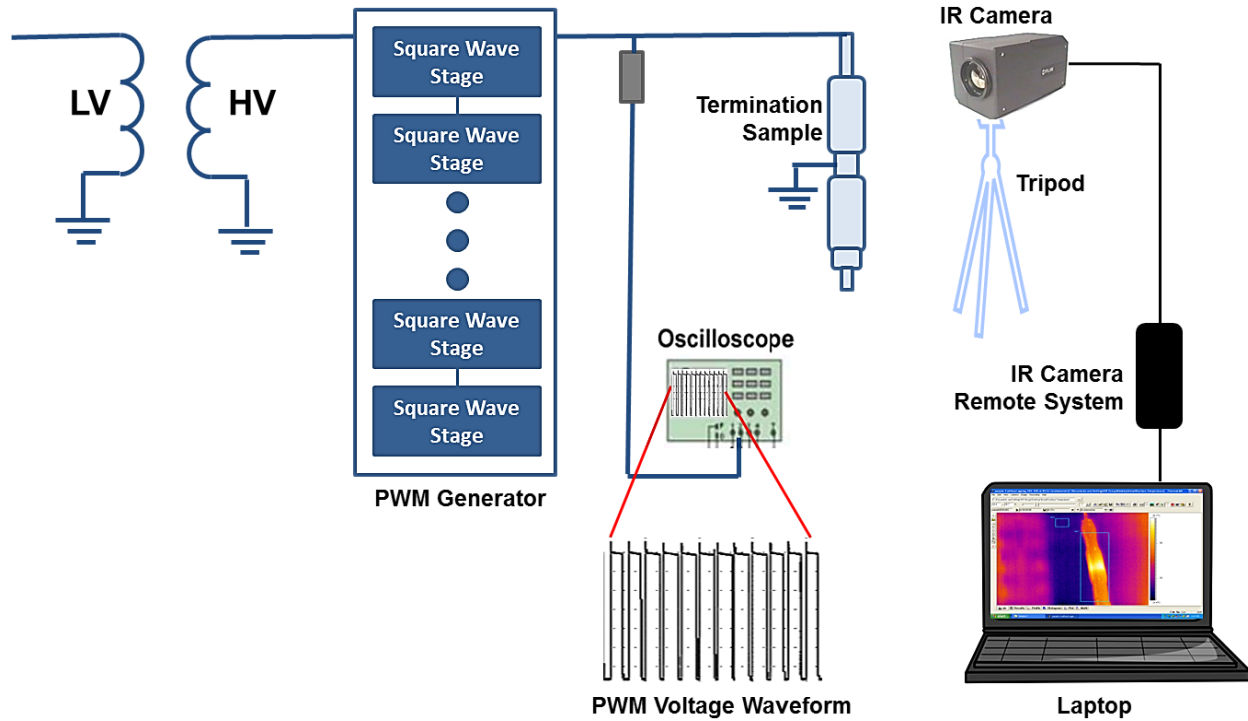
Figure 4.4: Experimental setup for infrared thermography of the cable termination sample during aging under the high frequency PWM voltage pulses

The emissivity used for termination sample was 0.95 to account for the dark gray outer silicone rubber housings. The acquisition software allowed different types of post-processing of the temperature distribution in the infrared image. The maximum surface temperature on the termination sample was continuously acquired every minute using the thermo-vision acquisition software. Figure 4.5 shows the ThermaCAM™ Researcher 2.8 Pro SR-3 thermo-vision acquisition with the thermal image and the measured time profile of change in temperature on the surface of the cable termination sample under high frequency PWM waveforms.

Figure 4.5: Thermal image and temperature plot of the termination sample's maximum surface temperature rise from the ThermaCAM™ Researcher 2.8 Pro SR-3 thermo-vision acquisition software

4.2.2 Electrostatic Voltmeter for Voltage Distribution Measurements in SG Systems
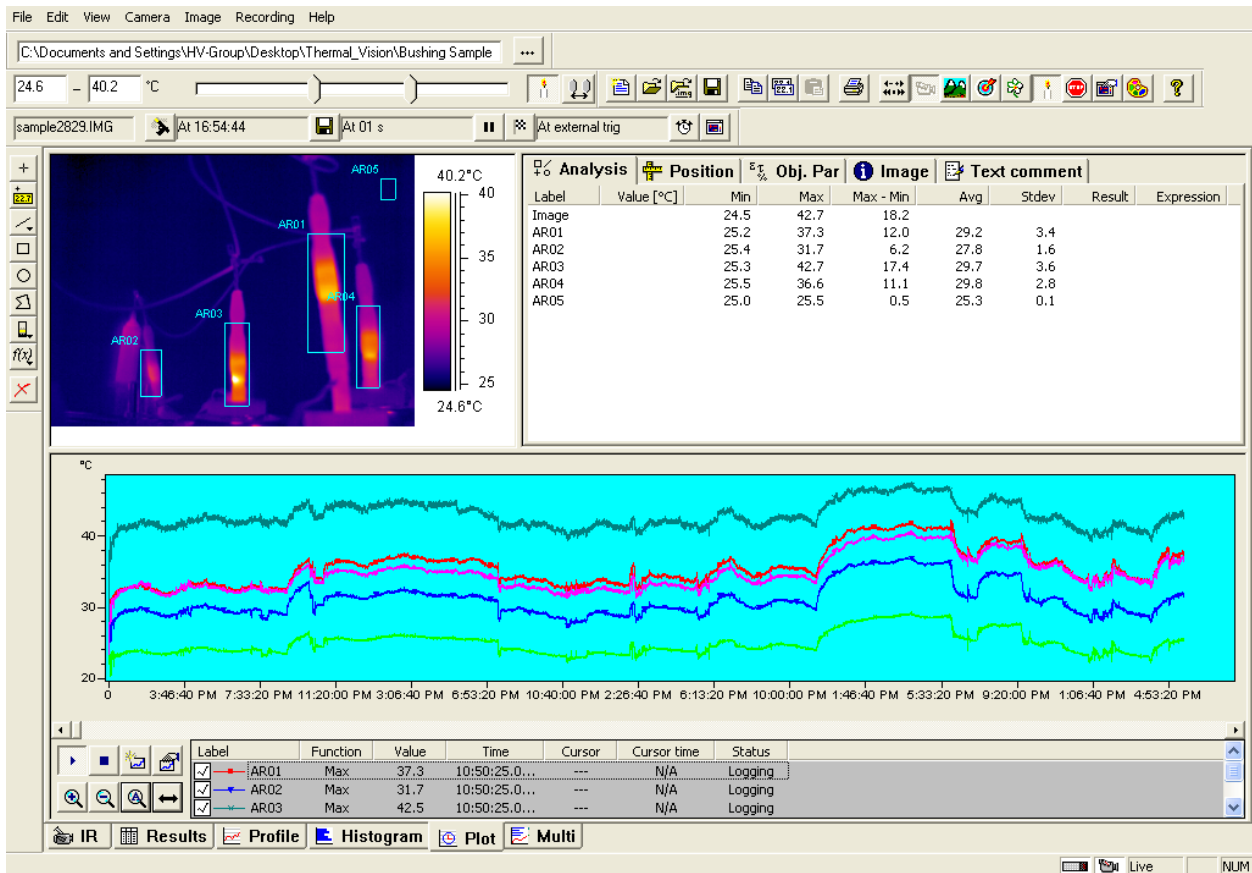
The quality of the SG system can be best determined by the direct measurement of the grading effect. A method of examining the grading effect on the SG systems is to measure the surface potential [111, 123-124]. For a better evaluation, the corresponding electric field must be extracted from the measured surface potentials because the surface potential distribution alone cannot effectively evaluate the SG performance. A simple method is to measure the potential in very small steps along the length of the SG system and then evaluate the corresponding electric field in the tangential direction. The SG system has high impedance so a regular voltmeter or a HV divider cannot be used to directly measure the voltage distribution. This is to avoid a transfer of charge between the source and the voltmeter, which changes the loading and the original value of the voltage. In this research, an advanced TREK model 341A electrostatic voltmeter (ESV) was used, which is a voltmeter that does not represent a considerable load

63

for the source of potential because it is a high impedance meter. This method was recently adopted for the SG system of the machine [111, 125]. The same method can be extended for the evaluation of the SG system of the cable termination, which is a unique diagnostic technique in the cable accessories division.

As opposed to potential measurement on a smooth and even surface of the SG system of the machine, there was a challenge with the potential measurement for the uneven SG surface of the cable termination. The distance from the surface in radial direction and the radial shape of the termination was another concern because the ESV probe had to be placed 3mm ± 1 mm perpendicular from the termination surface, within the specifications recommended for the instrument [126]. As a result, the ESV probe was mounted on a tripod with an adjustable plastic bar. The ESV probe was positioned and maintained very close to the surface of a termination sample between 2 mm and 4 mm perpendicular to the surface during the measurements. A reasonable precision was also achieved for the tangential distance between the two measuring points by reasonably adjusting the vertical position of the tripod. The angle of the ESV probe was also adjusted for every measuring point to make the probe as perpendicular as possible to the uneven surface. Figure 4.6 illustrates a schematic of the experimental setup for the voltage distribution measurements with the Electrostatic Voltmeter.
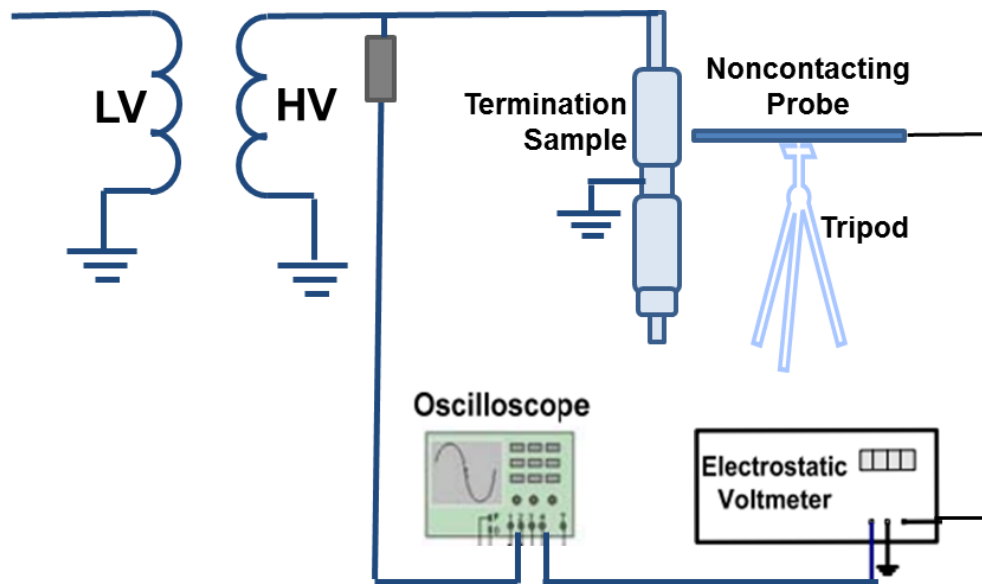

Figure 4.6: Experimental arrangement for measuring the termination surface potential

The TREK model 341A ESV uses a sensitive vibrating Kelvin probe that vibrates electromechanically in the direction perpendicular to the surface to be tested with a field-nulling technique (Kelvin technique) for

non-contacting measurements. The electric field nullifying process continues until the ESV probe housing has been driven to the same potential as that of the test surface. The ESV probe spatial resolution is limited and the instrument will read the resulting averaged electric field at a given location. Measurements with the ESV probe give an idea of the superposition of the field resulting from the surface charges. The field measurements are affected by the geometry of the measurement setup so it was important to consider the distance between the ESV probe sensor and the surface. Moreover, the ESV was calibrated for each test point to ensure that the potential measurements are taken for the surface within 1 mm to 3 mm distance. Capacitively coupling of the ESV probe strongly influences the measurement results so it was important to assure that capacitance of the surface under test to ground is larger than the capacitance between the ESV probe and the surface.

The maximum voltage of the ESV is 20 kV DC or 20 kV_{Peak} AC with ±0.1% accuracy and a response speed better than 200 μs for 1 kV_{Peak} [126]. The ESV has a limited frequency response, which is set by the probe's mechanical frequency. Operation around 2.5 kHz at 1 kV_{RMS} becomes a sampling rate issue. Depending on peak-peak voltage, high frequency, and the probe to surface spacing, the probe may produce a high voltage discharge to the viewing surface. This is caused by the integrator of Model 341A not being able to follow the changing voltage on the surface being viewed, thus when the two voltage sources are at different levels, a discharge may occur. This may cause damage to the probe if the testing unit and probe are allowed to continue to arc for a certain period of time. To quickly recover from such a discharge, 42077 signal pc board of the TREK model 341A ESV was modified by adding a few resistors in parallel with the existing resistor.

A precision voltage monitor provides a low-voltage replica of the measured electrostatic potential for monitoring purpose. The monitor output provides a low voltage signal (1/1000) similar to the voltage measured on the surface of the termination. For each probe position, calibration was done by zero adjustment of the output of the instrument. The calibration would ensure that phenomena such as contaminations, stray charges in the field of view of the probe, and contact potentials are minimized. In addition, the accuracy of measurements was tested by recording the line end voltage for 60Hz and 60Hz + distorted voltages, for each test case. Figure 4.7 shows the partial laboratory setup for the illustrated setup in Figure 4.6 in the High Voltage Engineering Laboratory (HVEL) at the University of Waterloo.
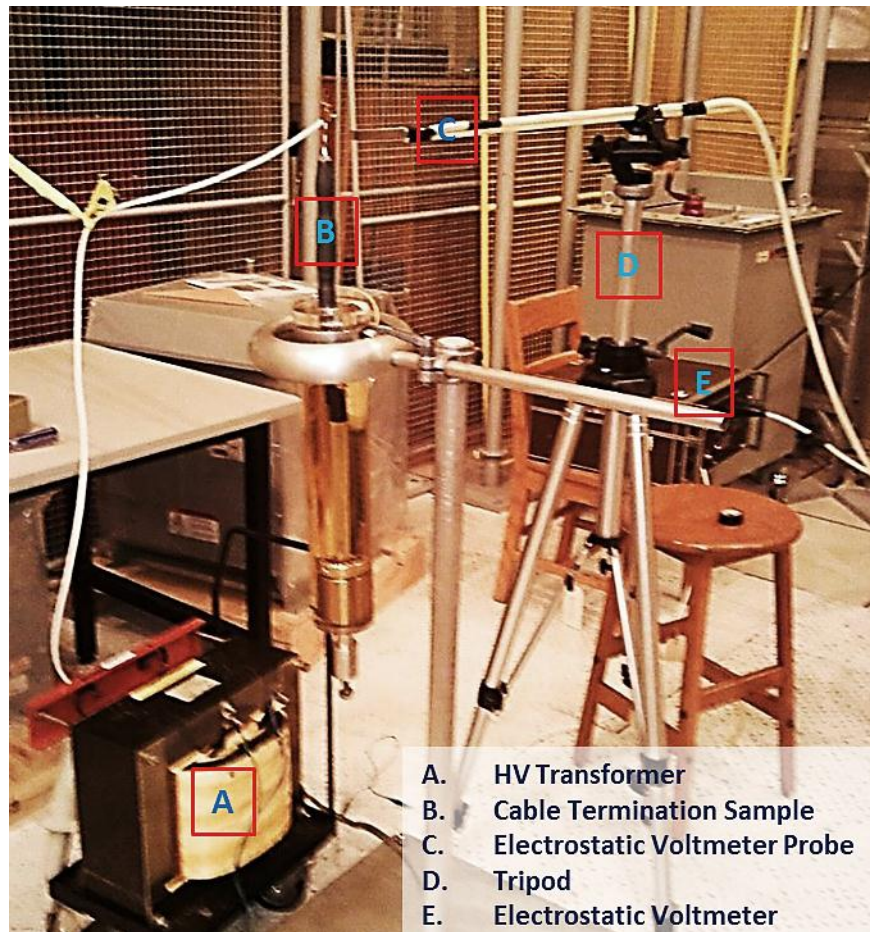
Figure 4.7: Laboratory setup for measuring the termination surface potential illustrated in Figure 4.6

4.2.3 Partial Discharge Measurements

PD measurement is an important test for the condition assessment of the HV insulation system. PD helps in detecting any poor workmanship in the initial stage and provides knowledge of the insulation condition during the periodic measurements. The PD measurement system used was a 0 kV - 150 kV/20 kVA AC dielectric test set (Hipotronics 7150-20AMAX-G) with a PD level < 2 ρC and a PD Detector (Tettex Instruments DDX-9101). The setup under the influence of low background noise in the laboratory of less than 3 ρC met all the IEC and ASTM standard requirements [127, 128].

The evaluation of the SG systems during the pulse aging test was carried out with the PD measurements in this study in order to analyze the PD trend due to aging in the insulation system. More importantly, PD measurement would serve in ensuring the test sample preparation quality before subjecting to the experiments listed in Section 4.3. The PD measurement procedure for the test terminations was adopted

from IEC 61442 for accessories with $V_{L-N} = 8.7$ kV$_{RMS}$ [119]. To ensure that the termination met the quality test with the PD measurements, the applied voltage was raised 25% above the testing voltage level for 10 seconds before lowering it back to the testing voltage level. If the detectable discharge at the testing voltage was less than 10 ρC, the test implied that the termination has successfully passed the quality test.

4.3 Experiment Procedure Sequence

Accelerated PWM aging tests were carried out on termination samples of both SG systems: Type-II and Type-I. Both types of samples were subjected to at least 200 hours and maximum 635 hours PWM pulse aging at nominal temperature, using the setup shown in Figure 4.5 with 17.0 kV$_{P-P}$ PWM pulses and 3 kHz repetition rate with 60 Hz carrier frequency. The reason for selecting such high levels of voltage and frequency was to accelerate the aging process by the application of high electric stress. The surface corona activity was periodically checked in the dark with a corona camera during the aging test. The surface temperature along the end portions of the samples was scanned for temperature hot spots using infrared thermography. Termination surface temperature along with the room temperature was continuously monitored in majority test protocols.

Table 4.1 summarizes the aging experiments carried out in this work. The drive behind each aging test is mentioned in the 'Remarks' column of Table 4.1. In Table 4.1 and Table 4.2, Type-II refers to 3M^{TM} Cold Shrink Silicone Rubber Termination QT-III, 7621-T-95 kit and Type-I refer to the 3M^{TM} Cold Shrink Silicone Rubber Termination QT-II, 5621K kit. A total of six samples of Type-II (i.e. Type-II A, Type-II B, Type-II C, Type-II D, Type-II E, and Type-II F) and two samples of Type-I (Type-I A and Type-I B) were used in the experiments. Though the focus of the research was on Type-II cable termination, Type-I samples were also tested in the later stage of the experimental work for comparison purposes.
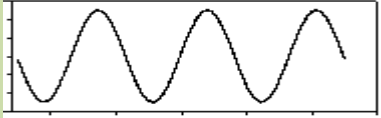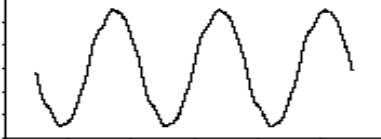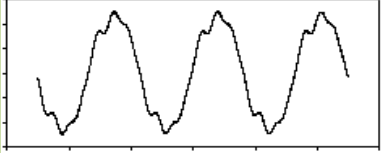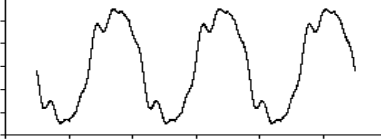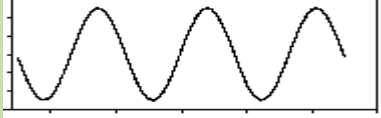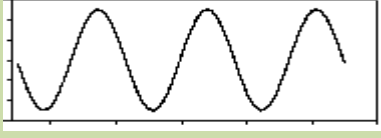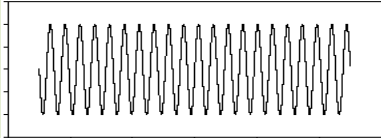
Figure 4.2 summarizes the test sequence and conditions for diagnosing terminations via ESV test under the influence of distorted waveform. The factors that varied included applied voltage, THD level, and harmonic components distribution. The ESV test was applied on terminations with varying age. The distorted voltage waveform which are composed of fundamental and THD different proportion chosen for each case are illustrated in the last column of Figure 4.2.

Table 4.1: Test Sequence for the accelerated aging experiments with infrared thermography

Test Case	Sample	Test Condition	Duration	Remarks
A	**New:** Type-II A, Type-II B, Type-II C, and Type-II D	PWM 17.2 $kV_{P-P(MAX)}$, 3.0 kHz	620 hours	Monitored termination surface and room temperature every minute to age the newly prepared terminations
B	**Aged (620 hrs):** Typ-II A **New:** Typ-II E	PWM 17.0 $kV_{P-P(MAX)}$, 3.0 kHz	15 hours	Monitored termination surface and room temperature every 10 seconds to compare the temperature rise between the aged and new termination
C	**Aged (620 hours):** Type-II C	Sinusoidal 35.0 - 38.0 kV_{RMS}, 60 Hz	22 hours	Monitored termination surface and room temperature every 10 sec as an attempt to age with higher but sinusoidal voltage and simultaneously detect any degradation via online PD monitoring
D	**New:** Type-I A	PWM 17.0 $kV_{P-P(MAX)}$, 3.0 kHz	200 hours	Occasionally monitored termination surface and room temperature to age the newly prepared Type-I termination and compare with Type-II termination
E	**New:** Type-I B	PWM 17.0 $kV_{P-P(MAX)}$, 3.0 kHz	500 hours	Rarely monitored the termination surface and room temperature to age the newly prepared Type-I termination and compare with the failed termination sample of test case D

For the designated ESV tests, the sample was energized at peak-peak voltage that varied from 3.0 kV_{P-P} to 10.0 kV_{P-P}. Reasonable voltage readings were possible along the cable termination length as long as the applied voltage was greater than 3.0 kV_{P-P}. The applied voltage level was not so crucial because the surface potential distribution would be proportional to the applied test voltage, which is a suitable requirement for the electric field computation. The fundamental frequency chosen was 60 Hz for all the test cases except for the test case Z-2.

Table 4.2: Test sequence and conditions for testing termination via ESV test on distorted waveform

Test Case	Sample	Voltage (@ 60 Hz)	THD Level	Harmonic Components Distribution	Voltage Waveform at the Test Sample (Voltage vs. Time)
X-1	**New:** Type-II A, Type-II B, Typ-II C, and Type-II D	5.0 kV$_{P-P}$	0%	• Only PF (60 Hz) component	
X-2	**New:** Type-II A, Type-II B, Type-II C, and Type-II D	5.0 kV$_{P-P}$	10%	• 3rd (180 Hz), 60° phase: 40% • 5th (300 Hz), 90° phase: 30% • 7th (420 Hz), 120° phase: 30%	
X-2	**New:** Type-II A, Type-II B, Type-II C, and Type-II D	5.0 kV$_{P-P}$	20%	• 3rd (180 Hz), 60° phase: 40% • 5th (300 Hz), 90° phase: 30% • 7th (420 Hz), 120° phase: 30%	
X-4	**New:** Type-II A, Type-II B, Type-II C, and Type-II D	5.0 kV$_{P-P}$	30%	• 3rd (180 Hz), 60° phase: 40% • 5th (300 Hz), 90° phase: 30% • 7th (420 Hz), 120° phase: 30%	
Y-1	**Aged (620 hrs):** Type-II C	10.2 kV$_{P-P}$	0%	• Only PF (60 Hz) component	
Y-2	**Aged (620 hrs):** Type-II C	10.2 kV$_{P-P}$	30%	• 15th (900 Hz), 0° phase: 100%	
Z-1	**Aged (635 hrs):** Type-II A **Aged (15 hrs):** Type-II E **New:** Type-II F	3.04 kV$_{P-P}$	0%	• Only PF (60 Hz) component	
Z-2	**Aged (635 hrs):** Type-II A **Aged (15 hrs):** Type-II E **New:** Type-II F	3.04 kV$_{P-P}$ (@ 420 Hz)	0%	• 1st (420 Hz), 0° phase: 100% [i.e. no harmonics but only fundamental of 420 Hz]	

The purpose of test cases X-1, X-2, X-3, and X-4 was to evaluate the electric field gradient before the PWM aging tests. Test procedure in Y-1 and Y-2 was used to access the effects of individual power frequency and a single 15th order harmonic on an aged test sample. In order to evaluate the electric field gradient between the aged and new termination sample, test cases Z-1 and Z-2 were chosen. Z-2 used higher frequency of 420 Hz as a fundamental without any distortion to evaluate the effects of harmonics separate from the 60 Hz fundamental.

Surface potential measurements were conducted at different positions along the cable termination length 2 mm to 4 mm away from the termination. Figure 4.8 illustrates the marked positions on the termination with 2 cm gaps. On each sample, ESV measurements were carried out at position (cm): 0, 1, 2, 3, 4, 5, 6, 7, 8, 8.5, 9, 9.5, 10, 10.5, and 11. From 0 cm to 11 cm, the potential distributes completely from the applied voltage to the zero potential. The Hi-K stress control tube and Hi-K stress control compound overlap with the insulation shield at around 9 cm of Figure 4.9. For measurement purposes, both applied voltage waveforms and voltage waveforms measured at the listed termination points were recorded and stored as a data file by a digital storage oscilloscope (DSO).
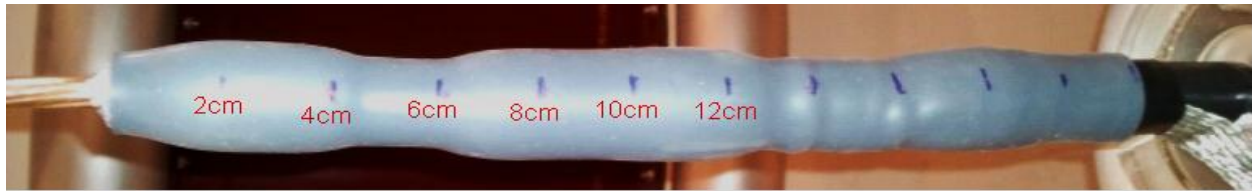
Figure 4.8: Termination sample with the marked positions to aid in the surface potential measurements

Before subjecting all the new cable termination under the tests listed above, PD measurements were performed. The PD measurements ensured that the each cable termination test sample was PD-free and verified the sample quality. As mentioned in Section 4.2.3, initial PD measurements were conducted according to IEC 61442 for accessories with $V_{L-N} = 8.7$ kV [119]. The indication of PD < 10 ρC for the 25% higher testing voltage level of 15 kV$_{RMS}$ ensured that the cable termination samples were prepared correctly without any human errors. This helped confirm that each installation was PD-free and any surface temperature rise observed during the applied stresses from the PWM and distorted waveform could be due to resistive heating as opposed to the PD activity in the termination sample. The PD measurements after the aging test were also used as a tool to detect the termination quality.

Chapter 5
Results and Discussion

This chapter presents the experimental results along with the discussions. The termination surface temperature rise observations are provided under the aging tests. Termination surface potential distribution plots and the tangential electric field distribution plots are provided under the electrostatic voltmeter measurements. Lastly, the results are discussed with the test termination sample analysis.

5.1 Experimental Results

Using the accelerated aging test procedures mentioned in Table 4.1 and the experimental setups explained in section 4.1.2 and section 4.21, the performance of the Type-II termination SG systems and Type-I termination SG systems was thermally examined for both HF and PF application. The effects of the stresses from the high frequency, high $\frac{dv}{dt}$ PWM voltage waveforms were investigated on the surface of the test samples.

Figure 5.1 shows the profile of change in maximum temperature on the surface of the Type-II A, Type-II B, and Type-II C under the testing conditions of Test Case A. The change in temperature is determined from the difference between the maximum hot-spot temperature and the room temperature, which were measured continuously for 620 hours (~26 days). The change in the temperature was saturated for Type-II A and Type-II D at 11°C, and Type-II C at 17°C after 4 hours under the test. Figure 5.2 illustrates a timeline that shows the thermal images captured at several intervals during the 620 hours of aging.
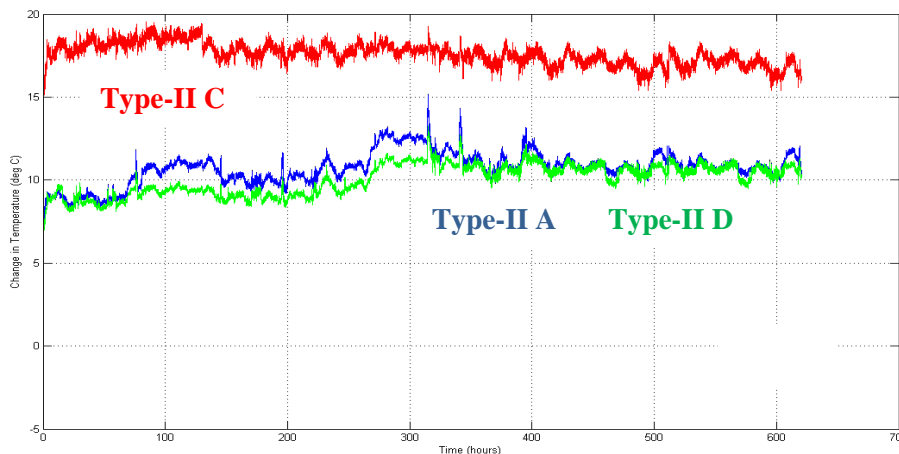

Figure 5.1: Change in maximum surface temperature profile of the Type-II A, Type-II B, and Type-II C under the aging conditions of PWM 17.2 kV$_{P-P}$ at 3.0 kHz for 620 hours
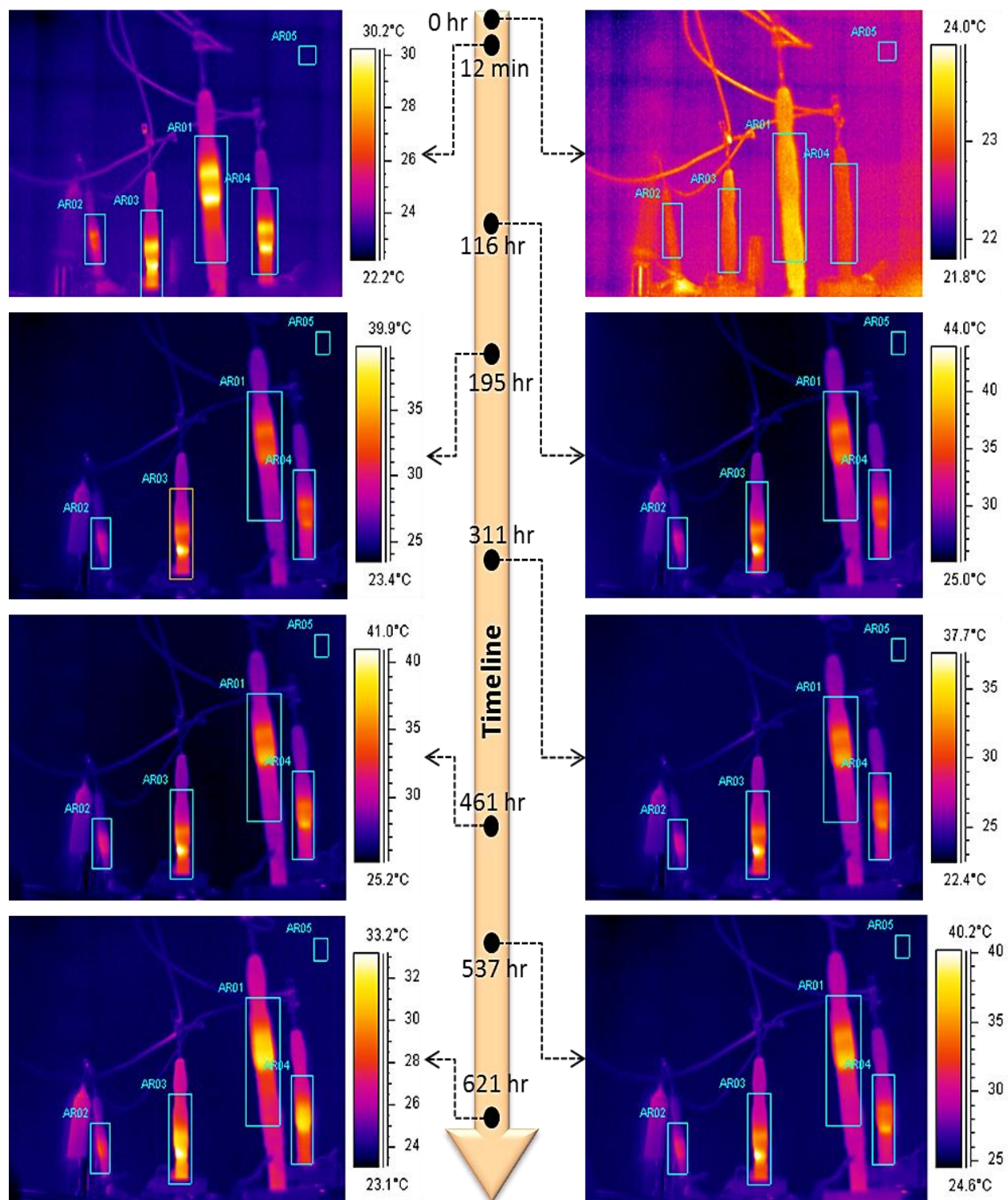
71

Figure 5.2: Thermal images illustrating the temperature variation with time during the aging of case A

From the experiment of Test Case A, it was observed that no PD was detected before or after 620 hours of aging. Moreover, the hot-spot temperature rise of as high as 17°C was observed without any influence of current circulation. The effect of the load current circulation would have stressed the cable insulation even more. The surface heating is thus caused by the application of high repetitive high $\frac{dv}{dt}$ voltage pulses without any external factors. In Test Case B, the aged sample Type-II A along with the new sample Type-II E were tested under the same testing conditions as Test Case A for 15 hours for comparative purpose. The maximum surface temperature profile rise for the aged sample Type-II A was expected to be steeper and greater compared to the new Type-II E sample. However, the surface temperature rise and distribution were very similar for both samples as shown in Figure 5.3. Figure 5.4 shows the profile of change in temperature on the surface of the aged sample Type-II A and new sample Type-II E under the testing conditions of Test Case B. In Test Case C, an aging test was attempted to determine the age of the sample at higher but sinusoidal voltage waveform using the PD setup described in section 4.2.3. The temperature rise was similar to that illustrated in Figures 5.1 and 5.4. The maximum surface temperature difference was 12°C when saturated after 1 hour 15 minutes. As shown in Figure 5.5, the surface temperature was significantly higher at the 2nd hour under PF component at the higher voltage of 38.0 kV_{RMS}, which is 4.75 times higher than the termination voltage ratings.
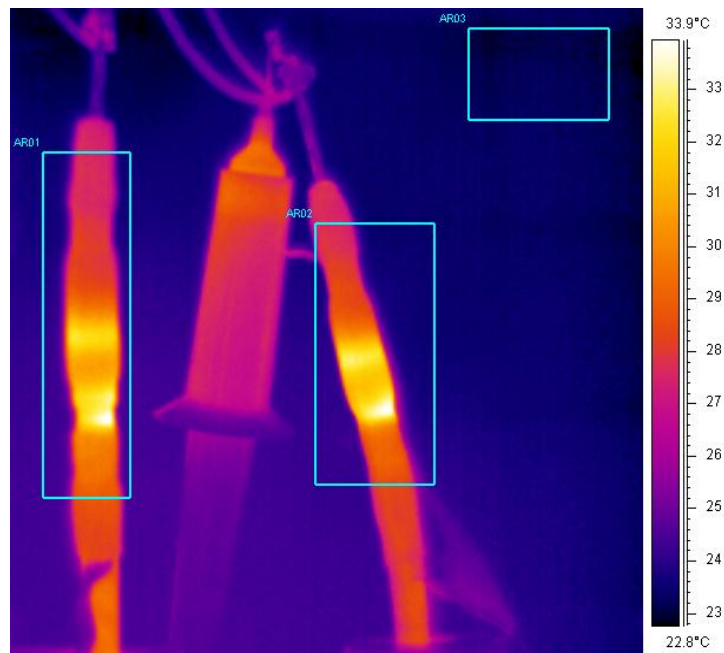
Figure 5.3: Thermal image of an aged sample Type-II A (right) and new sample Type-II E (left) at the 15th hour indicating temperature distribution and two hot-spots on each sample for Test Case A

Figure 5.4: Change in maximum surface temperature profile of aged Type-II A and new Type-II E under the testing conditions of PWM 17.2 kV$_{P-P}$ at 3.0 kHz for 15 hours

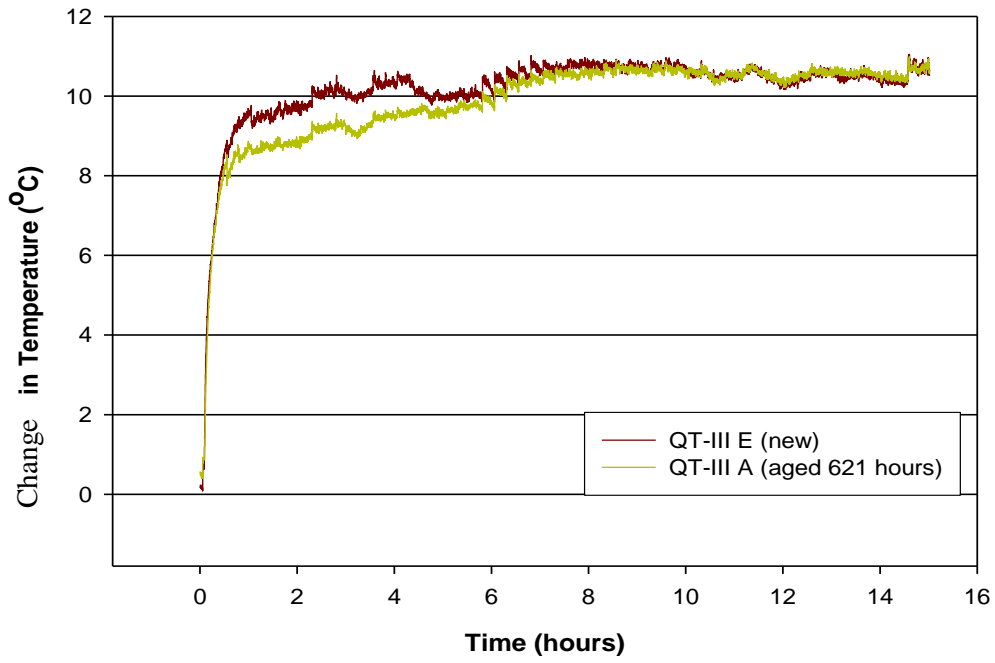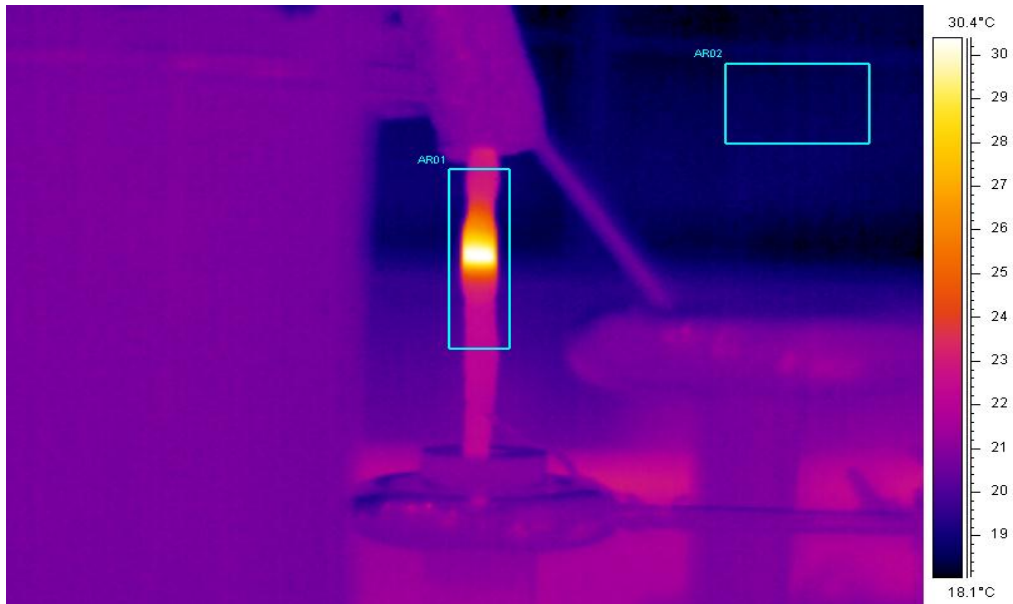**Figure 5.5:** Thermal image of an aged sample Type-II C at 1 hour 15 minutes mark indicating temperature distribution and a single hot-spot for Test Case C

The Type-II C sample did not show any PD during the online PD monitoring and aging for a span of 15 hours. An important observation of Test Case B is the formation of a two hot-spots under the HF PWM voltage waveform (Figure 5.3), as opposed to a single hot-spot as seen in Test Case C (Figure 5.5). The time duration for aging under the applied electric stresses of Test Case A, B, and C appeared to be short to degrade the newly prepared termination samples with BIL of as high as 95 kV_{RMS}. The aging tests on the Type-II samples were thus discontinued. The next case, Test Case D attempted to age the Type-I A sample under the PWM 17.0 kV_{P-P}, 3.0 kHz. Unlike Type-II samples, the Type-I A displayed a significantly lower change in the surface temperature. Periodic temperature monitoring indicated a maximum surface temperature rise of only 3°C. Relative to Type-II, the temperature change was significantly lower. When the Type-I A SG system integrity was checked using the PD setup after 200 hours, the sample punctured at the triple point with a snap sound that caused the protection signal to trigger and shut down the PD experiment. Figure 5.6 shows the dissected picture of a punctured Type-I A sample exactly at the triple point where the SG tape is overlapped on the region of XLPE insulation and the insulation shield. The breakdown occurred when the voltage level increased from 19 kV_{RMS} to 20 kV_{RMS}, at which the PD level rose significantly just before the breakdown. The failure in the SG system subjected to electric stress results from thermal deterioration; thus the SG layers and cable insulation may lose the mechanical strength, become more brittle, lose some mass, or even have lower electrical breakdown strength.

Figure 5.6: Punctured Type-I A at the triple point where the SG tape, XLPE insulation and insulation shield were connected during the PD measurements of Test Case D.

The purpose of the aging test of Test Case E was to re-verify the failure of the Type-I A. Type-I A SG layer was degraded in 200 hours of aging and failed thereafter. Following the failure of Type-I A, Type-I B was aged for 500 hours. Having aged the sample Type-I B for 500 hours, the maximum surface temperature rise observed was 3°C, which is insignificant and similar to that of Type-I A. No PD was detected at 30 kV$_{RMS}$ when Type-I B was measured after 500 hours.

In all the aging test cases, the end of the cable termination was expected in the functional accelerated aging test by a breakdown. No breakdown was observed within the insulation or the SG system of the Type-II even after aging for 635 hours. However, the only breakdown observed was for the case of Type-I A that occurred when conducting the PD measurements after aging of 200 hours.

The experimental surfaces potential measurements recorded using the ESV are presented. The SG system performance of the cable termination is evaluated with its ability to control the electric field below the breakdown strength of the surrounding. The setup introduced in Figure 4.7 and Figure 4.8 of Section 4.3 was used to measure the surface voltage waveform along the termination sample length at regular intervals indicated in Figure 4.9. The results of various test cases of Table 4.2 are combined to compare the behaviour of the termination samples under different levels of distortion. The applied THD voltage level was not an additional voltage built on top of the PF voltage component, but the THD component was incorporated within the original PF voltage waveform to have the same peak. In other words, when the distortion components were added, the original PF component was reduced so as to keep the peak-to-peak distorted voltage waveform same as the peak-to-peak voltage waveform without any distortion. Maintaining the constant peak-to-peak allowed to understand the influence of the distortion level while avoiding the influence of the increased voltage amplitude. In the power system grid, though, the harmonic components are added onto the PF component that increases the voltage amplitude, adding additional electric stresses.

Figure 5.7 illustrates the applied test voltage waveform and the measured voltage waveform at the region near the overlap of insulation shield and the stress control tube (i.e. 9 cm) on a new Type-II D sample for the test cases X-1, X-2, X-3, and X-4. As the applied THD level increases, the measured voltage waveform at 9 cm reflects the applied THD in a very similar manner, as noticed in Figure 5.7. The results of the peak-to-peak voltage measured at several points on the surface of Type-II termination samples are plotted in Figure 5.8 It can be observed from Figure 5.8 (a) to (d) that the surface potential remains almost similar for all the new Type-II samples under the THD level as high as 30% with very low order

harmonics. The THD level was changed from 0% to 30% to observe the dependency of the distortion on the stress control tube and Hi-K stress control compound.
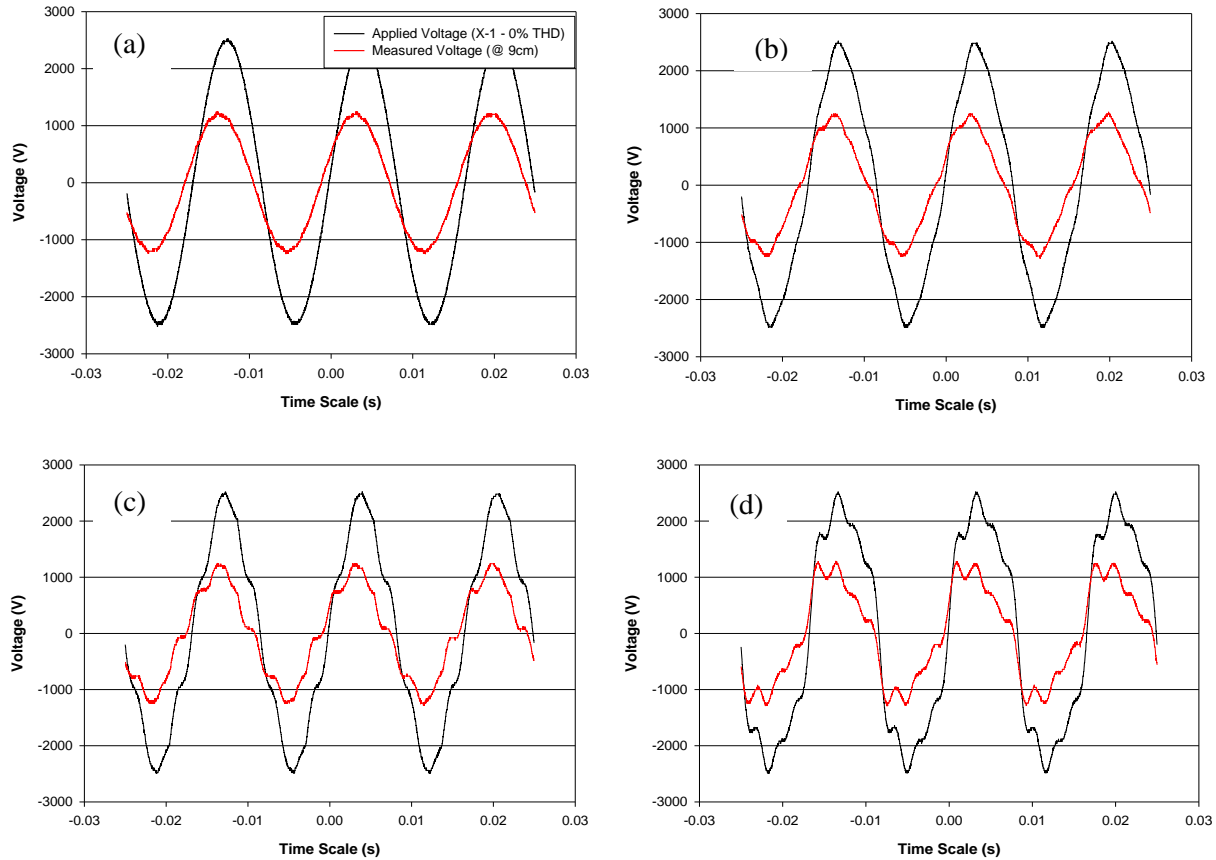

Figure 5.7: Voltage waveforms measured at the terminal (black) and at 9 cm from the top of the sealed termination (red) for the Test Case of (a) X-1 – 0% THD, (b) X-2 – 10% THD, (c) X-3 – 20% THD, and (d) X-4 – 30% THD

After the Type-II termination samples were aged for 620 hours, the observation on aged samples with the surface potential distribution and the associated electric field distribution was essential. The aged Type-II C sample was chosen for the study in Test Case Y-1 and Y-2 because Type-II C observed the hot-spot with the highest temperature difference of 17°C. A surface potential distribution at the high level of THD (30%) at 15th order harmonic was compared with the 60 Hz PF component, as provided in Figure 5.9. Similarly, test cases Z-1, Z-2, and Z-3 were executed to evaluate the potential distribution for the new and aged Type-II samples and to understand the behaviour purely under the distorted voltage component (i.e. only 420 Hz). The results of surface potential distribution for test cases Z-1-3 are provided in Figure 5.10.

77

(a)

Sample: QT-III A (New)
Applied Voltage: 5.0 kV$_{p-p}$

X-1 - 0% THD
X-2 - 10% THD
X-3 - 20% THD
X-4 - 30% THD

(b)

Sample: QT-III B (New)
Applied Voltage: 5.0 kV$_{p-p}$

X-1 - 0% THD
X-2 - 10% THD
X-3 - 20% THD
X-4 - 30% THD

SG   Semicon
XLPE
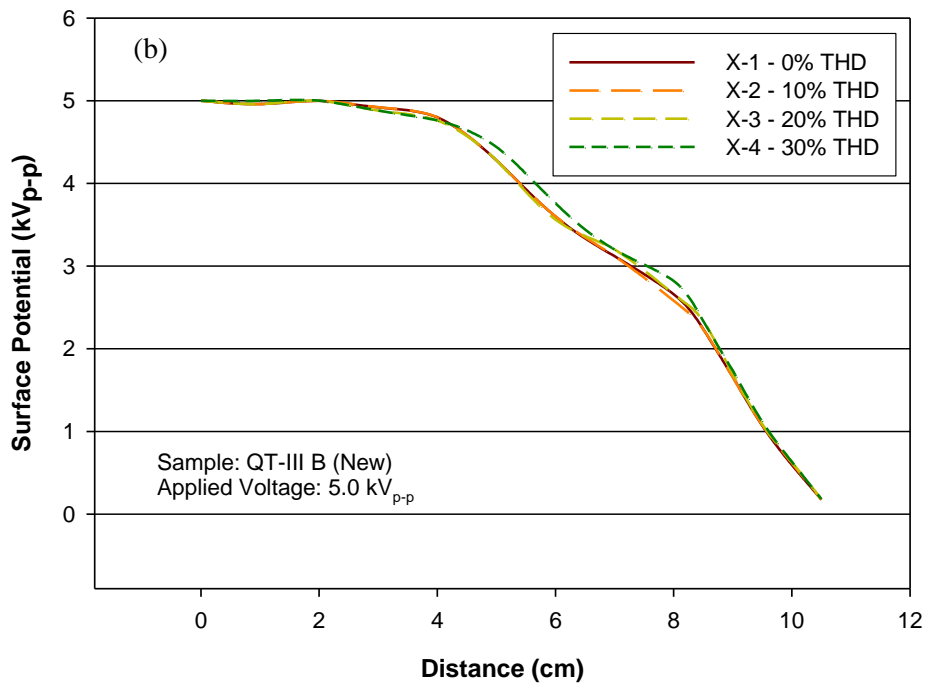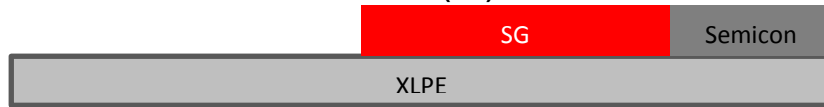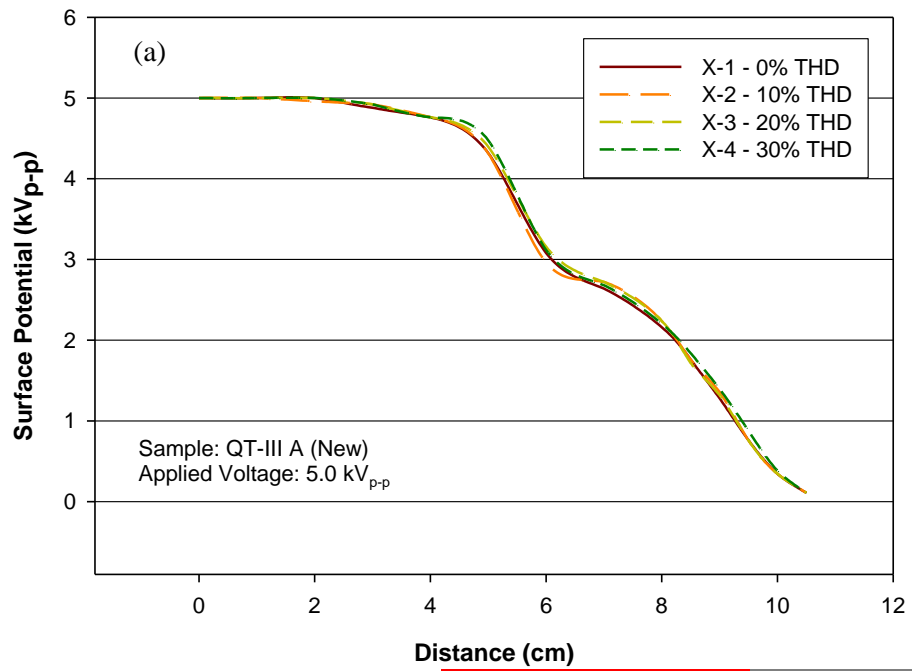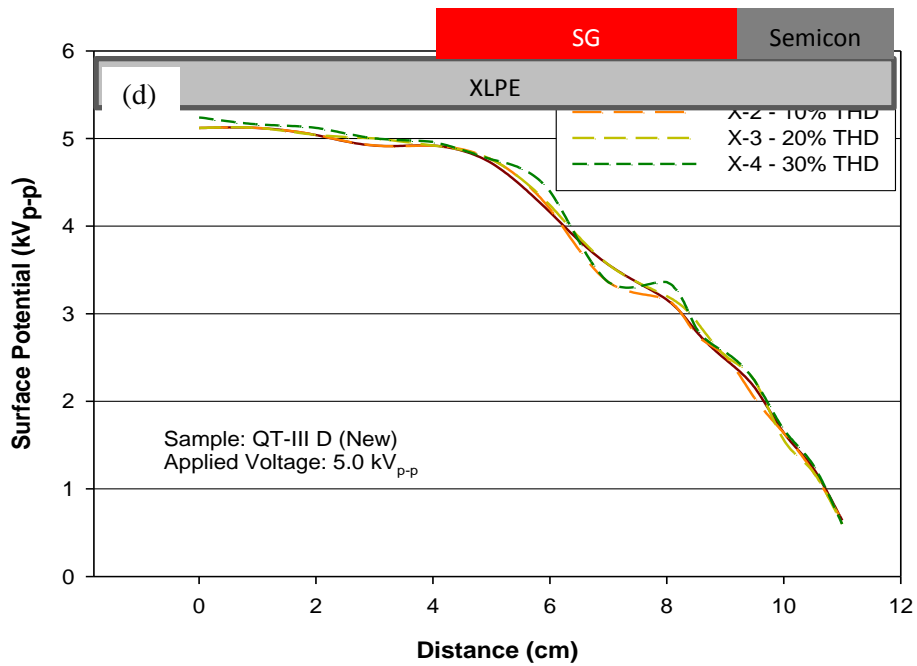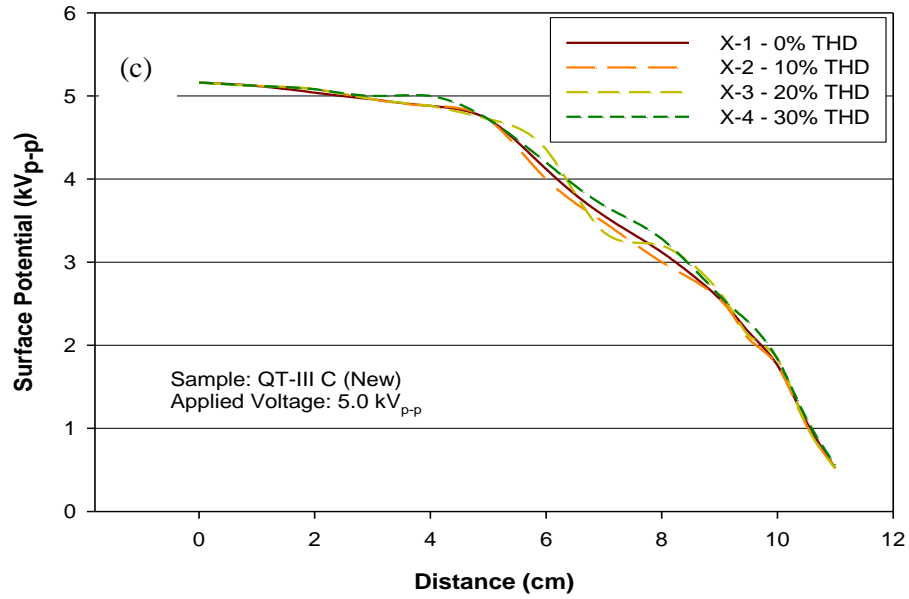
Figure 5.8: Electric surface potential distribution measured along the length of the new samples (a) Type-II A, (b) Type-II B, (c) Type-II C, and (d) Type-II D during the test cases of X-1, X-2, X-3, and X-4

Figure 5.9: Electric surface potential distribution measured along the length of an aged sample Type-II C during the test cases of Y-1 and Y-2
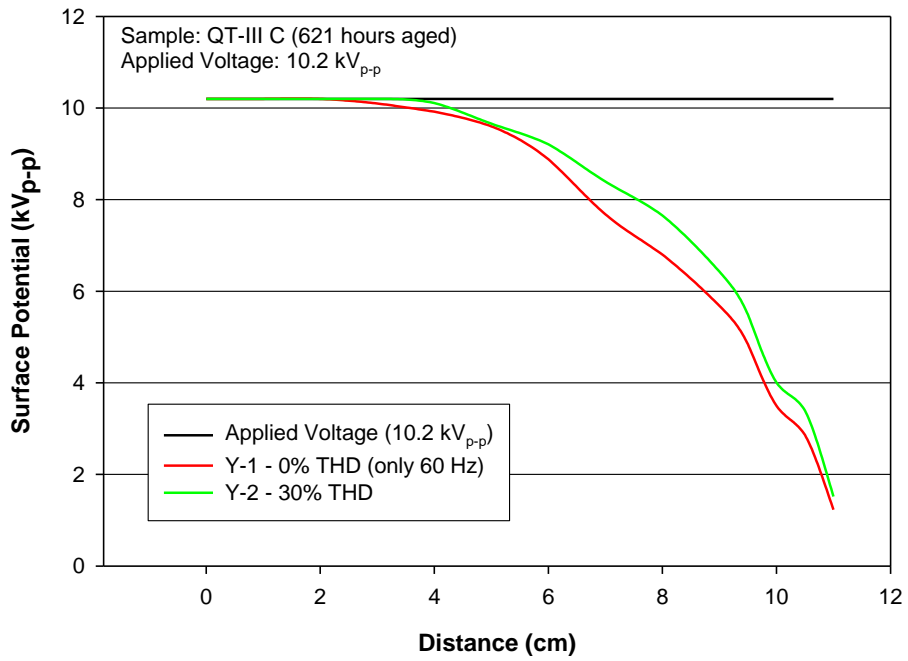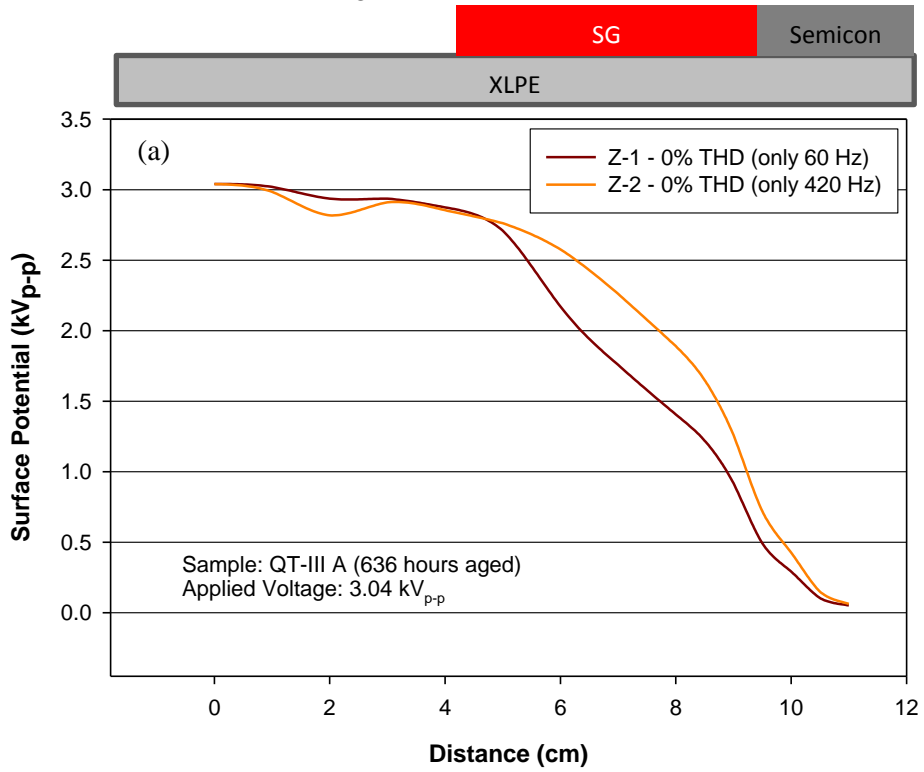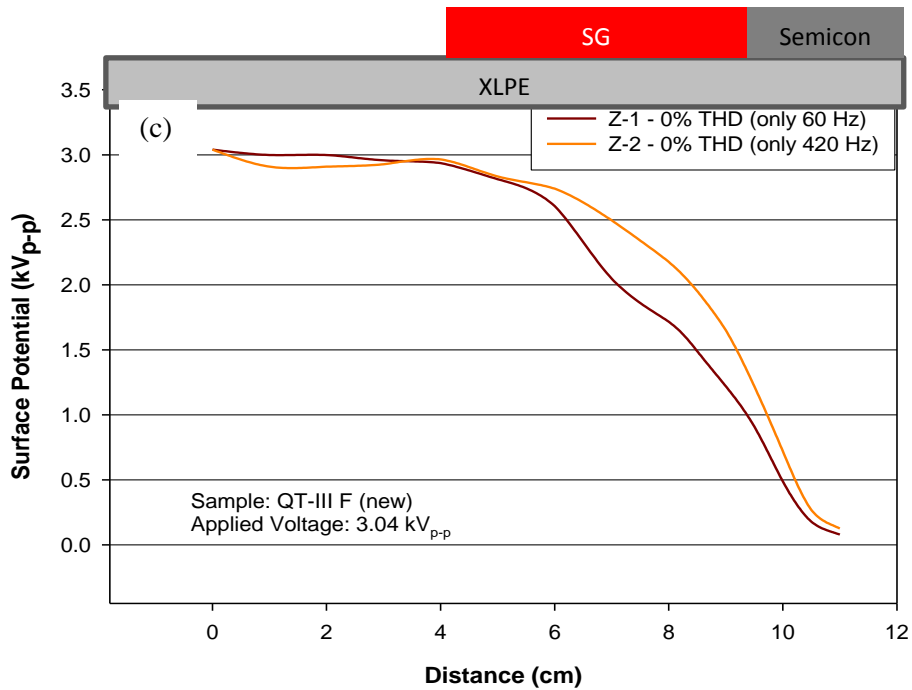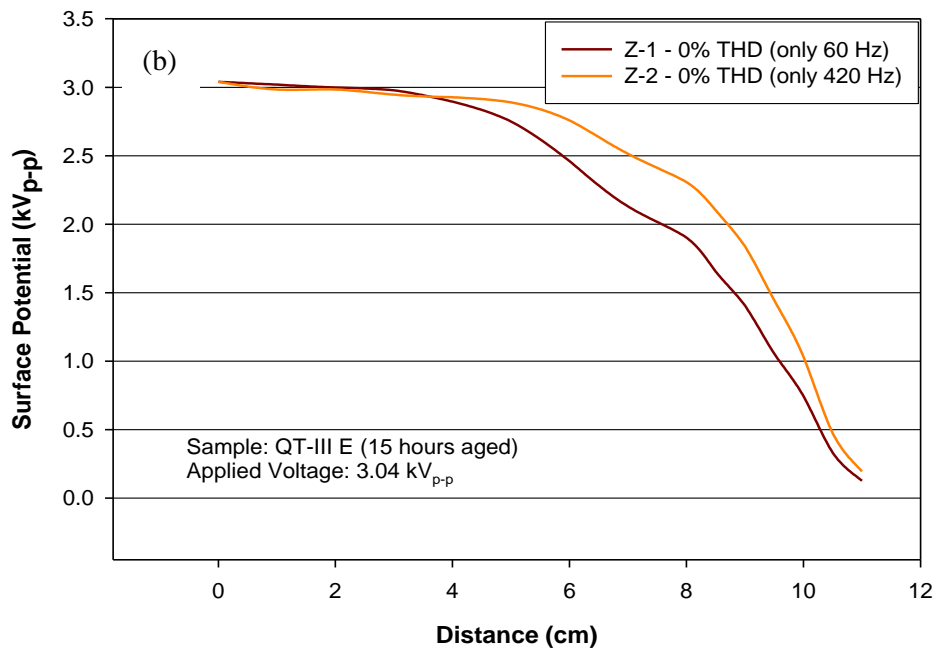
Figure 5.10: Electric surface potential distribution measured along the length of the (a) aged Type-II A, (b) little aged (15 hours) Type-II E, and (c) new sample Type-II F during the test cases of Z-1, Z-2, and Z-3

For the test cases of Y-1, Y-2, Z-1, Z-2, and Z-3, normalized quantities were plotted in Figure 5.9 and Figure 5.10 to ensure that the applied voltage and the measured voltage at the cable conductor (i.e. position of 0 cm) are exactly matched.

The performance of the SG systems at PF, and PF + THD was evaluated using the tangential electric field along the SG system, which is one of the most important factors and was calculated through the measurement of surface potential. The scalar quantity of distributed electric potential can be used to calculate the electric field. If the differential voltage change is calculated along a distance ds, then it is seen to be equal to the electric field component in that direction times the distance ds, as indicated in equation 5.1.

$$dV = -\vec{E} \cdot \vec{ds} = -E_s ds = -E_x dx - E_y dy - E_z dz \tag{5.1}$$

The electric field can then be expressed as:

$$E_s = -\frac{dV}{ds} = -\frac{\partial V}{\partial s} \tag{5.2}$$

The electric field in the partial derivative form of equation 5.2 can be expressed in the cylindrical coordinates as:

$$E_z = -\frac{\partial V}{\partial z} \tag{5.3}$$

Given the potential distribution along the surface of the termination (i.e. in the tangential direction), the electric field was computed in MATLAB™ in a tangential direction, E_z. The electric field plots for the test cases listed in Table 4.2 are provided in Figure 5.11, 5.12, and 5.13.
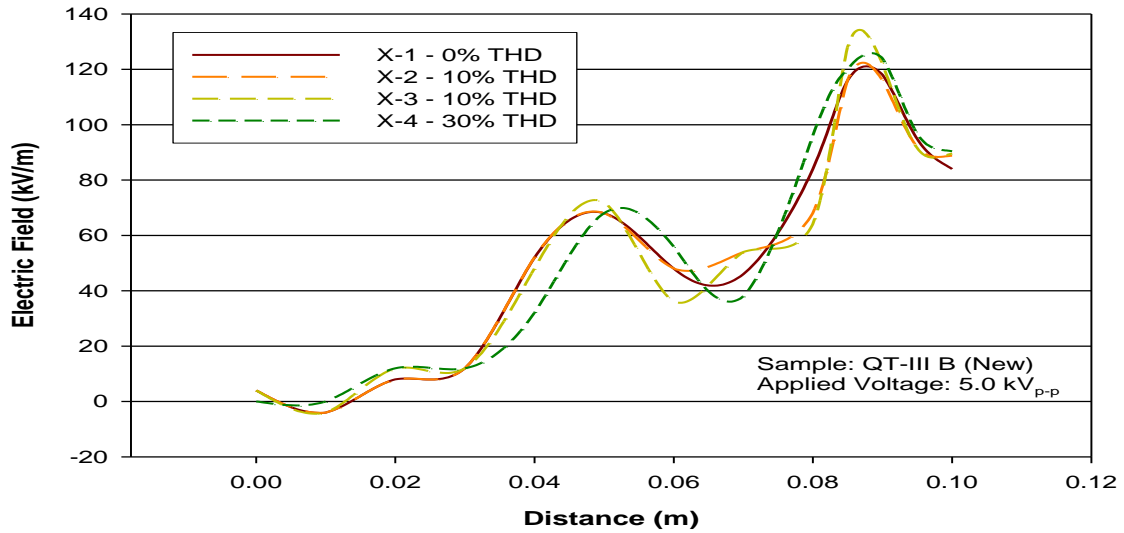
Figure 5.11: Electric field distribution along the length of the new sample Type-II B for the test cases of X-1, X-2, X-3, and X-4
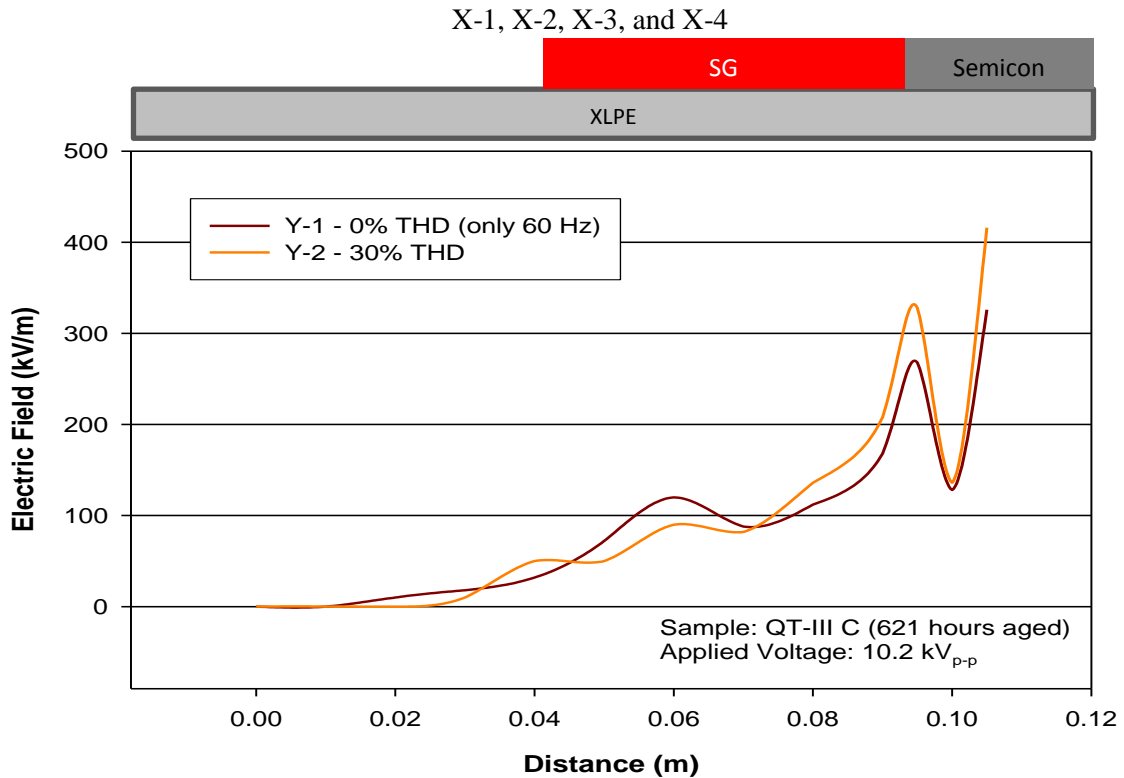
Figure 5.12: Electric field distribution along the length of the aged sample Type-II C for the test cases of Y-1 and Y-2
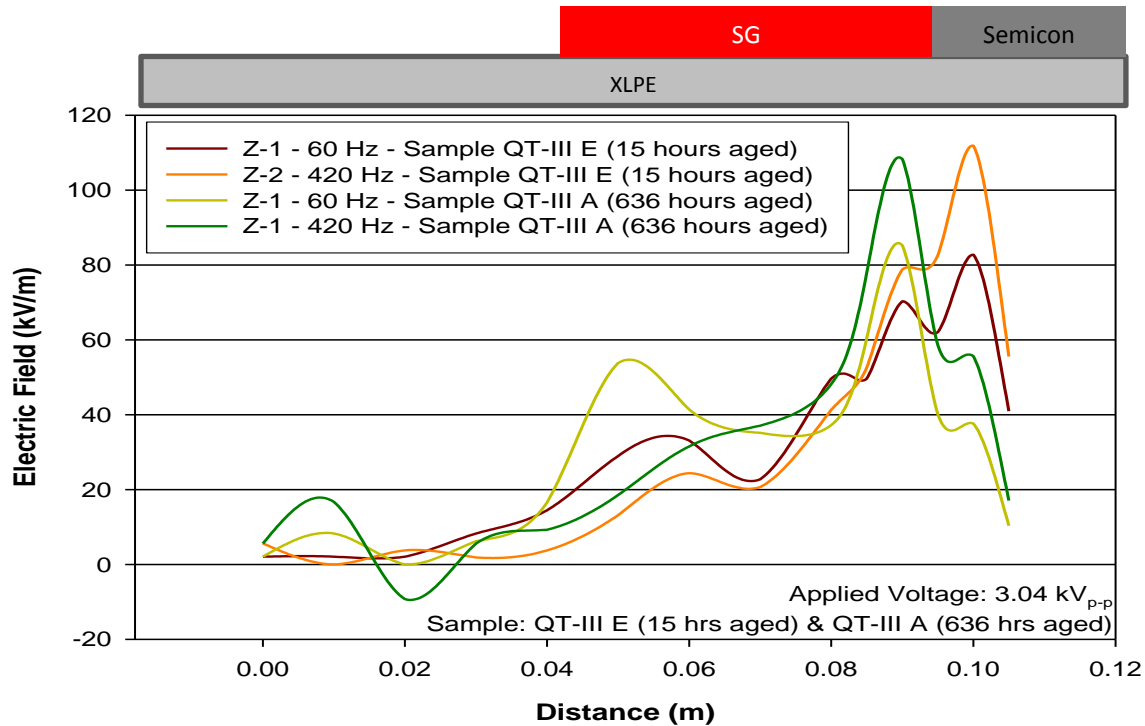
Figure 5.13: Electric field distribution along the length of the 15 hours aged sample Type-II E and 635 hours aged sample Type-II C for the test cases of Z-1 and Z-2

The electric field enhances greatly in the overlap region (i.e. at around 9 cm) for all the test cases as expected. The region where the SG tube and Hi-K SG compound intersect the insulation shield and XLPE insulation, observes higher electric stress with an increased level of distortion and frequencies. The increment in the electric field relative to the electric stress applied by PF 60 Hz component at this triple point region is: 0% (10% THD), 10.3% (20% THD), and 5.1% (30% THD) for the Test Case X (Figure 5.11); 23.8% for the Test Case Y (Figure 5.12); 22.5% (15 hours aged Type-II E) and 27.1% (635 hours aged Type-II A) for the Test Case Z (Figure 5.13). The electric field enhancement for Test Case Y (Figure 5.12) and Test Case Z (Figure 5.13) was significant because of a noticeable steep change in the surface potential distribution in the overlap region of Figure 5.9 and Figure 5.10. The magnitude of the electric field was low because of the lower than rated applied voltage for the surface potential measurements, which serves the purpose of comparing the two cases.

The method adopted in this study of measuring the surface potential in one dimension restricted the computation of electric field only in the tangential direction along the surface of the sample. Though away from the cable ends, the electric field is purely radial and confined within the outer conductor; the field in the cable's end is no longer radial and a tangential field component is introduced. So the

84

tangential component was expected to be the major electric field component along the SG system. However, because the stress grading layers are not homogeneous and uniform, particular at overlaps, the normal of the electric field must be studied separately. In Appendix C, a 2D-axial FEM simulation using COMSOL^{TM} Multiphysics was conducted to get an idea of the normal component of the electric field.

5.2 Discussions

This section discusses the experimental results presented in Section 5.1. The experimental results are being related to the theories from the literature. The discussion reasons the distortion and frequency observed in the experimental results. Analysis of the test terminations is also presented. Additional material characterization results are used to interpret the behaviour of Type-II and Type-I samples. The results of the scanning electron microscopy/energy dispersive microscopy (SEM/EDAX) are presented in Appendix B. The results of the FEM simulation are presented in Appendix C.

The aging tests of Table 4.1 under PWM waveforms on the Type-II samples were discontinued because there were hardly any signs of aging through the PD under the applied testing conditions. During the test, no surface discharge and after the test, no change in PD level was observed. However, the temperature rise in the non-linear resistive SG system increased significantly when energized with relatively smaller applied stress with the PWM repetitive fast pulses under the severe electric stress. The testing conditions were much severe than the actual service conditions. The actual MV motor drives with multi-level PWM drives generally having a slower rise time, and lower switching frequency than those used in this study. Thus, the possible small degradation was only through the resistive losses that were noticed through the rise in the surface temperature and formation of hot-spots. As observed in Test Case B, new sample Type-II E saw a very similar change in temperature rise profile to that of the 620 hours aged sample Type-II A. The surface temperature rise remained constant throughout the 620 hours duration. Thus, the surface temperature rise observed under HF stress was attributed to resistive heating and not the PD activity. The maximum temperature rise of 17°C is related to the percolation theory which is related to the statistical distribution of the conductive filler in the host polymer matrix. The stress control tube and compound of the Type-II was percolated (i.e. the threshold or critical filler concentration has reached beyond which the matrix is electrically conductive).

Aging test results indicated that the SG system of the Type-I samples had a much lower temperature rise than the non-linear resistive SG system of Type-II. The maximum surface temperature rise of only 3°C and no formation of hot-spot implied that Type-I sample was capacitively graded at the applied electric

field (i.e. HF stresses using PWM generator). Dissipation factor plot of Figure 3.3 indicates that Type-I could start to behave as a non-linear resistive field grading material under very high electric field due to increasing dissipation factor. The percolation of the stress grading layers of the Type-I had not reached to make the mixture electrically conductive. The attribute of the capacitively graded SG system gave such a low temperature rise. There is no significant resistive loss associated to the silicone tape, stress control compound, and silicone grease of the Type-I, which is reflected in the negligible surface temperature rise. However, the performance of the Type-I SG system during a long term aging was susceptible to degradation in the region where the silicone grease is applied. The fact that a 200 hours aged sample Type-I A breakdown at the overlap of the taped silicone and the insulation shield when the PD measurements were conducted showed that a capacitively graded SG system is vulnerable to long term aging under the HF electric stress. Another possible cause of the Type-I sample breakdown was the disappearing of the silicone lubricant on the overlap region due to absorption by the insulation material. The lubricant composed of fluid and solid filler could have dried-out during the aging. This would have resulted in the decrease in breakdown strength along the interface of the silicone tape and insulation shield. Other possible cause of the puncture in the termination was treeing in the XLPE insulation. Combination of these issues possibly caused significant rise in the PD just before the breakdown at the triple point.

Power dissipation is an obvious issue related to designing of a non-linear SG material. Power dissipation during a lighting impulse or rare transients is not of much consequence, as the event is normally too short to cause appreciable heating [93]. Even the joule heating problem can be solved by increasing the strength of the non-linearity (suggested non-linearity factor, $\alpha = 20$ by ABB). However, the steady state power dissipation is problematic for the non-linear SG materials that could even cause hot-spots. The two hot-spots in the motor coils were observed by F.P. Espino-Cortés and E. Sharifi-Ghazvini, who analyzed how the waveform parameters affect the resistive heat produced in stress grading coatings of motor coils fed by adjustable speed drives and the intensity of both the hot-spots [68, 111]. For a cable termination, a similar formation of two hot-spots under the HF PWM was observed for Test Case B (Figure 5.3), while a single hot-spot was observed in Test Case C (Figure 5.5). The cause of the formation of two hot-spots in the termination is similar to that in a motor coil insulation system [111]. Electric field enhancement and surface discharge are the two main causes of the second hot spot (i.e. the hot spot near the region of ground conductor and insulation shield), which are sensitive to the pulse rise time and the repetition rate of the PWM voltage waveform. A smaller rise time (faster pulses) caused an intense hot spot at the

86

insulation shield end, while a larger rise time (slower pulses) caused a slightly higher temperature in the SG region.

Referring to Figure 2.9, the non-linear resistively graded SG system is described with the impedances and admittances. To account for both, conductivity and permittivity, the equivalent circuit model consists of resistor in parallel with a capacitor. Ignoring the resistance of the XLPE insulation along the capacitance of the SG system will reduce the circuit into a lumped R-C cascade network. The total power loss thus becomes:

$$P_{Loss} = \sum_{k=1}^{n} \frac{|V_{k+1} - V_k|^2}{R_k}$$

(5.4)

where k = 1, 2, ..n, n is the number of resistive SG segments, node voltage V_k and R_k represents the resistance of the kth segment of the SG system.

Though increasing the SG length would reduce the chances of flashover and tracking, the increase of the length of the SG system through the use of more segments would increase the power loss in the SG system. The frequency of the applied voltage has a direct effect on the insulation lumped capacitive reactance, which in turn will affect both the voltage and impedance values.

SEM/EDAX results (Appendix B) suggests that stress control tube was formulated by filling a polymeric dielectric with conducting particles (carbon) below percolation in order to raise the field in the dielectric between particles. The Hi-K stress control tube was likely the dielectric filled with a non-linear material based on SiC, both of which are used commercially in non-linear SG materials. The dielectric constant and dissipation factor of the Hi-K stress control compound with respect to electric stress was computed by the 3M engineers involved in the design of the Hi-K stress control compound, which is provided in Figure 5.14 illustrating its stability at electrical stresses up to 2050 V/mm [115].
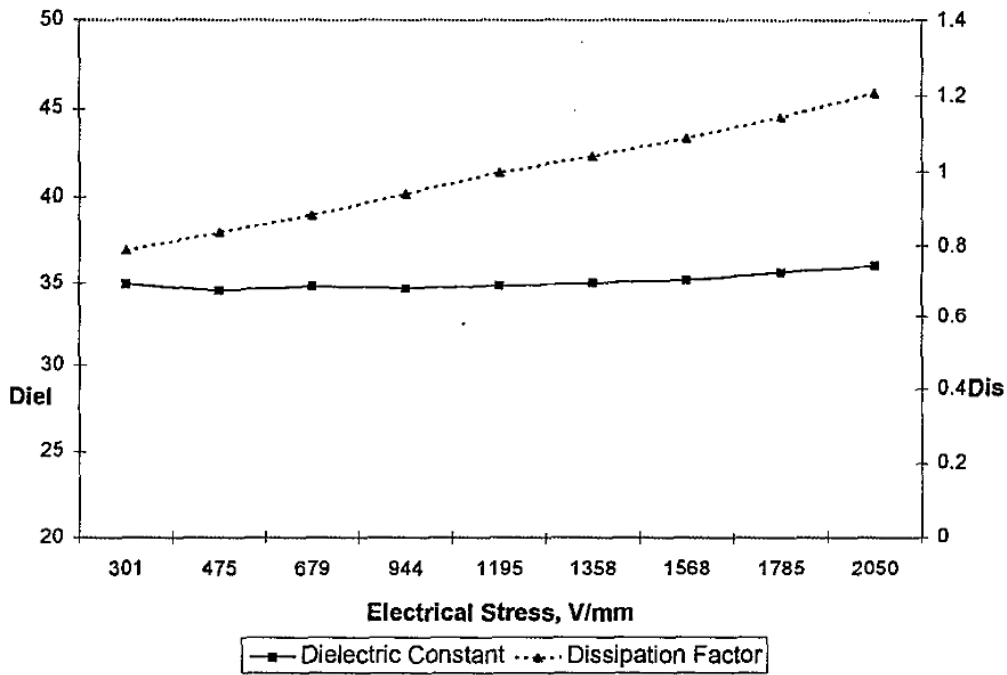
Figure 5.14: Dielectric constant and dissipation factor of the Hi-K stress control compound as a function of electric stress [115]

For the Hi-K stress control compound, the maximum electrical stress adjacent to the end of the insulation shield was about 550 V/mm on the inside of the termination and 350 V/mm on the outside of the termination for a 15 kV tubular termination on a 1/0 AWG conductor with 5.6 mm (220 mils) thick insulation at 8.7 kV [115]. The lower electric stress inside the termination was expected to produce low dielectric heating when subjected to power frequency for extended periods and withstand PF voltage, which was verified in the experiments. Moreover, the lower electric stresses on the outside of the termination allowed a suitable flashover withstand voltage, particularly during the PWM waveforms.

R.A. Wandmacher, et al. did not provide the dielectric constant and dissipation factor results of the other overlapped SG layer, i.e. the stress control tube [115]. An experimental report (Figure 3.3) provided by the suppliers, the Type-I stress control tube, which is still an integral part of the Type-II termination, had a dissipation factor of as high as 17 at the electric stress of 30 V/mil or 1180 V/mm. Overlapping both the SG layers would certainly add to the reported dissipation factor of Figure 3.3 (e.g. the dissipation factor would become approximately 8.8 when the electric stress is 1180 V/mm).

Figure 5.8 - 5.10 show how the potential increases away from the conductor towards the insulation shield along the SG layers. The dependency of the distortion level on the SG layers of the termination was

88

observed through the incremental electric field. The insulation shield acts almost like a ground potential while all the stress relief occurs in the stress control tube and Hi-K stress control compound. The potential distribution is disturbed under the distorted voltage waveforms. High field strength was present at the triple point location at overlap of insulation shield, XLPE insulation, and Hi-K stress control compound. The experimental electric field profiles of Figures 5.11 - 5.13 correlate with the simulated normalized electric field profiles, as indicated in Appendix C. There is a reasonable agreement between the FEM simulations and the measurements with the ESV.

The conductivity of the non-linear stress control tube in the high field region will become very high unless the dielectric time constant becomes comparable to the time constant of the applied voltage. In other words, the space charge formation in the dielectric must limit the electric field; otherwise, the electric field will become very high. The electric field must cause the non-linear conductivity to adopt a value which results in a dielectric time constant comparable to the time constant of the applied voltage, which can be formulated mathematically as:

$$\tau = \frac{\varepsilon}{\sigma(E)} = \frac{1}{\omega} \quad \text{or} \quad \sigma(E_{lim}) = \varepsilon\omega \tag{5.5}$$

where τ is the dielectric time constant which is also inverse of the applied frequency ω.

In a non-linear SG material, the conductivity is an exponential function of electric field in the form of equation 4.1. The effective frequency increases as the harmonic n^{th} order increases and the distortion level increases, which also increases the space charge limited field. As the space charge limited field region concentrates, the electric field enhances since the integral of the electric field is equal to the applied voltage. This is the reason for seeing higher and dispersed electric field distribution in Figures 5.10 – 5.13 for the case of increased THD level. The effect of frequency on the field distribution over the SG system was significant. The stress control tube conductivity at normal operating fields of 60 Hz would probably be relatively low that the system would be capacitively graded rather than being graded by the non-linear properties of the tube.

Chapter 6

Conclusion and Suggestions for Future Work

This chapter summarizes the research work on the cable termination SG system under the influence of poor power quality, and important conclusions and recommendations are derived based on the results obtained from the surface potential measurements, surface temperature monitoring, and partial discharge measurements. Suggestions to continue the cable termination research work in this field are also made.

6.1 Summary and Conclusions

In this work, the performance of the stress grading system of a commercial cable termination was studied under the condition of poor power quality, associated with the increasing penetration of the distribution generation and increased use of the power electronic components in the power system grid. In particular, the effects of the low order harmonics and the high frequency and high $\frac{dV}{dt}$ voltage waveforms on two types of termination samples, Type-I and Type-II, were studied. Aging tests were performed using the pulse width modulated high-voltage generator to understand the impact of high frequency stress on stress grading system of the cable terminations. Thermal diagnostic technique was utilized to observe the temperature rise and hot-spot development on the surface of the cable termination. Moreover, the potential was measured using the electrostatic voltmeter along the length of the termination samples under the application of power frequency, experimentally generated distorted voltage waveforms composed of fundamental and low order harmonics. The surface tangential electric field was computed based on the gradient of the termination surface potential for analysis. The stress grading layers for both the samples were examined under the scanning electron microscopy/energy dispersive microscopy to understand the material properties.

From this work, the following conclusions are derived:

1. The electrical field enhancement occurred near the triple point of the Type-II sample where the stress grading layers overlap with the insulation shield and XLPE insulation when the voltage waveform was distorted with the added low order harmonic components. The level of total harmonic distortion reflected the electric field enhancement on the termination sample.

2. The aging test with high frequency and high $\frac{dV}{dt}$ components increased surface temperature of the Type-II sample significantly and developed two hot-spots near the triple point region, while the

temperature rise for the Type-I sample was negligible and no hot-spots were developed. The two hot-spots developed primarily are due to electric field enhancement which is sensitive to the pulse rise time and repetition rate. The cause of the heating in the Type-II stress grading system was resistive loss and not the discharges as identified by the partial discharge measurements. This implies faster insulation degradation with the increase in the dissipation factor which is caused by the resistive heating. A likely early cable termination failure is not only a reliability issue but also a loss of asset which translates to the financial loss. The Type-I cable terminations currently aging under the grid could spontaneously see the end of its life due to deteriorating power quality from the DG integration. The temperature rise in both types of terminations is essentially caused by the resistive losses under the application of high frequency component. Such resistive losses are of a great concern when the DGs would be integrated to the power system network as the power electronic components of the DGs add high frequency components to the network.

3. The stress grading system of the Type-I termination samples behaved as capacitively graded under the PF and HF components, while Type-II termination samples behaved as a non-linear resistively graded under the high frequency components and capacitively graded under low frequency components (i.e. low electric field). This claim can be supported by (A) the significant temperature rise seen on the surface of the Type-II under HF electric stresses and negligible temperature rise on the Type-I surface, (B) dissipation factor vs. electric field plot (Figure 3.1 and Figure 5.14) showing the escalation of dissipation factor significantly beyond DF = 1 as a function of electric field, and (C) the presence of large conductive elements in the stress grading layers as observed through the scanning electron microscopy/energy dispersive microscopy (Appendix B).

4. Type-I has a better capacitively graded stress grading system even at higher electric fields compared to the Type-II below the rated voltage. This can be concluded since (A) the surface temperature rise for the Type-I was much lower compared to that of the Type-II during the aging tests and (B) Type-I have a lower dissipation factor for a field below 866 V/mm (22 V/mil).

5. In this work it is demonstrated that the electrostatic voltmeter can be utilized to scan the cable termination surface for the potential measurements, which can be used to compute the electric field distribution in the tangential direction along the termination length to identify the electric stress enhancement.

It is recommended to apply the capacitively graded termination in the grid where the distortion levels are low. Under the increased total harmonic distortion levels and HF components, capacitively graded termination may not be adequate and non-linear resistively grading becomes more beneficial. Since non-linear resistively graded termination dissipate energy at levels that are not acceptable under normal operating conditions, the nonlinearity of the resistive stress grading must be improved that lowers the dissipation factor and resistive losses at the higher electric field while aiming for a uniform surface potential distribution. A high degree of stress grading nonlinearity can bring a great simplicity, which can be achieved with the use of ZnO as opposed to the SiC filler in Hi-K stress control compound. If the nonlinearity of the resistive stress grading material is improved, the additional stresses posed by the high frequency components and harmonics can be tolerated to a greater degree. Such a change in the power system network to replace the currently aging cable terminations having low nonlinearity comes with a huge financial cost, which is not practical. The improved terminations can be applied wherever the power system expansion is taking place.

To address the issue of the currently installed cable termination with low degree of nonlinearity, the utilities could get involved to take preventive maintenance on medium voltage power cable accessories by testing and analyzing the overall insulation of the cable termination, and determine the serviceability of the termination through the data trending to prevent the termination failure before it actually occurs. The experimental results suggesting electric field rise of as high as 27.1% and surface temperature rise of as high as 17°C at the triple point of the cable termination envisions a threatening futuristic power system network problem. The integration of the DGs in the power system network should be viewed more broadly by considering the potential serious side-effects of the poor power quality.

6.2 Suggestions for Future Work

This section gives some suggestions for future work to take the cable termination study to a next level to increase the knowledge base about the subject.

To degrade the cable termination samples even further such that partial discharges are detected, an experiments conducted over a longer aging term are suggested. The applied electric stress should be increased by increasing the applied voltage and frequency from the generator source. The voltage capacity of the PWM generator at the HVEL should thus be improved to add additional electric stresses. The experimental work can be extended to other cable accessories such as cable splices or higher voltage cable terminations (69 kV or greater). Testing the termination sample on a live power system grid is

suggested at the point of common coupling where the wind farm is connected as a realistic test case. A termination can also be tested on different locations of the grid where the level of total harmonic distortion differs. A high frequency electrostatic voltmeter should be used to scan the termination surface for potential measurements under the high frequency electric stresses.

An experiment can be performed with different types of power quality issues including voltage transients. Long term instantaneous voltage data from utilities would help in identifying the power quality issues and generate similar waveforms in the research laboratories. As a diagnostic technique, the diameter of the termination surface at the triple point should be monitored to detect any thermal expansion of the stress grading layers caused by the joule heating.

The terminations should be divided in different classes for operation under different types of waveforms and different levels of total harmonic distortion. Better stress grading layers with superior non-linearity should be developed in the HVEL and then tested against long term aging experiments.

A development of a computational model is suggested to precisely understand the joule heating phenomenon that would translate the termination surface temperature rise to the resistance and operating condition of the termination (i.e. capacitively behavior or non-linear resistively graded behaviour).

Further study in this area should allow utilities to develop a framework to allow a coherent view of the interaction between models of failure mechanisms and network performance. A framework should provide a platform for integrated asset management using existing knowledge of dielectric ageing mechanism and condition monitoring. A solid plan by utility to monitor the failure of the electrical insulation components including cable terminations under the rise of the DG would prove the authenticity of this work.

Cable manufacturers are suggested to develop robust cable terminations with increased nonlinearity that can sustain distorted voltage and high frequency pulses over the entire duration of cable termination's nominal design life. With the awareness of the potential threat on the cable termination, researchers are suggested to focus in the area of distribution generation to investigate and resolve the rising power quality issues. Moreover, the idea of adding a DC feeder to the distribution network could be further explored to resolve the cable termination insulation integrity problem described in this work for the future termination installations on the DC network.

References

[1] "IEEE Standard Dictionary of Electrical & Electronics Terms," IEEE Journals and Magazines, Geoscience and Remote Sensing, IEEE Transaction on, Volume: GE-18, Issue: 1, 1980.

[2] "IEEE Recommended Practice for Monitoring Electric Power Quality," *IEEE Std 1159-2009 (Revision of IEEE Std 1159-1995)*, pp.c1-81, June 26 2009.

[3] J.K. Phipps, J.P. Nelson, and P.K. Sen, "Power quality and harmonic distortion on distribution systems," *Industry Applications, IEEE Transactions on*, vol.30, no.2, pp.476-484, Mar/Apr 1994.

[4] M.I. Marei, E.F. El-Saadany, and M.M.A. Salama, "A novel control algorithm for the DG interface to mitigate power quality problems," *Power Delivery, IEEE Transactions on* , vol.19, no.3, pp. 1384- 1392, July 2004.

[5] M.S. Witherden, R. Rayudu, and R. Rigo-Mariani, "The influence of nonlinear loads on the power quality of the New Zealand low voltage electrical power distribution network," *Universities Power Engineering Conference (AUPEC), 2010 20th Australasian*, pp.1-6, 5-8 Dec. 2010.

[6] Ontario Power Authority. "What is Feed-in Tariff Program?" Internet: http://fit.powerauthority.on.ca/what-feed-tariff-program, 2010 [Apr. 23, 2012].

[7] U.S. Department of Treasury. "Renewable Energy Grants." Internet: http://www.dsireusa.org/incentives/incentive.cfm?Incentive_Code=US53F, Nov. 19, 2011 [Apr. 23 2012].

[8] L. Paulsson, B. Ekehov, S. Halen, T. Larsson, L. Palmqvist, A.A. Edris, D. Kidd, A.J.F. Keri, and B. Mehraban, "High-frequency impacts in a converter-based back-to-back tie; the Eagle Pass installation," *Power Delivery, IEEE Transactions on*, vol.18, no.4, pp. 1410- 1415, Oct. 2003.

[9] H. Bevrani, A. Ghosh, and G. Ledwich, "Renewable energy sources and frequency regulation: survey and new perspectives," *Renewable Power Generation, IET*, vol.4, no.5, pp.438-457, Sept. 2010.

[10] B. Florkowska, M. Florkowski, J. Roehrich, and P. Zydron, "The influence of PWM stresses on degradation processes in electrical insulation systems," *Electrical Insulation and Dielectric Phenomena (CEIDP), 2010 Annual Report Conference on*, pp.1-4, 17-20 Oct. 2010.

[11] D. Patel, R.K. Varma, R. Seethapathy, and M. Dang, "Impact of wind turbine generators on network resonance and harmonic distortion," *Electrical and Computer Engineering (CCECE), 2010 23rd Canadian Conference on*, pp.1-6, 2-5 May 2010.

[12] Garrad Hassan and Partners Limited. "The Impacts of Increased Levels of Wind Penetration on the Electricity Systems of the Republic of Ireland and Northern Ireland: Final Report." Internet: http://www.cer.ie/cerdocs/cer03024.pdf, Feb.2003 [Apr 25, 2012].

[13] H. Jinwei, Y. Wei Li, and M.S. Munir, "A Flexible Harmonic Control Approach Through Voltage-Controlled DG–Grid Interfacing Converters," *Industrial Electronics, IEEE Transactions on*, vol.59, no.1, pp.444-455, Jan. 2012.

[14] S. Bahadoorsingh and S.M. Rowland, "The Relationship Between Insulation Ageing and Power Network Performance," *Solid Dielectrics, 2007. ICSD '07. IEEE International Conference on*, pp.180-183, 8-13 July 2007.

[15] A. Laxson, M.M. Hand, and N. Blair, "High Wind Penetration Impact on U.S. Wind Manufacturing Capacity and Critical Resources." Internet: http://www.nrel.gov/docs/fy07osti/40482.pdf, Oct. 2006 [Apr 25, 2012].

[16] N. Miller and Z. Ye, "Report on Distributed Generation Penetration Study." Internet: http://www.nrel.gov/docs/fy03osti/34715.pdf, Aug. 2003 [Apr 23, 2012].

[17] M.S. Witherden, R. Rayudu, and R. Rigo-Mariani, "The influence of nonlinear loads on the power quality of the New Zealand low voltage electrical power distribution network," *Universities Power Engineering Conference (AUPEC), 2010 20th Australasian*, pp.1-6, 5-8 Dec. 2010.

[18] Y. Tang; P.C. Loh, P. Wang, F. H. Choo, F. Gao, and F. Blaabjerg, "Generalized Design of High Performance Shunt Active Power Filter With Output LCL Filter," *Industrial Electronics, IEEE Transactions on*, vol.59, no.3, pp.1443-1452, Mar. 2012.

[19] A. A. Rockhill, M. Liserre, R. Teodorescu, and P. Rodriguez, "Grid-filter design for a multimegawatt medium-voltage voltage-source inverter," *IEEE Trans. Ind. Electron.*, vol. 58, no. 4, pp. 1205–1217, Apr. 2011.

[20] P. Mitra and G.K. Venayagamoorthy, "An Adaptive Control Strategy for DSTATCOM Applications in an Electric Ship Power System," *Power Electronics, IEEE Transactions on*, vol.25, no.1, pp.95-104, Jan. 2010.

[21] M.K. Mishra, A. Ghosh, and A. Joshi, "Operation of a DSTATCOM in voltage control mode," *Power Delivery, IEEE Transactions on*, vol.18, no.1, pp. 258- 264, Jan. 2003.

[22] M.I. Marei, E.F. El-Saadany, and M.M.A. Salama, "A Flexible DG Interface Based on a New RLS Algorithm for Power Quality Improvement," *Systems Journal, IEEE* , vol.6, no.1, pp.68-75, Mar. 2012.

[23] S.M.M. Agah and H.A. Abyaneh, "Distribution Transformer Loss-of-Life Reduction by Increasing Penetration of Distributed Generation," *Power Delivery, IEEE Transactions on*, vol.26, no.2, pp.1128-1136, Apr. 2011.

[24] M. Reza, P.H. Schavemaker, J.G. Slootweg, W.L. Kling, and L. van der Sluis, "Impacts of distributed generation penetration levels on power systems transient stability," *Power Engineering Society General Meeting, 2004. IEEE*, pp.2150-2155 Vol.2, 10-10 June 2004.

[25] M.C. Alvarez-Herault, D. Picault, R. Caire, B. Raison, N. HadjSaid, and W. Bienia, "A Novel Hybrid Network Architecture to Increase DG Insertion in Electrical Distribution Systems," *Power Systems, IEEE Transactions on*, vol.26, no.2, pp.905-914, May 2011.

[26] R. Zavadil, N. Miller, A. Ellis, E. Muljadi, E. Camm, and B. Kirby, "Queuing Up," *Power and Energy Magazine, IEEE* , vol.5, no.6, pp.47-58, Nov.-Dec. 2007.

[27] Square D, "Power System Harmonics: Causes & Effects of Variable Frequency Drives Relative to the IEEE 519-1992 Standard." Internet: http://www.schneider-electric.us/documents/customers/mechanical-engineers/power.pdf, Aug. 1994 [Apr. 25, 2012].

[28] Athula Rajapakse, Dharshana Muthumuni, and Nuwan Perera, "Grid Integration of Renewable Energy Systems." Internet: http://www.intechopen.com/source/pdfs/9325/InTechGrid_integration_of_renewable_energy_syste ms.pdf [Apr. 25, 2012]

[29] K.W. Louie, P. Wilson, R.A. Rivas, A. Wang, and P. Buchanan, "Discussion on Power System Harmonic Analysis in the Frequency Domain," *Transmission & Distribution Conference and Exposition: Latin America, 2006. TDC '06. IEEE/PES*, pp.1-6, 15-18 Aug. 2006.

[30] ABS, "Control of Harmonics in Electrical Power Systems." Internet: http://www.eagle.org/eagleExternalPortalWEB/ShowProperty/BEA%20Repository/Rules&Guides/

Current/150_CtrlofHarmonicsinElecPowerSystems/Pub150_ElHarmonics, May 2006 [Apr. 25, 2012].

[31] Power Studies, "An Introduction to Power System Harmonics." Internet: http://www.powerstudies.com/articles/Harm_Intro.pdf, [Apr. 25, 2012].

[32] *IEEE Standard for Recommended Practices and Requirements for Harmonic Control in Electrical Power System.* IEEE 519 – 92, August 28, 2010.

[33] A.F. Abdul Kadir, A. Mohamed, and H. Shareef, "Harmonic impact of different distributed generation units on low voltage distribution system," *Electric Machines & Drives Conference (IEMDC), 2011 IEEE International*, pp.1201-1206, 15-18 May 2011.

[34] [34] Pedro González, Enrique Romero-Cadaval, Eva González, and Miguel A.Guerrero "Impact of Grid Connected Photovoltaic System in Power Quality of a Distribution Network," Power Electrical and Electronic Systems (PE&ES), IFIP Advances in Information and Communication Technology, Vol. 349/2011, pp. 466-473, 2011.

[35] C. Yang, K. Liu, and D. Wang, "Harmonic Resonance Circuit's Modeling and Simulation," *Power and Energy Engineering Conference, 2009. APPEEC 2009. Asia-Pacific* , pp.1-5, 27-31 Mar. 2009.

[36] R. Zheng, M.H.J Bollen, and J. Zhong, "Harmonic resonances due to a grid-connected wind farm," *Harmonics and Quality of Power (ICHQP), 2010 14th International Conference on*, pp.1-7, 26-29 Sept. 2010.

[37] D. Patel, R. K. Varma, R. Seethapathy, and M. Dang. "Impact of wind turbine generators on network resonance and harmonic distortion" 23rd Canadian Conference on Elec. and Comp. Engineering, pp.1-6, 2010.

[38] R.A. Hanna and S.W. Randall, "Medium Voltage Adjustable-Speed Drive Retrofit of an Existing Eddy-Current Clutch Extruder Application," IEEE Transactions on Industry Applications, Vol. 36, pp. 1750-1755, Nov/Dec 2000.

[39] R. H. Engelmann and W. H. Middendorf, Handbook of Electric Motors. Marcel and Dekker NY. 1995.

[40] B.K. Bose, Modern Power Electronics and AC Drives. Upper Saddle River, NJ: Prentice Hall, 2002.

[41] R. Teodorescu, F. Blaabjerg, J.K. Pedersen, E. Cengelci, "Multilevel Inverter by Cascading Industrial VSI," IEEE Transactions on Industrial Electronics, Vol. 49, pp. 832-838, Aug. 2002.

[42] Y. Montasser, "Design and Development of a Power Modulator for Insulation Testing," Master's thesis, University of Waterloo, Waterloo, Ontario, Canada, 2006.

[43] N. Mohan, T.M. Underland, and W. Robbins, "Power Electronics, Converters, Applications, and Design," John Wiley and Sons, Inc. 2003.

[44] B.R. Andersen, L. Xu, P.J. Horton, P. Cartwright., "Topologies for VSC Transmission", IEE Power Engineering Journal, Vol. 16, Issue 3, pp. 142-150, 2002.

[45] Y. Shakweh, "Power devices for medium voltage PWM converters", IEE Power Engineering Journal, Vol. 13, Issue: 6 pp. 297-307, 1999.

[46] E. Persson, "Fast Switching Adjustable Speed Drives and Overview," IEE Power Engineering Journal, Vol. 14, pp. 148-157, 2000.

[47] Y. Shakweh, "MV Inverter stack topologies," IEE Power Engineering Journal, Vol. 15, pp. 139-149, 2001.

[48] R. Teichmann and S. Bernet, "A Comparison of Three-Level Converters Versus Two-Level Converters for Low-Voltage Drives, Traction, and Utility Applications," IEEE Trans. on Industry Applications, Vol. 41, pp. 855-865, 2005.

[49] E. Ozdemir, S. Ozdemir, L. Tolbert, and B. Ozpineci, "Fundamental frequency modulated multilevel inverter for three-phase stand-alone photovoltaic application," in Applied Power Electronics Conference and Exposition, 2008. APEC 2008. Twenty-Third Annual IEEE, pp. 148-153, Feb. 2008.

[50] L. Gyugi and N. Hingorani, Understanding FACTS: Concepts and Technology of Flexible AC Transmission Systems. New York: IEEE, 2000

[51] N. Mohan, T.M. Underland, W. Robbins, "Power Electronics, Converters, Applications, and Design," John Wiley and Sons, Inc. 2003.

[52] Qualification and Acceptance Tests for Type II Electrical Insulation Systems used in Rotating Electrical Machines Fed from Voltage Converters, IEC/TC 60034-18-42, Ed. 1.0, 2008.

[53] J.C.G. Wheeler, "Effects of Converter Pulses on the Electrical Insulation in Low and Medium Voltage Motors," IEEE Electrical Insulation Magazine, Vol. 21, No. 2, pp. 22-29, Mar/Apr 2005.

[54] E. Sharifi, "Over-voltage Transient on Motor Terminal Fed by PWM-Voltage Source Converter and Long Cable (Factors, Suppression Methods & Simulation)," University of Waterloo, Waterloo, Ontario, Canada, 2007.

[55] B. Sonerud, T. Bengtsson, J. Blennow, and S. Gubanski, "Dielectric heating in insulating materials subjected to voltage waveforms with high harmonic content," Dielectrics and Electrical Insulation, IEEE Transactions on, vol. 16, pp. 926-933, Aug. 2009.

[56] S. Ul Haq, "A Study on Insulation Problems in Drive Fed Medium Voltage Induction Motors," PhD thesis, University of Waterloo, Waterloo, Ontario, Canada, 2007.

[57] S. Ul Haq, S.H. Jayaram, and E.A. Cherney "Insulation Problems in Medium Voltage Stator Coils under Fast Repetitive Voltage Pulses," 53rd IEEE Pulp and Paper Industry Technology Conference, June 2007.

[58] J.C.G. Wheeler, "Effects of Converter Pulses on the Electrical Insulation in Low and Medium Voltage Motors," IEEE Electrical Insulation Magazine, Vol. 21, No. 2, pp. 22 – 29, Mar/Apr. 2005.

[59] S. Bell, T.J. Cookson, S.A. Cope, R.A. Epperly, A. Fischer, D.W. Schlegel, and G.L. Skibinski, "Experience with Variable-Frequency Drives and Motor Bearing Reliability," IEEE Transactions on Industry Applications, Vol. 37, no. 5, pp. 1438-1446 Sept/ Oct. 2001.

[60] S. Ul Haq, Shesha H. Jayaram, and Edward A. Cherney, "Evaluation of Medium Voltage Enamelled Wire Exposed to Fast Repetitive Voltage Pulses," IEEE Transactions on Dielectrics and Electrical Insulation, Vol. 14, No. 1, pp. 194-903, 2007.

[61] T.L. Koltunowicz, R. Kochetov, G. Bajracharya, D. Djairam, and J.J. Smit, "Repetitive transient aging, the influence of repetition frequency," *Electrical Insulation Conference (EIC), 2011*, vol., no., pp.444-448, 5-8 June 2011.

[62] T. Koltunowicz, G. Bajracharya, D. Djairam, and J. Smit, "Investigating the effects of repetitive transients on paper insulation," in Developments in Power System Protection (DPSP 2010). Managing the Change, 10th IET International Conference on, pp. 1-5, Apr. 2010.

[63] L. Ming, F. Sahlen, S. Halen, G. Brosig, and L. Palmqvist, "Insulation Performance of Cable terminations with Resistive Stress-grading under High Frequency Voltages", XIVth International Symposium on High Voltage Engineering, Paper I-18, pp. 1-4, 2005.

[64] INCOPR, "Clean Energy Assuring Wind Plant Availability." Internet: http://www.imcorptech.com/Papers/NA%20CleanEnergy%20Assuring%20Wind%20Plant%20Availability%202011.pdf, [Apr. 25, 2012].

[65] M. Moore, "The testing methodologies of service aged medium voltage power cables as applied to an operating wind farm," *Electrical Insulation Conference (EIC), 2011*, pp.423-429, 5-8 June 2011.

[66] C.H. Lee, M.Y. Chiu, C.H. Huang, S.S Yen, K.K. Chen, "The study on diagnostics for aging trend of cable termination," *Condition Monitoring and Diagnosis, 2008. CMD 2008. International Conference on*, pp.336-339, 21-24 Apr. 2008.

[67] S. Banerjee, "A Study of High Frequency Voltage Effects in Medium Voltage Cable Terminations" Master's thesis, University of Waterloo, Waterloo, Ontario, 2008.

[68] F.P. Espino-Cortés, "A Study of Field-Dependent Stress Grading Systems Working under Fast Rise Time Pulses," PhD thesis, University of Waterloo, Waterloo, Ontario, 2007.

[69] L. Cabot, "Conductive Carbon Black Selection Guide for Semi-Conductive Power Cable Compounds," *International Symposium on Electrical Insulation*, pp. 214-221, Sept. 2002.

[70] J.C. Fothergill and R.N. Hampton, "Chapter 10: Polymer Insulated Power Cable on GlobalSpec." *GlobalSpec - Engineering Search & Industrial Supplier Catalogs*. Internet: http://www.globalspec.com/reference/31558/203279/chapter-10-polymer-insulated-power-cable, June 2004 [Apr. 25, 2012].

[71] S.J. Han, A.M. Mendelsohn, and R. Ramachandran, "Overview of Semiconductive Shield Technology in Power Distribution Cables," *Transmission and Distribution Conference and Exhibition, 2005/2006 IEEE PES*, pp.641-646, 21-24 May 2006.

[72] J. H. Mason, "In Progress in Dielectrics", vol. 1. J. S. Birks, and J. H. Shulman, editors, London: Heywood and Co., 1959.

[73] M.S. Mashikian and J.H. Groeger, "Ionic Impurities In Extruded Cable Insulation: Analytical Detection Techniques, Sources, Nature, and Effects", Proceedings of the JICABLE International Conference On Polymeric Cable Insulation, Versailles, 1987.

[74] S. Bamji, A. Bulinski, and J. Densley, "Final breakdown mechanism of water treeing," Annual Report of the Conference on Electrical Insulation and Dielectric Phenomena, pp. 298–305, 1991.

[75] S. Boggs, J. Densley, and J. Kuang, "Mechanism for conversion of water trees to electrical trees under impulse conditions," IEEE Trans. Power Delivery, vol. PD-13, pp. 310–315, Apr. 1998.

[76] G. Bahder, C. Katz, J. Lawson, and W. Vahlstrom, "Electrical and electrochemical treeing in polyethylene and crosslinked polyethylene cables," IEEE Trans. Power App. and Syst., vol. PAS 93, pp. 979–990, May/June 1974.

[77] N. Hampton, R. Hartlein, H. Lennartsson, H. Orton, and R. Ramachandran "Long-life XLPE Insulated Power Cable", JiCable07, 2007.

[78] S.J. Han, L.H. Gross, and J. Lastovica, "New Semiconductive Compound Technology for Solid Dielectric Insulated Power Cables." *International Symposium on Electrical Insulation*, pp. 354-357, Sept. 2004.

[79] M. Masuda, A. Ogata, M. Nitta, and T. Tani, "A study of volume resistivity for high voltage power cable semiconducting layer," *Properties and Applications of Dielectric Materials, Proceedings of the 5th International Conference on* , vol.1, pp.398-401 vol.1, 25-30 May 1997.

[80] T. Liu, J. Fothergill, S. Dodd, and U. Nilsson, "Influence of semicon shields on the dielectric loss of XLPE cables," *Electrical Insulation and Dielectric Phenomena, 2009. CEIDP '09. IEEE Conference on*, pp.246-249, 18-21 Oct. 2009.

[81] L. H. Gross, J.S. Furno, C.G. Reid, and A. Mendelsohn, "XLPE Materials for Extruded High/Extra-High Voltage Transmission Cables," *CIGRE WG* 15, Boston, MA, Aug. 1997.

[82] N.H. Malik, A.A Al-Arainy, M.I. Qureshi, and F.R. Pazheri, "Calculation of electric field distribution at high voltage cable terminations," *High Voltage Engineering and Application (ICHVE), 2010 International Conference on*, pp.24-27, 11-14 Oct. 2010.

[83] F. P. Espino-Cortes, E.A. Cherney, and S. Jayaram, "Impact of Inverter Drives Employing Fast-Switching Devices on Form-Wound AC Machine Stator Coil Stress Grading," IEEE Electrical Insulation Magazine, Vol. 23, No. 1, pp. 16-28 Jan/Feb. 2007.

[84] X. Qi, Z. Zheng, and S. Boggs, "Engineering with Nonlinear Dielectrics," IEEE Electrical Insulation Magazine, Vol. 20, No. 6, pp. 27-34, 2004.

[85] G. C. Stone, E. A. Boulter, I. Culbert, and H. Dhirani, "Electrical Insulation for Rotating Machines," IEEE Press, 2004.

[86] "Draft Standard for Test Procedures and Requirements for Alternating Current Cable Terminations Used on Shielded Cables Having Laminated Insulation Rated 2.5 kV Through 765 kV or Extruded Insulation Rated 2.5 kV Through 500 kV (Revision of IEEE 48-1996)," *IEEE Unapproved Draft Std P48/D5.1, May 2008* , 2008.

[87] Robert Goodman and William Osborn, "Power Cable Splicing and Terminating." Internet: http://multimedia.3m.com/mws/mediawebserver?mwsId=SSSSSu7zK1fslxtUNx_UlxMSev7qe17z HvTSevTSeSSSSSS--, [Apr. 25, 2012].

[88] B. Taylor and G. Morrison, "Evaluating Medium Voltage Cable Splices and Terminations", IEEE Pulp & Paper Industry Technical Conference, pp. 188 – 194, 2000.

[89] ABB Data Sheet, Kabeldon terminations for XLPE-insulated cable for extremely high demands. Alingsas: ABB Kabeldon, 2003.

[90] L. Ming, F. Sahlen, S. Halen, G. Brosig, and L. Palmqvist., "Impacts of high frequency voltage on Cable-Terminations with Resistive Stressgrading", IEEE International Conference on Solid Dielectrics (ICSD), Vol. 1 pp. 300-301, 2004.

[91] L.G. Virsberg and P.H. Ware, "A New Termination for Underground Distribution," *Power Apparatus and Systems, IEEE Transactions on*, vol.PAS-86, no.9, pp.1129-1135, Sept. 1967.

[92] S.V. Nikolajevic, N.M. Pekaric-Nad, and R.M. Dimitrijevic, "A new concept in construction of cable terminations for medium voltages," *Power Delivery, IEEE Transactions on*, vol.13, no.3, pp.712-717, Jul 1998.

[93] T. Christen, L. Donzel, and F. Greuter, "Nonlinear resistive electric field grading part 1: Theory and simulation," *Electrical Insulation Magazine, IEEE*, vol.26, no.6, pp.47-59, Nov/Dec. 2010.

[94] W. Guo, Y. Wang, R. Zhang, and Z. Li , "Research on application of nonlinear insulation composites in cable termination," *Strategic Technology (IFOST), 2011 6th International Forum on* , vol.1, pp.133-136, 22-24 Aug. 2011.

[95] F.P. Espino-Cortes, S.H. Jayaram, and E.A. Cherney, "Stress grading materials for cable terminations under fast rise time pulses," *Electrical Insulation and Dielectric Phenomena, 2005. CEIDP '05. 2005 Annual Report Conference on*, pp. 621- 624, 16-19 Oct. 2005.
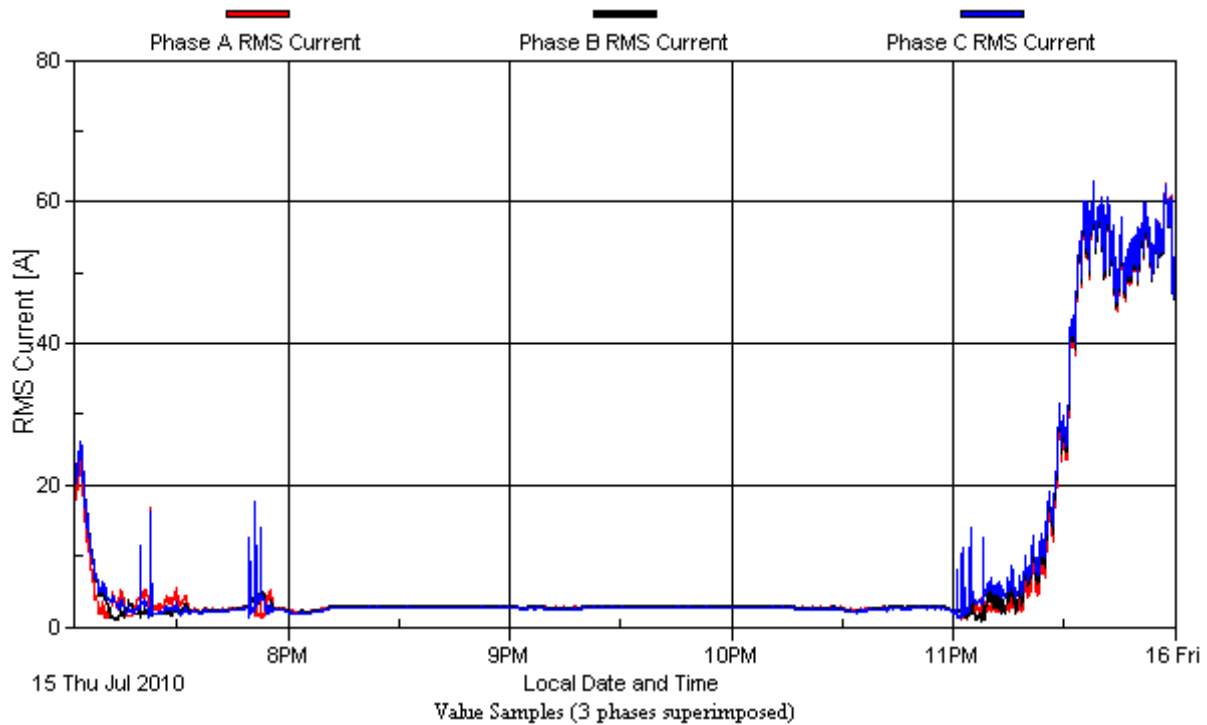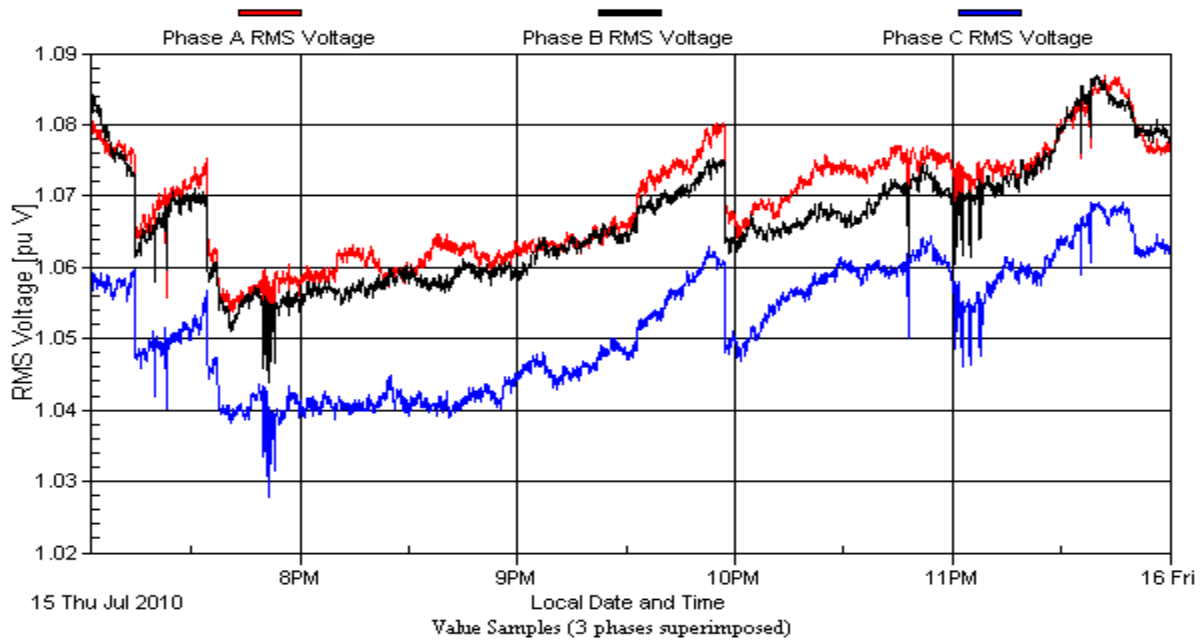
[96] "Electrical Solutions for Wind Farms." 3M Projects for Electrical Networks: Wind Farm Capabilities. Internet: http://multimedia.3m.com/mws/mediawebserver?mwsId=kkkkkmN6cwZLdp4MGqsMgpz7YON3YwN69OlkYOlkYkkkkkk--, [Apr. 25, 2012].

[97] "22 kV Cable Termination Failure at Switchgears and Transformers - A Common Cause of Voltage Dip in Singapore," Internet: http://www.jmpangseah.com/index_files/article/chapter-6.pdf –, [Apr. 25, 2011].

[98] D. Stuart-Smith, "Failure of 11 kV Cable Termination on 11 kV Ring Main Switchgear." Internet: http://engineering.railcorp.nsw.gov.au/Disciplines/Electrical/ETN_07_06.pdf, June 2010, [Apr. 25, 2012].

[99] Elichem, "Medium and High Voltage (6.6 - 36 kV) Cable Terminations." Internet: http://www.elichem.com.au/jointmaster3.htm, [Apr. 25, 2012].

[100] Northeast Power Systems, "Cable Selection for Medium Voltage Capacitor Banks and Harmonic Filter Banks." Internet: http://www.nepsi.com/cablewebpage.htm, 2009, [Apr. 25, 2012].

[101] Rolray Lty Ltd., "High and Medium Voltage Cable Termination." Internet: http://www.rolray.com.au/services.html, [Apr. 25, 2012].

[102] "Electrical Installation." Internet: http://electricalinstallationblog.blogspot.com/2011/04/neutral-link-pictures.html, Apr. 2011[Apr. 25, 2012].

[103] S. Haddock and A. Naderian, "Root Cause Failure Analysis of Termination and Cable." Internet: http://www.kinectrics.com/Case-Studies/Pages/Root-Cause-Failure-Analysis-of-Termination-and-Cable.aspx, [Apr. 25, 2012].

[104] C. Lee, L. Yu-Chih, M. Chiu, H. Chih-Hsien, S. Yen, and C. Haeng,"Recognition of partial discharge defects in cable terminations," *Condition Monitoring and Diagnosis, 2008. CMD 2008.International Conference on*, pp.1242-1245, 21-24 Apr. 2008.

[105] K. Uchida, H. Tanaka, K. Hirotsu, "Study on detection for the defects of XLPE cable lines", IEEE Trans. On Power Delivery, Vol. 1, No. 2, pp663-669, Apr. 1996.

[106] Z.A.A. Zarim, A.B.A. Ghani, S.K. Tiong, "The measurement and temperature profile of cable insulation failure due to loose connection at the cable termination," *Electrical Insulating Materials, 2008. (ISEIM 2008). International Symposium on*, pp.570-572, 7-11 Sept. 2008.

[107] A.H. Bonnett, "Analysis of the Impact of Pulse-Width Modulated Inverter Voltage Waveforms on AC Induction Motors", IEEE Trans. on Industry Applications, Vol. 32, 1996.

[108] J.C.G. Wheeler, "Effects of converter pulses on the electrical insulation in low and medium voltage motors", IEEE Electrical Insulation Magazine, Vol. 21, pp. 22 – 29, 2005.

[109] S.U. Haq, S.H. Jayaram, and E.A. Cherney, "Aging Characterization of Medium Voltage Groundwall Insulation Intended for PWM Applications", IEEE Symposium on Electrical Insulation, pp. 143-146, 2006.

[110] F.P. Cortes, E.A. Cherney, and S.H. Jayaram, "Effectiveness of Stress Grading Coating on Form Wound Stator Coil Groundwall Insulation Under Fast Rise Time Pulse Voltages", IEEE Trans. On Energy Conversion, Vol. 20, pp. 844-851, 2005.

[111] E. Sharifi-Ghazvini, "Analysis of Electrical and Thermal Stresses in the Stress Relief System of Inverter Fed Medium Voltage Induction Motors," PhD thesis, University of Waterloo, Waterloo, Ontario, Canada, 2010.

[112] M. Hamid, "Effects of Power System Harmonics on Distribution Transformer Insulation Performance," Master's thesis, University of Waterloo, Waterloo, Ontario, Canada, 2011.

[113] "Cable Termination Failure." Internet: http://www.eng-tips.com/viewthread.cfm?qid=308601, Oct 2011, [Apr. 25, 2012].

[114] 3M QT-III Cold Shrink Silicone Rubber Termination Datasheet,"Electrical Solutions for Wind Farms." Internet: http://multimedia.3m.com/mws/mediawebserver?mwsId=kkkkkmN6cwZLdp4MGqsMgpz7YON3YwN69OlkYOlkYkkkkkk--, [Apr. 25, 2012].

[115] R.A. Wandmacher, J.A. Morris, J.A., T.J.D. Heyer, and L.C.K. Chor, "New silicone cold shrink termination," *Transmission and Distribution Conference, 1996. Proceedings., 1996 IEEE*, pp.391-395, 15-20 Sept. 1996.

[116] Haefely Data Sheet, KEV-50 cable test terminations. Basel: Haefely High Voltage Test, 1997.

[117] Shell Product Data Sheet, Diala AX lubricants. Toronto: Shell Canada Limited, 2006.

[118] Imperial Oil (Esso) Product Data Sheet, Voltesso electrical insulating oils. Toronto: Imperial Oil Limited, 2003.

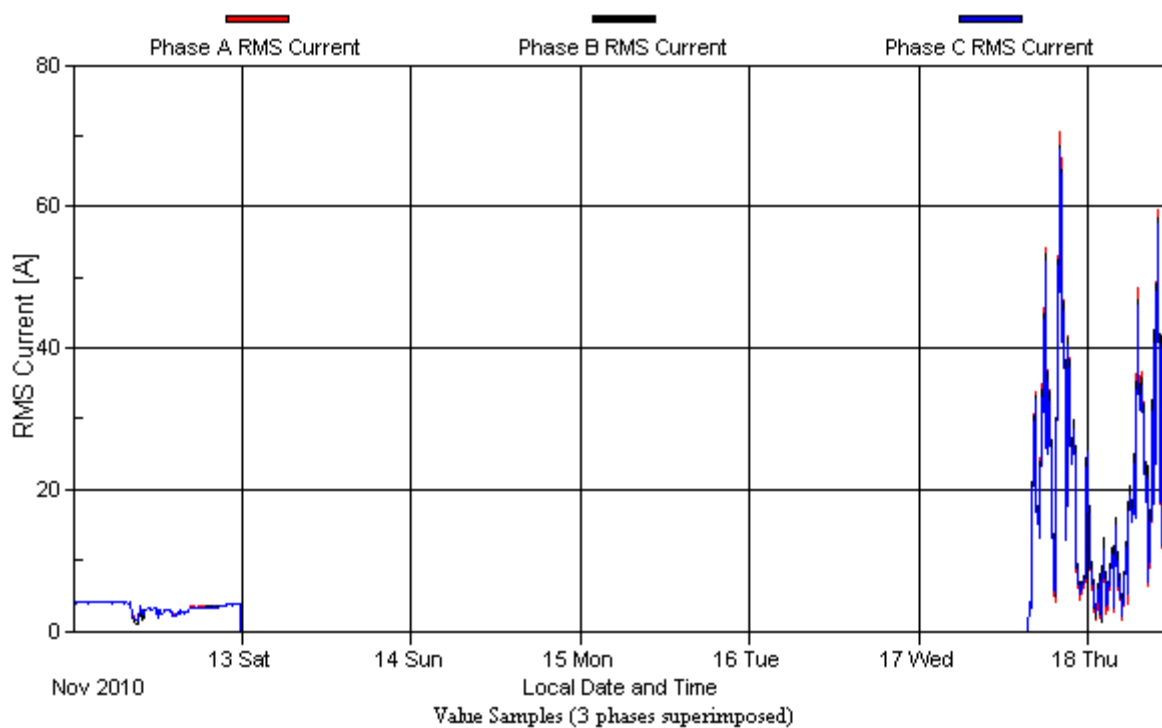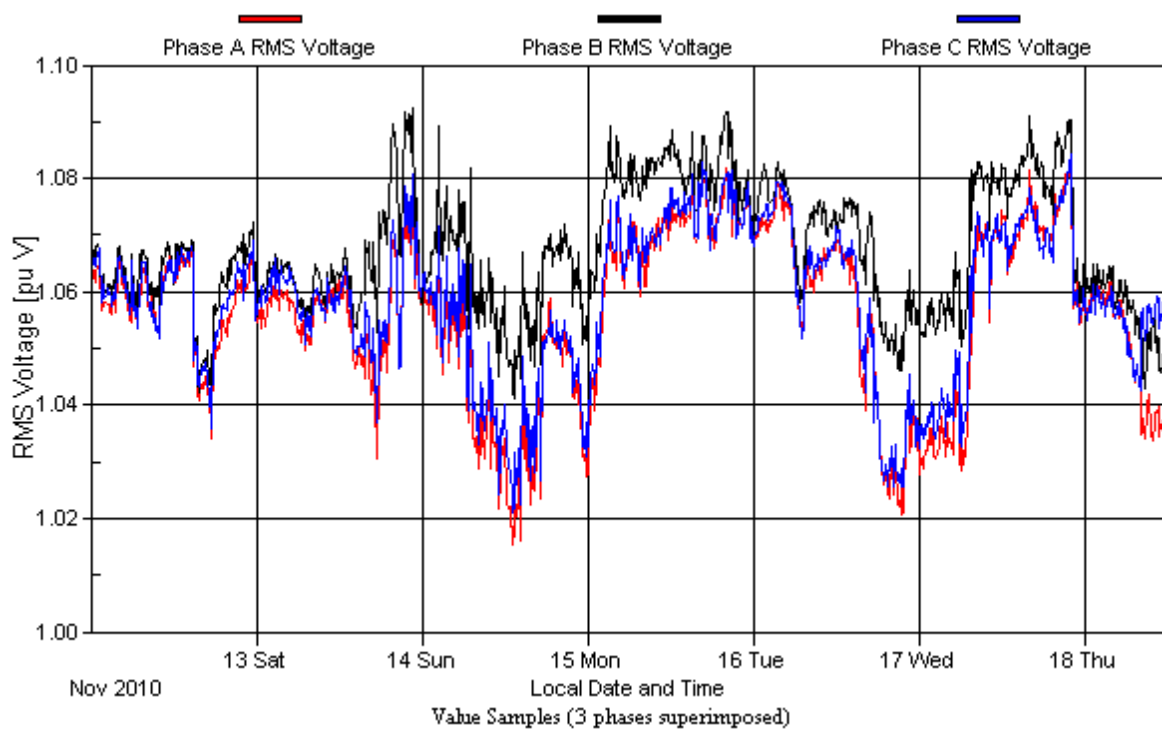[119] IEC 61442, "Test methods for accessories for power cables with rated voltages from 6 kV (Um = 7.2 kV) up to 30 kV (Um = 36 kV). Geneva: International Electrotechnical Commission, 2001.

[120] R. Ghunem, M. Hamid, S.H. Jayaram, R. Seethapathy, A. Naderian, "Transformer Insulation Risk Assessment Under Smart Grid Environment Due to Enhanced Aging Effects," *Electrical Insulation Conference, 2011. EIC 2011. IEEE* , pp.276-279, May 2011.

[121] Y.T. Yu and S.H. Jayaram, "High Voltage Square Wave Generator for Motor Coil Insulation Testing," *IEEE International Power Modulators and High Voltage Conference, Proceedings of the 2008*, pp.436-438, 27-31 May 2008.

[122] ThermaCAM^{TM} SC500, Operator's Manual, FLIR Systems.

[123] F. P. Espino-Cortes, E.A. Cherney, and S. Jayaram, "Impact of Inverter Drives Employing Fast-Switching Devices on Form-Wound AC Machine Stator Coil Stress Grading," IEEE Electrical Insulation Magazine, Vol. 23, No. 1, pp. 16-28 Jan/Feb. 2007.

[124] X. Qi, Z. Zheng, and S. Boggs, "Engineering with Nonlinear Dielectrics," IEEE Electrical Insulation Magazine, Vol. 20, No. 6, pp. 27-34, 2004.

[125] Maciej A. Noras, "Non-contact Surface Charge/Voltage Measurements Field-meter and Voltmeter Methods," Trek Application Note, Number 3002.

[126] Operator's Manual, Treck Model 341A, electrostatic voltmeter.

[127] High-Voltage Test Techniques - Partial Discharge Measurements, IEC 60270, Ed. 3.0, 2000.

[128] Standard Test Method for Detection and Measurement of Partial Discharge (Corona) Pulses in Evaluation of Insulation Systems, ASTM D1868, 2007.

[129] Qualification and Acceptance Tests for Type II Electrical Insulation Systems used in Rotating Electrical Machines Fed from Voltage Converters, IEC/TC 60034-18-42, Ed. 1.0, 2008.

[130] COMSOL Multiphysics AC/DC Module Documentation. Stockholm: COMSOL AB, 2006.
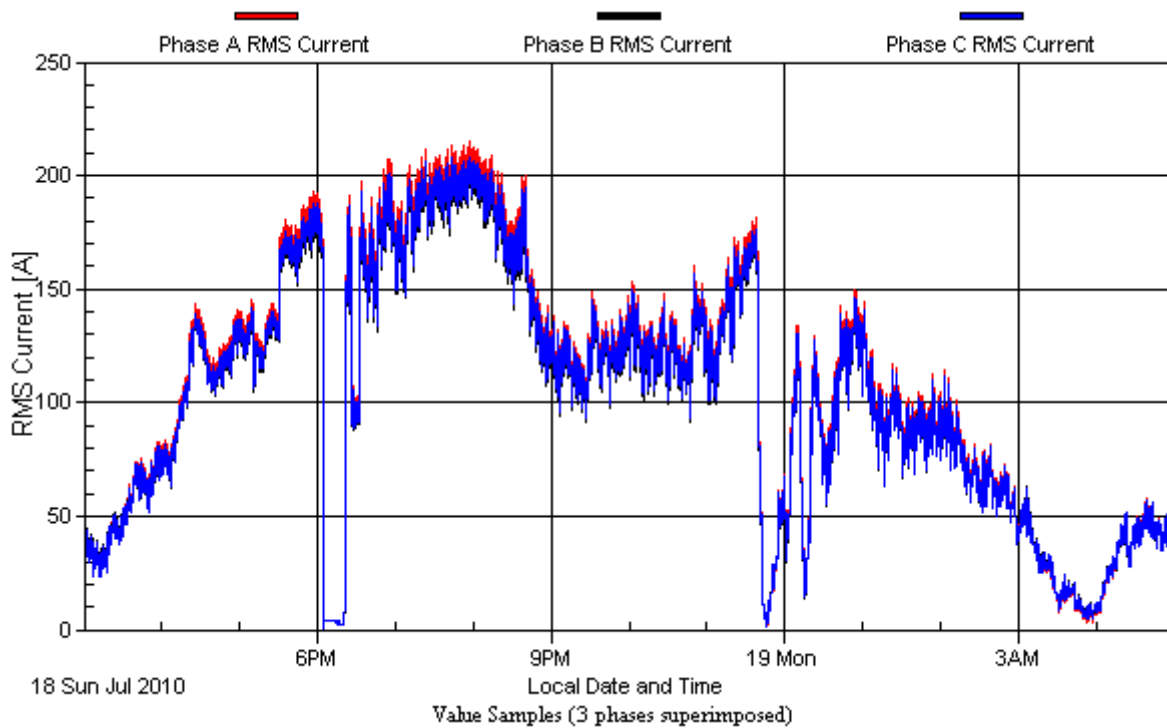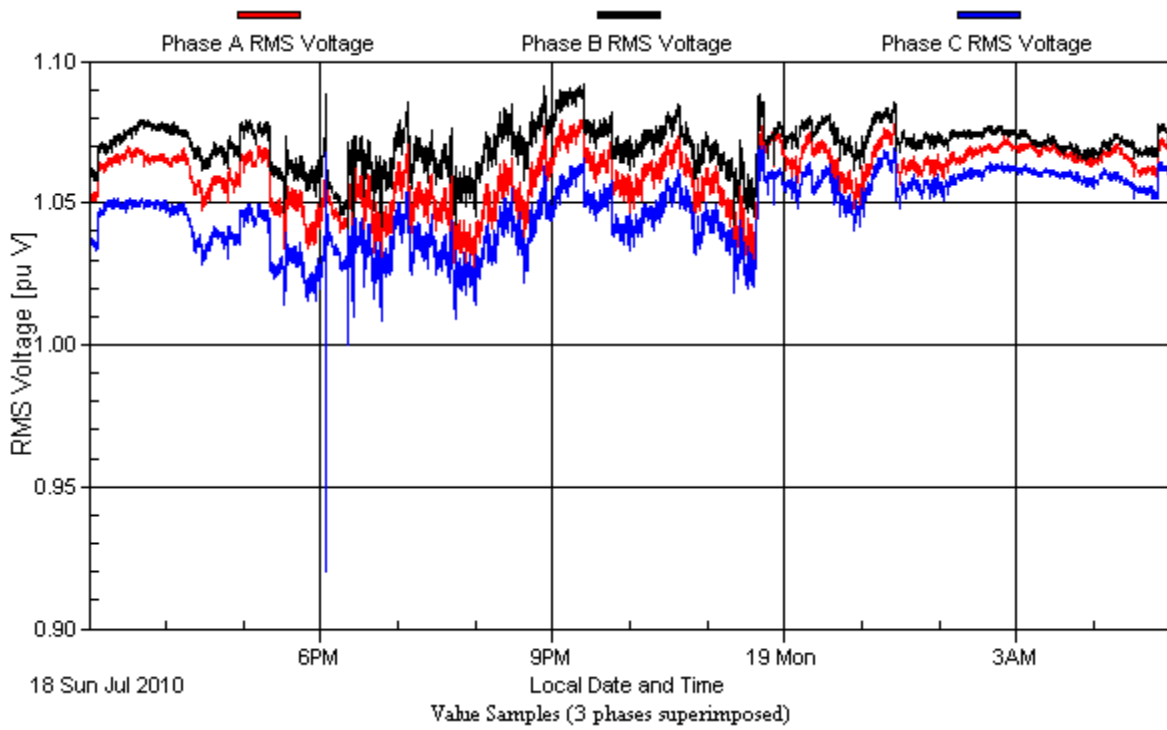
Appendix A: Data at the Wind Farm Output

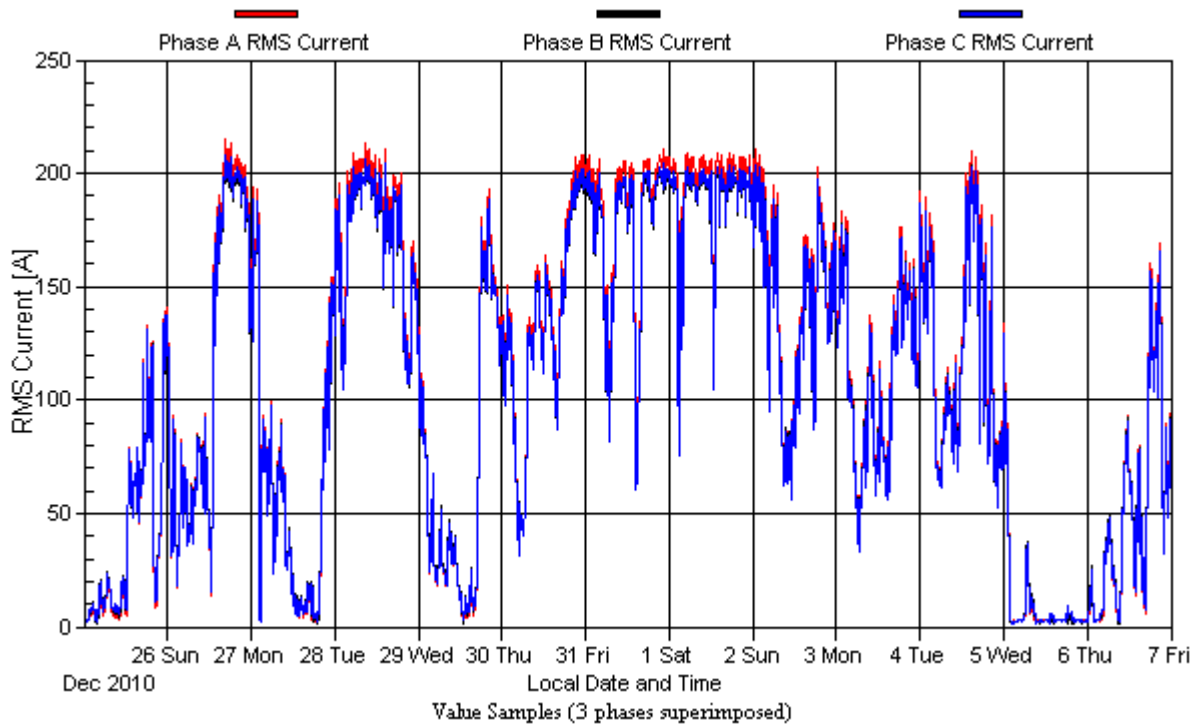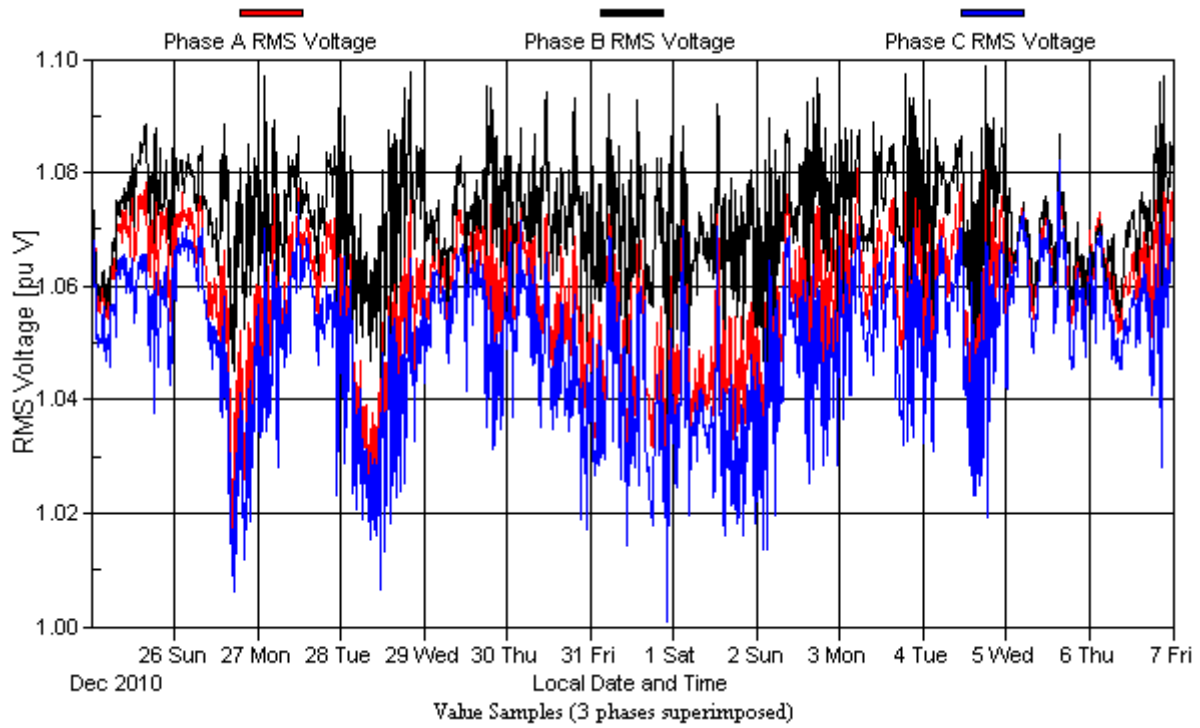## Steady State – DG – OFF (July 15, 2010)

106

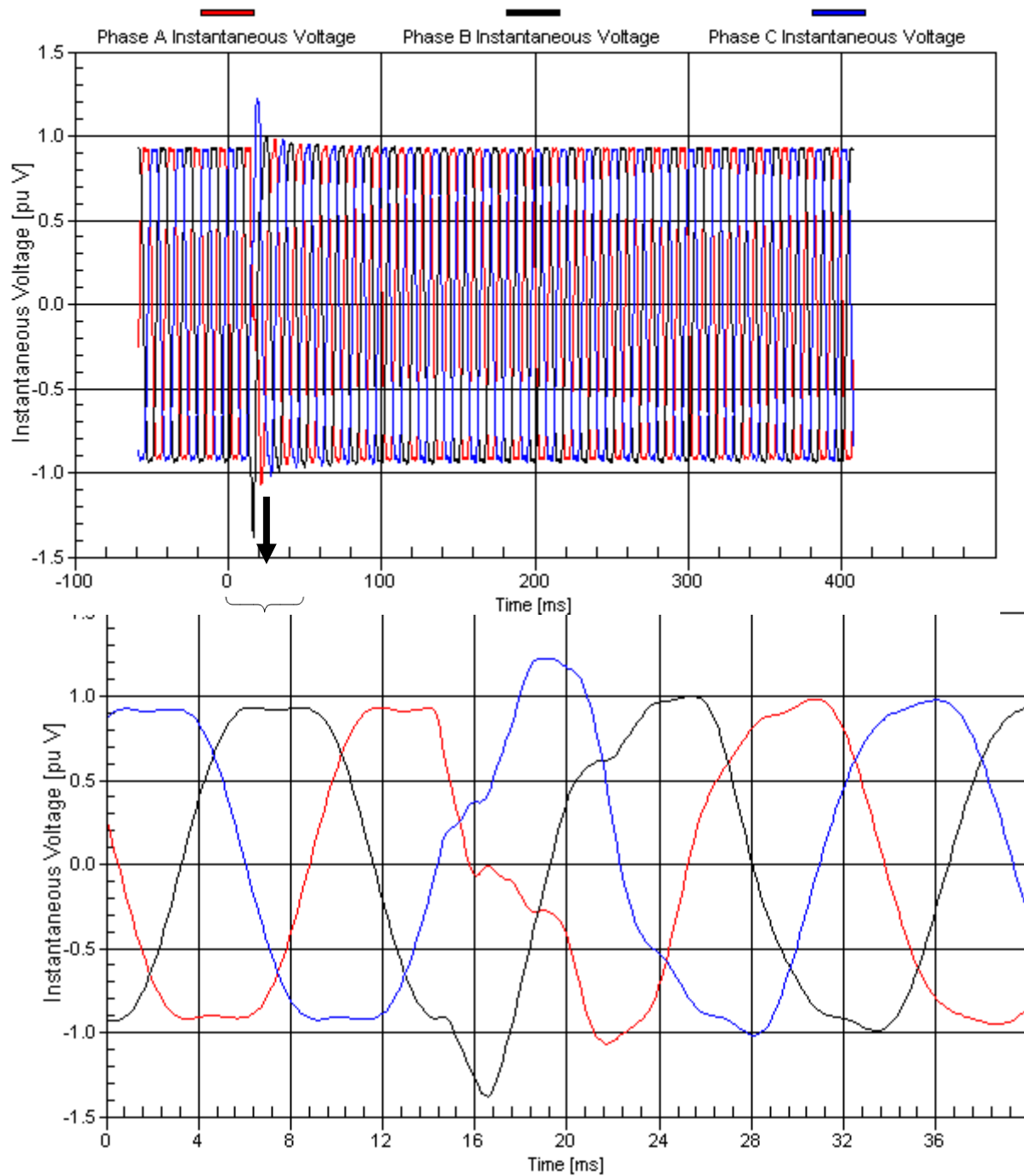## Steady State – DG – OFF (Nov 12, 2010)
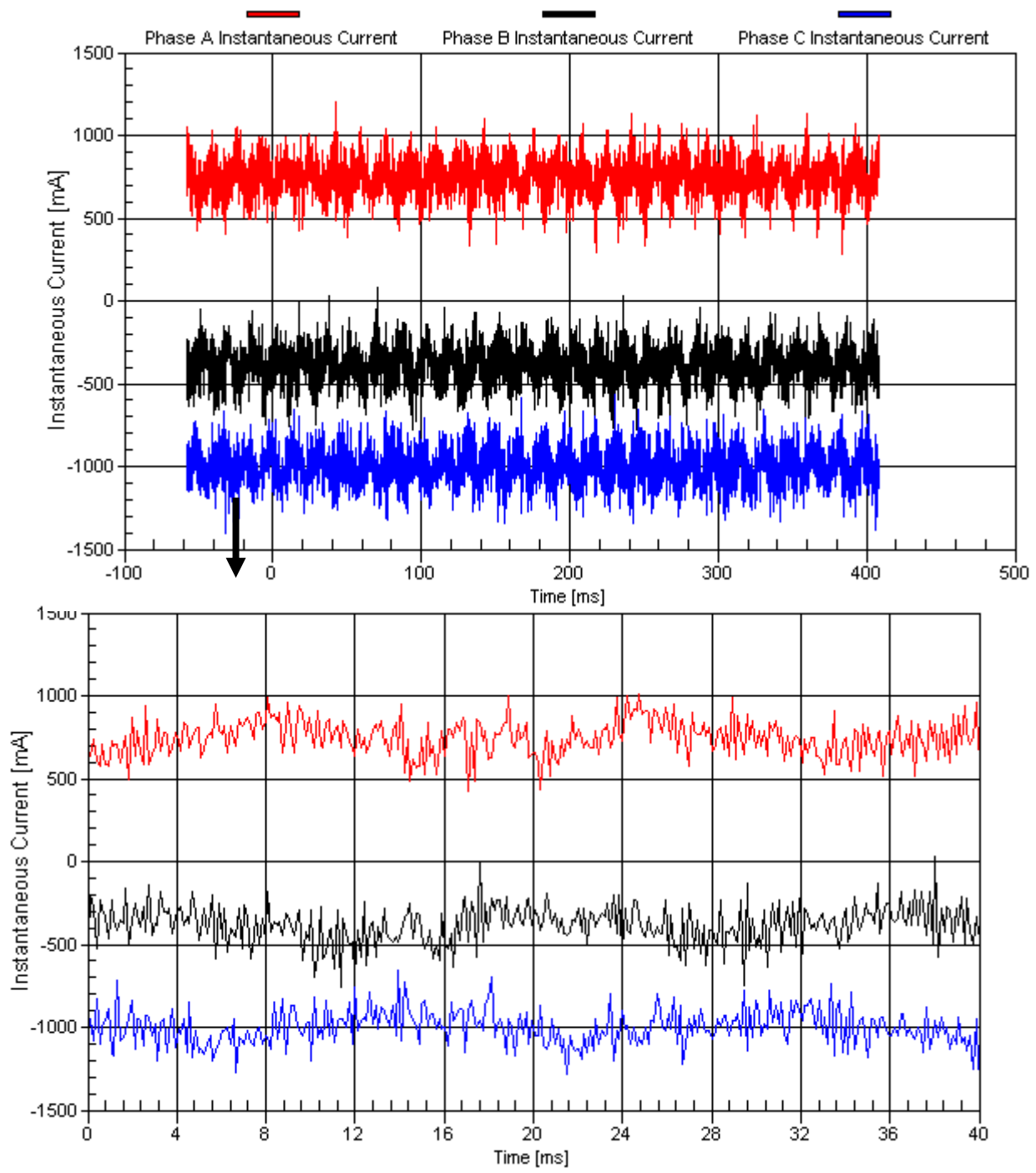

107

Steady State – DG – ON (July 18, 2010)
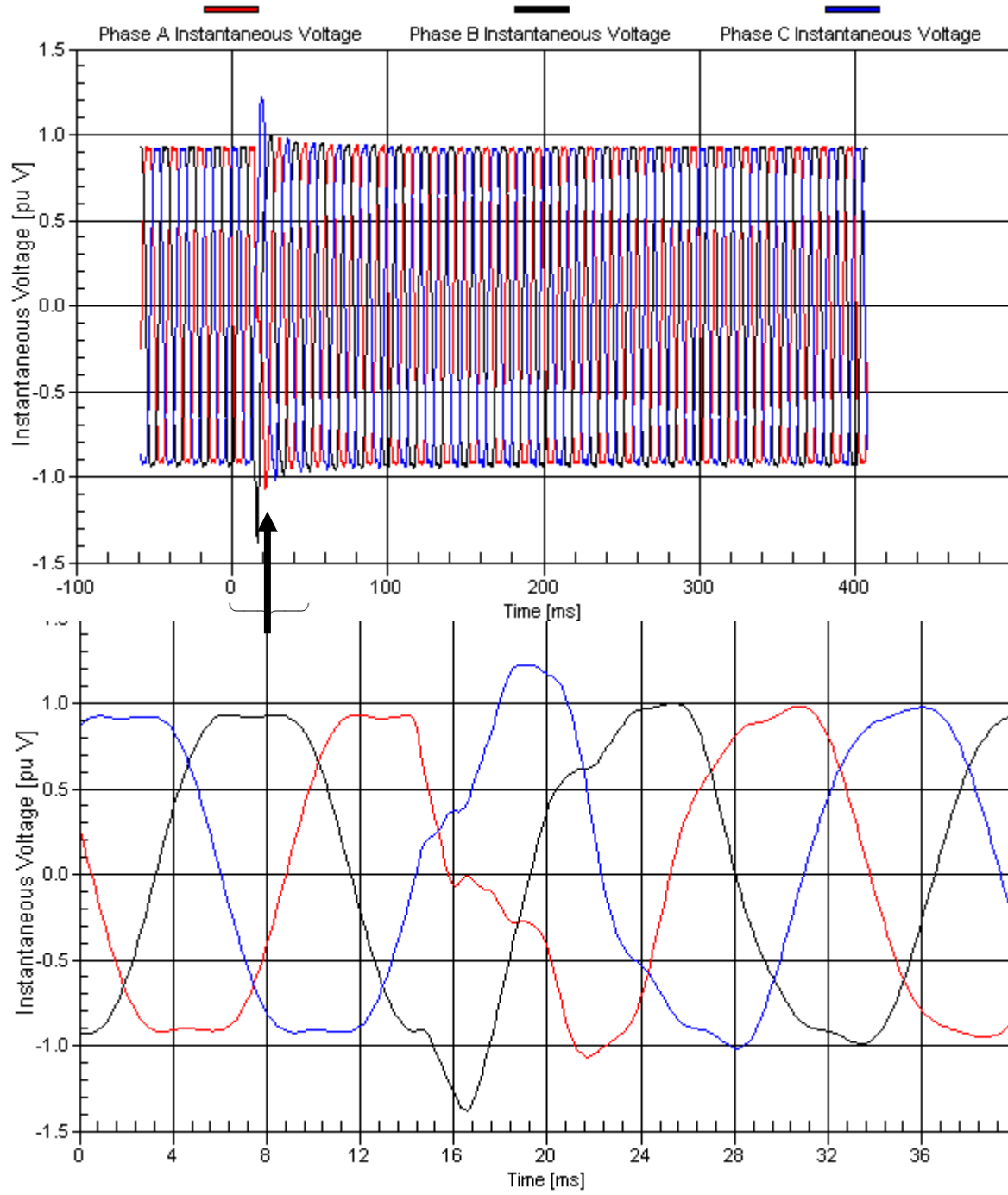
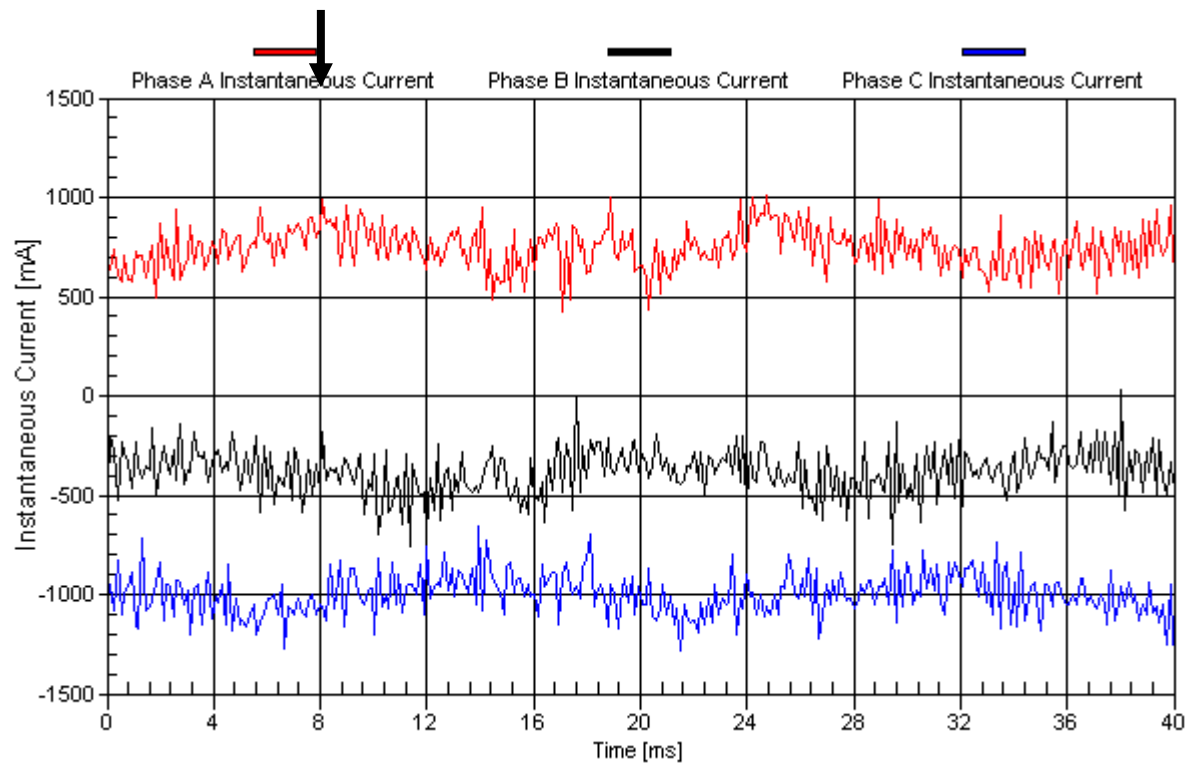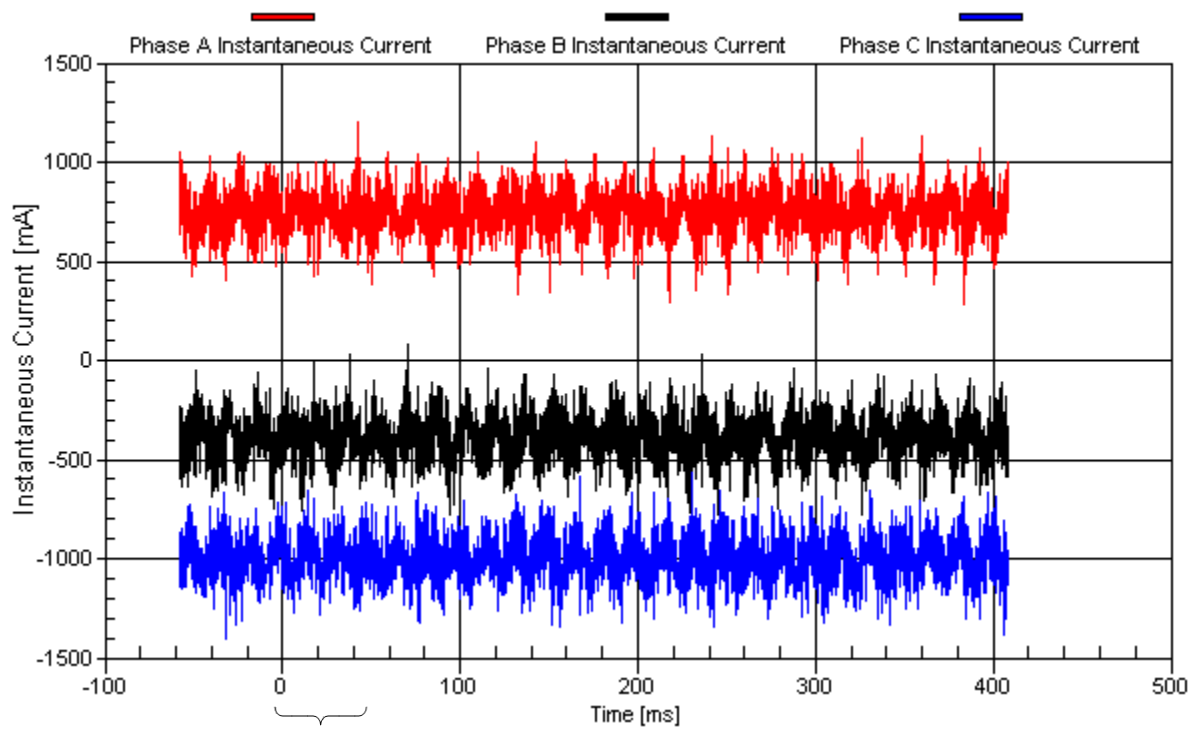# Steady State – DG – ON (Dec 25, 2010)

Phase A RMS Voltage   Phase B RMS Voltage   Phase C RMS Voltage

Value Samples (3 phases superimposed)

Phase A RMS Current   Phase B RMS Current   Phase C RMS Current

Value Samples (3 phases superimposed)

109

Transient State – DG OFF (Mar 14, 2010)

110

111

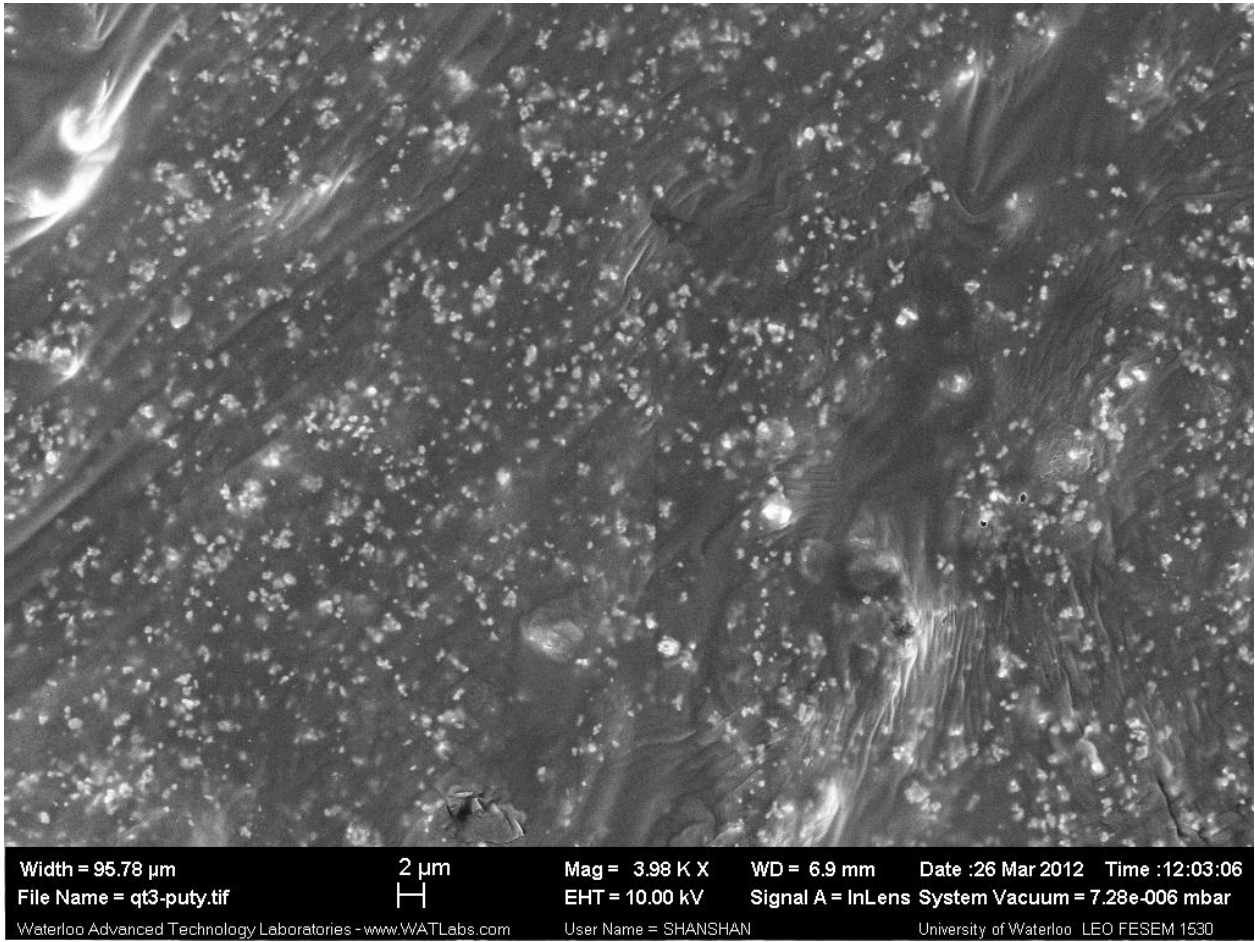## Transient State – DG ON (Mar 09, 2011)

112

Appendix B: SEM Results

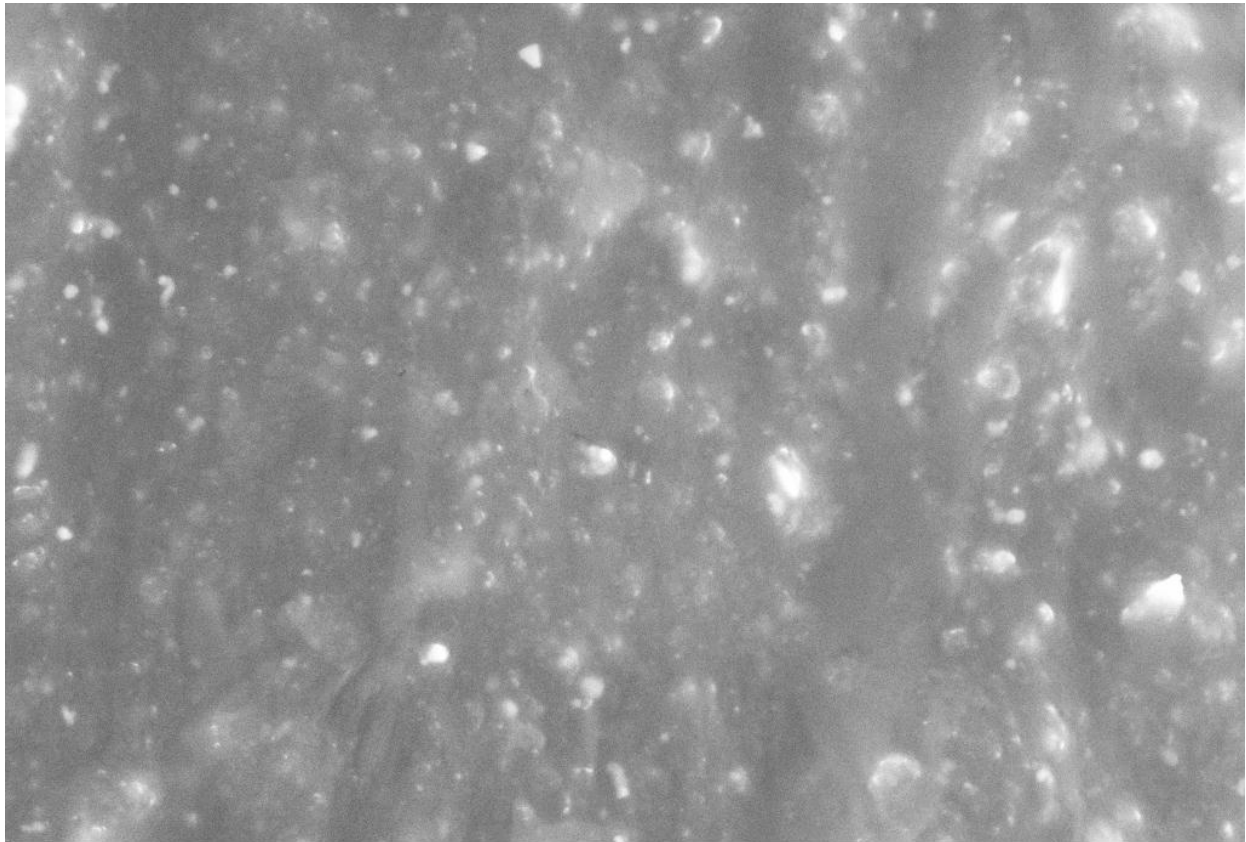## Type-II (SG Tube)

Type-II (Putty)

Width = 95.78 µm   2 µm   Mag = 3.98 K X   WD = 6.9 mm   Date :26 Mar 2012   Time :12:03:06
File Name = qt3-puty.tif   EHT = 10.00 kV   Signal A = InLens   System Vacuum = 7.28e-006 mbar
Waterloo Advanced Technology Laboratories - www.WATLabs.com   User Name = SHANSHAN   University of Waterloo LEO FESEM 1530
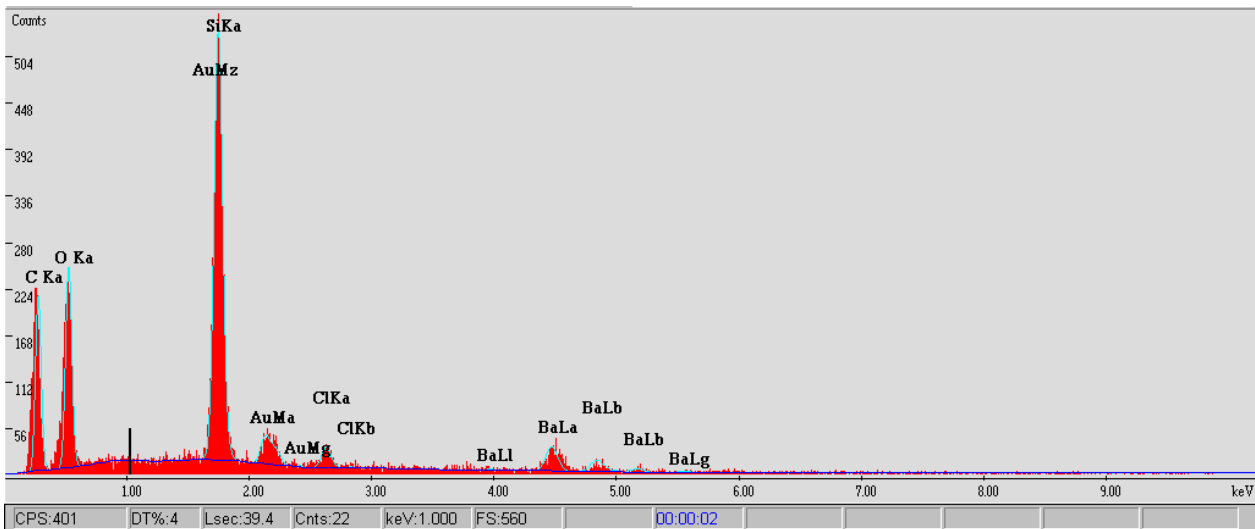
Type-I (SG Tube)

Width = 24.09 µm   1 µm   Mag = 15.82 K X   WD = 7.3 mm   Date :26 Mar 2012   Time :12:16:24
File Name = qt2-sglayer.tif   EHT = 10.00 kV   Signal A = InLens   System Vacuum = 4.38e-006 mbar
Waterloo Advanced Technology Laboratories - www.WATLabs.com   User Name = SHANSHAN   University of Waterloo   LEO FESEM 1530
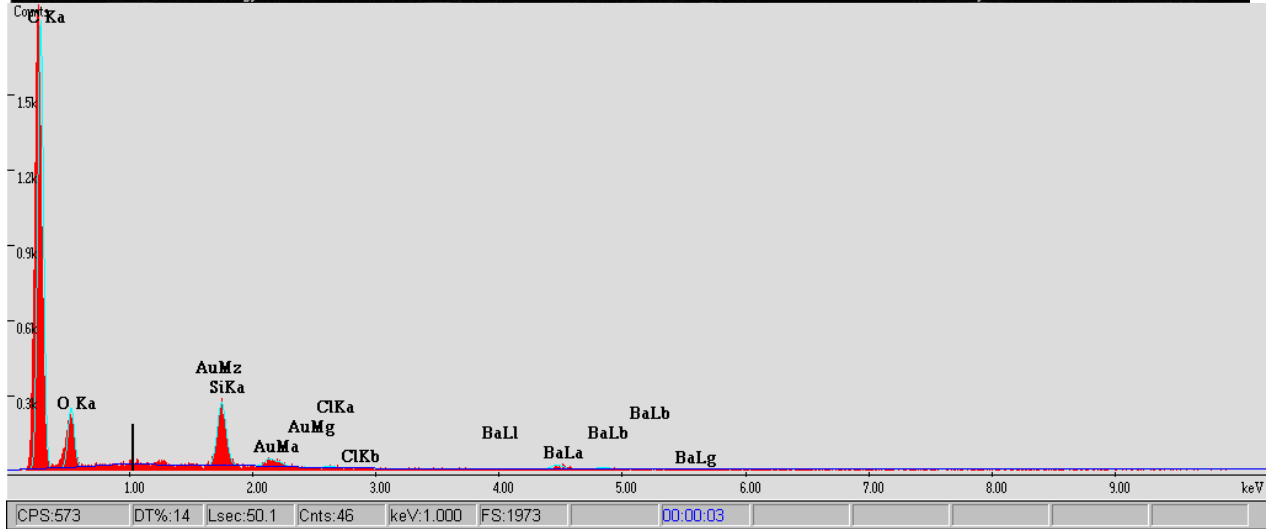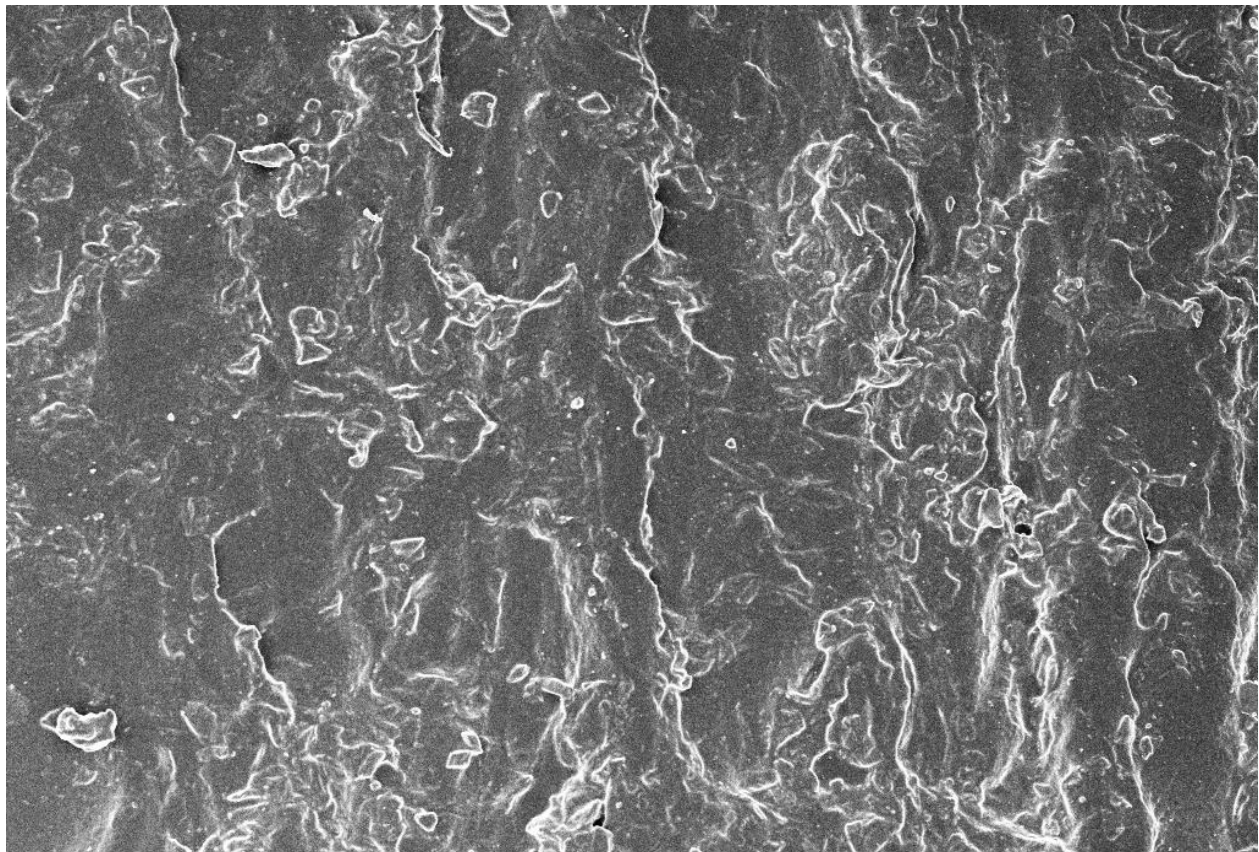

CPS:573   DT%:14   Lsec:50.1   Cnts:46   keV:1.000   FS:1973   00:00:03

Type-I (SG Tape)

Width = 850.2 μm   20 μm   Mag = 450 X   WD = 7.9 mm   Date :26 Mar 2012   Time :12:24:28
File Name = sg2tape.tif   EHT = 10.00 kV   Signal A = InLens System Vacuum = 3.84e-006 mbar
Waterloo Advanced Technology Laboratories - www.WATLabs.com   User Name = SHANSHAN   University of Waterloo LEO FESEM 1530

CPS:325   DT%:2   Lsec:60.3   Cnts:23   keV:1.000   FS:1727   00:00:02
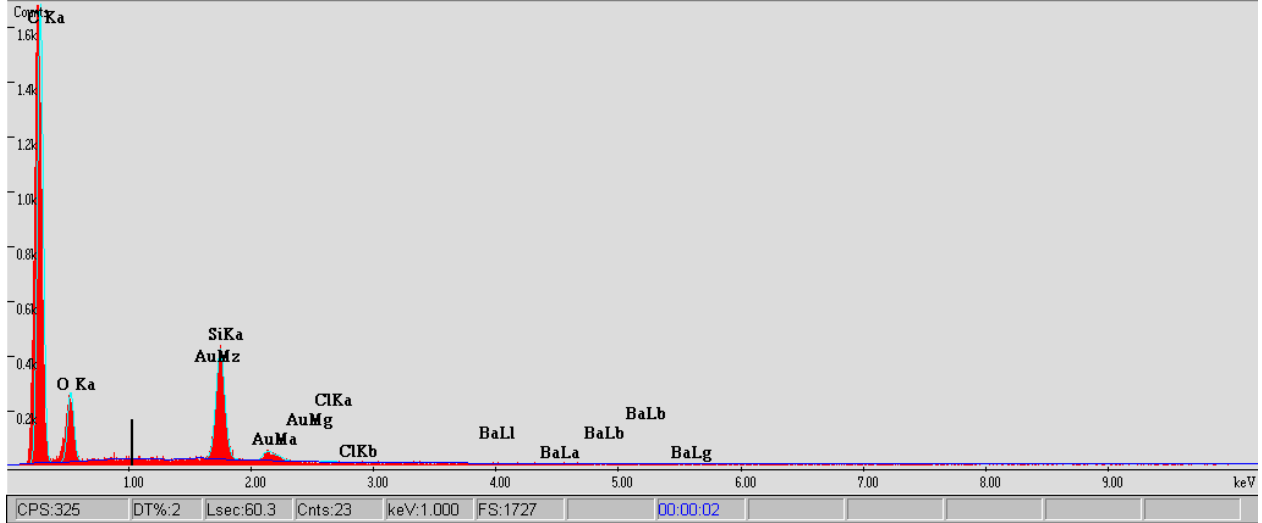
Appendix C: FEM Simulation Results

The appendix presents the methodology of finite element modeling (FEM) simulations. In order to understand the electric field distribution in a cable termination to complement the experiments, a Type-II cable termination was simulated in COMSOL[TM] Multiphysics 4.0a for electric field calculations. The COMSOL[TM] FEM study has already been conducted in previous studies of cable terminations with field-dependent SG materials [67, 90]. The FEM application modes, boundary settings, and meshing techniques are primarily based on the experimentally validated simulations by [67, 90]. The COMSOL[TM] FEM method in this work also utilized the material properties of the SG systems and cable based on the experimental values from [67, 90].

The partial differential equations in discretized domains are solved with electromagnetic simulations using FEM based on Maxwell's unified electromagnetic theory [129]. FEM approximates the solution to the partial differential equations in a domain composed of a mesh of elements whose vertices are known as nodes. A messed cross-section of the Type-II termination design is shown in Figure 4.9. An FEM problem can be broken down in four steps [130] as follows: (1) discretize the solution region in a finite number of sub-regions names elements, (2) define the equations that describe a typical element, (3) combine all the elements in the solution region, and (4) solve the system of equations described.

Cross-sectional view of the Type-II terminatinon COMSOL model on a 2D-axial geometry
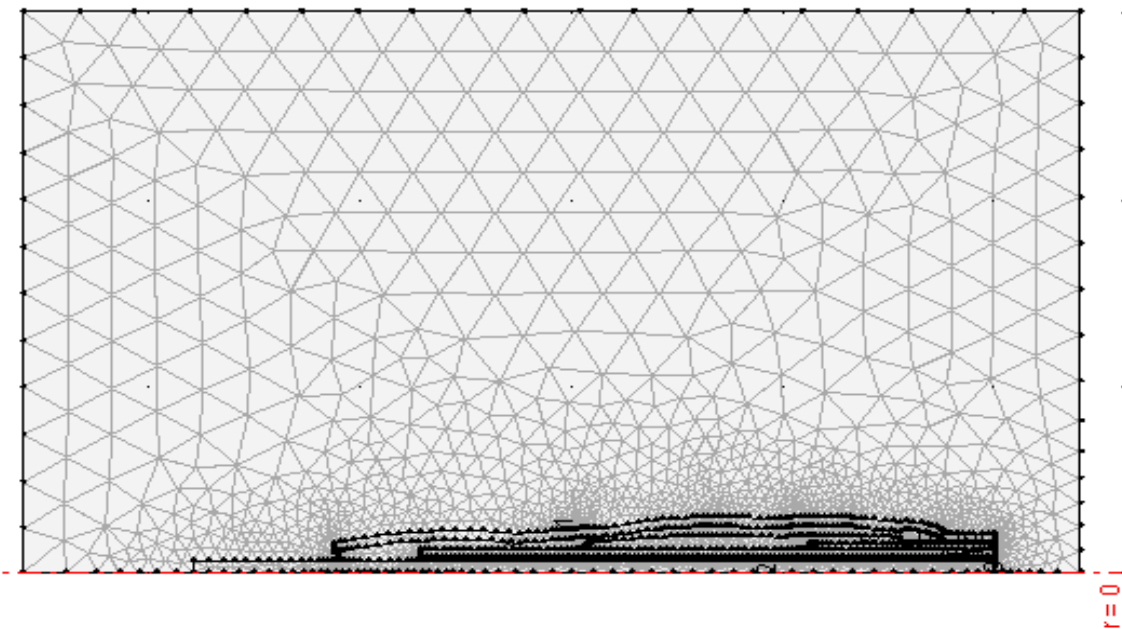
The cable termination geometry in this FEM model of Figure 4.10 is represented as subdomains of conductor, dielectrics: air and XLPE, semi-conductive screens; conductor shield and insulation shield, stress grading materials; stress control tube and Hi-K stress control compound, and cable termination housing; silicone sealing compound and silicone rubber insulator. Relative permittivity and electrical conductivity are assigned as subdomain properties. The SG material conductivity is dependent on the electric field E, as defined by:

$$\sigma(E) = \sigma_0 \, e^{\kappa E} \tag{4.1}$$

Here, σ_0 and κ are positive constants obtained from fitting experimental data and $E = |\mathrm{E}|$. A preselected combination of constants σ_0 and κ from [67] are adopted for this research. Temperature dependencies are not considered and permittivities were constant as the materials were considered isotropic for simplicity. Table 3-1 lists the conductivity constants (σ_0 and κ) and relative permittivities (ε_r) of the stress grading systems used in the simulations. The voltage level, and frequency parameters were selected to correspond with the ESV experimental test conditions, discussed in Section 4.3. Moreover, sensitivity analysis was conducted for the surface electric field in the model termination by varying the applied voltage amplitude, distortion level, and frequency. The conductor voltage was varied between $0.5V_{\text{L-G}}$ to $2V_{\text{L-G}}$, the THD level was varied from 0% to 30%, and the harmonic order was varied from 3rd to 21st.

Conductivity constants (σ_0 and κ) and relative permittivities (ε_r) used in the FEM model for the stress grading system of the Type-II termination sample [67]

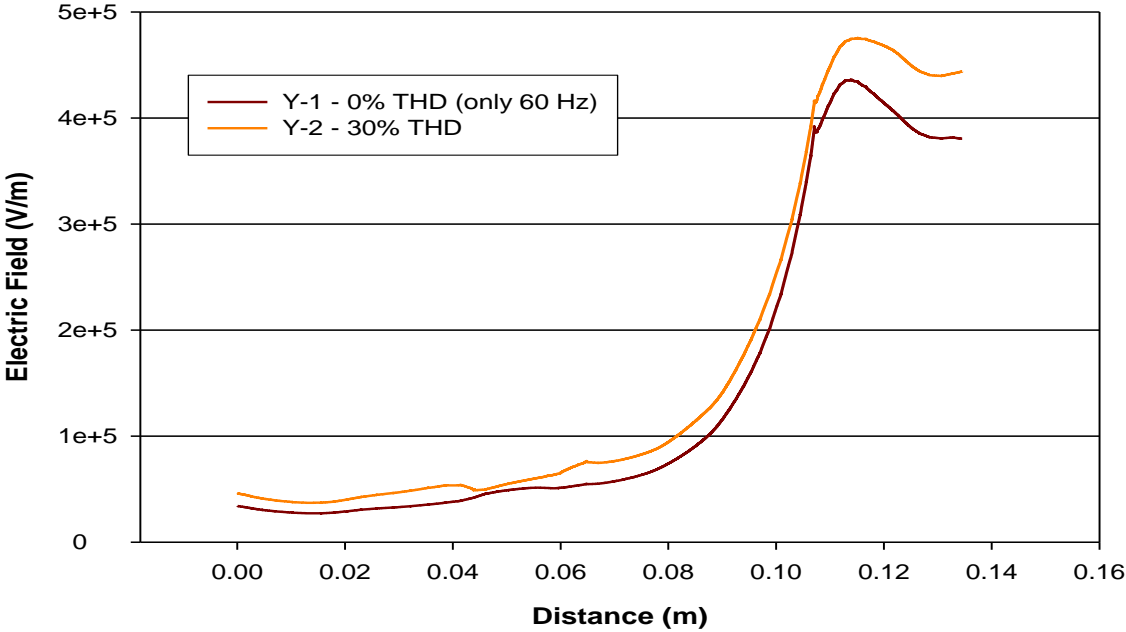| Component of the SG System	Field-Dependent Conductivity Parameters		Relative Permittivity (ε_r)
	σ_0 [S/m]	κ [m/V]	
Stress Control Tube	1.2E-10	8.50E-06	10
Hi-K stress control compound	2.7E-11	7.54E-06	23

Based on the boundary settings and material properties of the SG systems described in Section 4.4, Type-II surface potential and electric field on a Type-II FEM COMSOL™ model under the testing conditions listed in Table 4.2 is simulated and results of which are presented. As mentioned in Section 4.4, FEM application modes, boundary settings, meshing techniques, and even material properties of the SG systems and cable were primarily based on the experimentally validated simulations by [67, 90]. Similar

to the experimental electric field distribution, the simulated electric field plots for the test cases listed in Table 4.2 are provided in Figure 5.14, 5.15, and 5.16. The electric filed used in the simulation is the magnitude of the electric field,$|E|$, combined from all three axes of the rectangular coordinates. The simulated and the experimental electric field distribution show a very similar trend.

Electric field distribution across the termination length for the test cases of X-1, X-2, X-3, and X-4
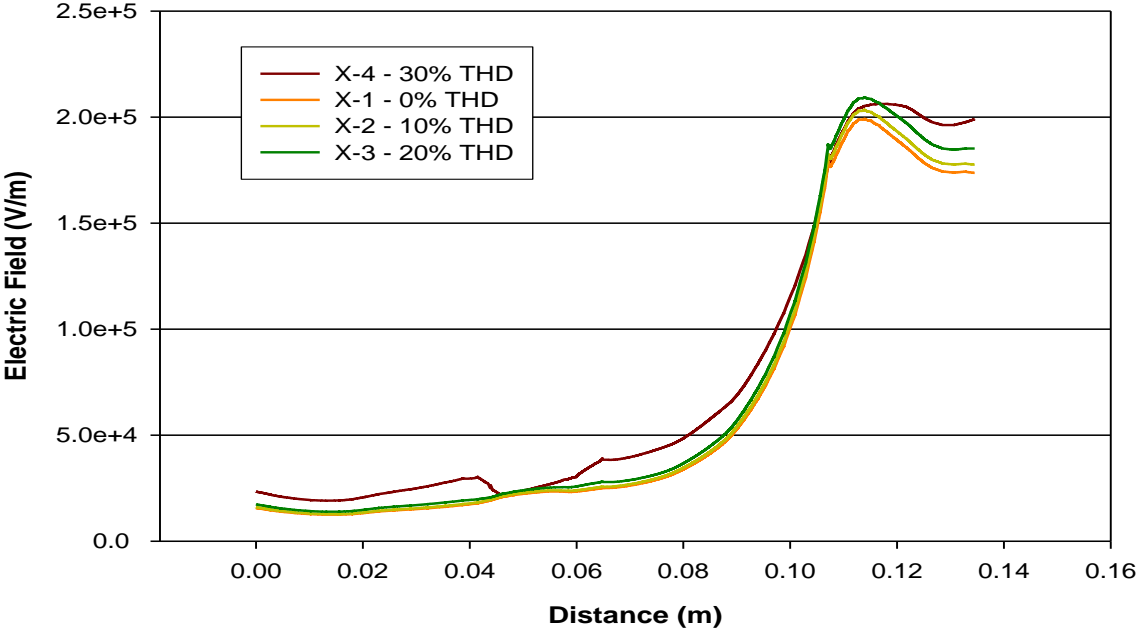
Electric field distribution across the termination length for the test cases of Y-1 and Y-2

Electric field distribution across the termination length for the test cases of Z-1 and Z-2